Aminoglycoside tolerance in *Vibrio cholerae* engages translational reprogramming associated to queuosine tRNA modification

Louna Fruchard [1,2,#], Anamaria Babosan [1,#], Andre Carvalho [1], Manon Lang [1], Blaise Li [3], Magalie Duchateau [4], Quentin Giai-Gianetto [4,5], Mariette Matondo [4], Frédéric Bonhomme [6], Isabelle Hatin [7], Hugo Arbes [7], Céline Fabret [7], Guillaume Sanchez [8], Virginie Marchand [8], Yuri Motorin [8], Olivier Namy [7], Valérie de Crécy-Lagard [9,10], Didier Mazel [1,*], Zeynep Baharoglu [1,*].

# equal contribution
*Corresponding authors: baharogl@pasteur.fr, mazel@pasteur.fr

1. Institut Pasteur, Université de Paris Cité, Unité Plasticité du Génome Bactérien, UMR3525, CNRS, 75015, Paris, France
2. Sorbonne Université, Collège Doctoral, F-75005, Paris, France
3. Institut Pasteur, Université Paris Cité, Bioinformatics and Biostatistics Hub, F-75015 Paris, France
4. Institut Pasteur, Université de Paris, Proteomics Platform, Mass Spectrometry for Biology Unit, UAR2024, CNRS 2000, Paris, France.
5. Institut Pasteur, Université de Paris, Department of Computation Biology, Bioinformatics and Biostatistics Hub, Paris, France.
6. Institut Pasteur, Université Paris cité, Epigenetic Chemical Biology Unit, UMR 3523, CNRS, 75015, Paris, France
7. Université Paris-Saclay, CEA, CNRS, Institute for Integrative Biology of the Cell (I2BC), F-91198, Gif-sur-Yvette, France
8. Université de Lorraine, CNRS, Inserm, UAR2008/US40 IBSLor, Epitranscriptomics and RNA Sequencing Core Facility and UMR7365 IMoPA, F-54000, Nancy, France
9. Department of Microbiology and Cell Science, University of Florida, Gainesville, Florida 32611, United States.
10. University of Florida Genetics Institute, Florida 32611, United States

Abstract

Tgt is the enzyme modifying the guanine (G) in tRNAs with GUN anticodon to queuosine (Q). *tgt* is required for optimal growth of *Vibrio cholerae* in the presence of sub-lethal aminoglycoside concentrations. We further explored here the role of the Q in the efficiency of codon decoding upon tobramycin exposure. We characterized its impact on the overall bacterial proteome, and elucidated the molecular mechanisms underlying the effects of Q modification in antibiotic translational stress response. Using molecular reporters, we showed that Q impacts the efficiency of decoding at tyrosine TAT and TAC codons. Proteomics analyses revealed that the anti-SoxR factor RsxA is better translated in the absence of *tgt*. RsxA displays a codon bias towards tyrosine TAT and overabundance of RsxA leads to decreased expression of genes belonging to SoxR oxidative stress regulon. We also identified conditions that regulate *tgt* expression. We propose that regulation of Q modification in response to environmental cues leads to translational reprogramming of genes bearing a biased tyrosine codon usage. *In silico* analysis further identified candidate genes possibly subject to such translational regulation, among which DNA repair factors. Such transcripts, fitting the definition of modification tunable transcripts, are plausibly central in the bacterial response to antibiotics.

Introduction

Antimicrobial resistance is an increasingly serious threat to global public health. Our recent finding that many tRNA modification genes are involved in the response to antibiotics from different families (1) led to further investigate the links between environmental factors (e.g. traces of antibiotics), tRNA modifications and bacterial survival to antibiotics.

The regulatory roles of RNA modifications was first proposed for eukaryotes(2) and their importance in human diseases has recently emerged(3,4). In bacteria, while some tRNA modifications are essential(5), the absence of many RNA modification shows no growth phenotype in unstressed cells(6). At the molecular level, the roles of tRNA modifications in differential codon decoding have been described in various species(7-10). In most cases, no growth phenotype was associated with these variations in decoding in bacteria. Recent studies, however, do highlight the links between tRNA modifications and stress responses in several bacterial species(6,11-17), and new modifications are still being discovered(18). Until recently, few tRNA modification factors have been clearly linked with resistance and persistence to antibiotics, via differential codon decoding in cell membrane and efflux proteins (TrmD(19), MiaA(8)). A link between stress and adaptation was described to occur via the existence of modification tunable transcripts, or MoTTs.

MoTTs were first (and mostly) defined in eukaryotes as transcripts that will be translated more or less efficiently depending on the presence or absence of tRNA modifications(20), namely upon stress(21). In bacteria, links between tRNA modifications and the response to several stresses are highlighted by studies focusing on the following MoTT/codon and tRNA modification couples (reviewed in(6)): differential translation of RpoS/leucine codons via MiaA (*E. coli*)(12); Fur/serine codons via MiaB, in response to low iron (*E. coli*)(13); MgtA/proline codons via TrmD, in response to low magnesium(14); catalases/phenylalanine and aspartate codons via TrmB, during oxidative stress (*P. aeruginosa*)(11). Mycobacterial response to hypoxic stress(15) also features MoTTs. In this latter study, specific stress response genes were identified *in silico,* through their codon usage bias, and then experimentally confirmed for their differential translation. tRNA modification-dependent translational reprogramming in response to antibiotic stress has not been the focus of a study so far in bacteria.

During studies in *V. cholerae*, we recently discovered that t/rRNA modifications play a central role in response to stress caused by antibiotics with very different modes of action (1), not through resistance development, but by modulating tolerance. The identified RNA modification genes had not previously been associated with any antibiotic resistance phenotype. The fact that different tRNA modifications have opposite effects on tolerance to different antibiotics highlights the complexity of such a network, and shows that the observed phenotypes are not merely due to a general mistranslation effect. Since tRNA modifications affect codon decoding and accuracy, it is important to address how differential translation can generate proteome diversity, and eventually adaptation to antibiotics.

In particular, deletion of the *tgt* gene encoding tRNA-guanine transglycosylase (Tgt) in *V. cholerae* confers a strong growth defect in the presence of aminoglycosides at doses below the minimal inhibitory concentration (sub-MIC)(1). Tgt incorporates queuosine (Q) in the place of guanosine (G) in the wobble position of four tRNAs with GUN anticodon (tRNA-Asp GUC, tRNA-Asn GUU, tRNA-Tyr GUA, tRNA-His GUG)(22). The tRNAs with “AUN” anticodons are not present in the genome, and thus each one of the four GUN tRNAs decodes two synonymous codons (aspartate GAC/GAT, asparagine AAC/AAT, tyrosine TAC/TAT, histidine CAC/CAT which differ in the third position). Q is known to increase or decrease translation error rates in eukaryotes in a codon and organism specific manner(22,23). Q was shown to induce mild oxidative stress resistance in the eukaryotic parasite *Entamoeba histolytica*, the causative agent of amebic dysentery, and to attenuate its virulence(24). In *E. coli*, the absence of Q modification was found to decrease mistranslation rates by tRNA-Tyr, while increasing it for tRNA-Asp(25,26). No significant biological difference was found in *E. coli Δtgt* mutant, except for a slight defect in stationary phase viability(27). Recent studies show that the *E. coli tgt* mutant is more sensitive to aminoglycosides but not to ampicillin nor spectinomycin and is more sensitive to oxidative stress but the molecular mechanisms were not elucidated(28).

We asked here how queuosine (Q) modification by Tgt modulates the response to sub-MIC aminoglycosides. We find that *V. cholerae* Δ*tgt* displays differential decoding of tyrosine TAC/TAT. Molecular reporters, coupled to proteomics and *in silico* analysis, reveal that several proteins with codon usage biased towards TAT (versus TAC) are more efficiently translated in Δ*tgt*. One of these proteins is RsxA, which prevents activation of SoxR oxidative stress response regulon(29). We propose that sub-MIC TOB treatment leads to increased expression of *tgt* and Q modification, which in turn allows for more efficient Sox regulon related oxidative stress response, and better response to sub-MIC TOB. Lastly, bioinformatic analysis identified DNA repair gene transcripts with TAT codon bias as transcripts modulated by Q modification, which was confirmed by decreased UV susceptibility of *V. cholerae* Δ*tgt.*

Materials and methods

Media and Growth Conditions

Platings were done at 37°C, in Mueller-Hinton (MH) agar media. Liquid cultures were grown at 37°C in MH in aerobic conditions, with 180 rotations per minute.

Competition experiments were performed as described(1): overnight cultures from single colonies of mutant *lacZ*+ and WT *lacZ*- strains were washed in PBS (Phosphate Buffer Saline) and mixed 1:1 (500 µl + 500 µl). At this point 100 µl of the mix were serial diluted and plated on MH agar supplemented with X-gal (5-bromo-4-chloro-3-indolyl-β-D- galactopyranoside) at 40 µg/mL to assess T0 initial 1:1 ratio. At the same time, 10 µl from the mix were added to 2 mL of MH or MH supplemented with sub-MIC antibiotics (concentrations, unless indicated otherwise: TOB: tobramycin 0.6 µg/ml; GEN: 0.5 µg/ml; CIP: ciprofloxacin 0.01 µg/ml, CRB: carbenicillin 2.5 µg/ml), PQ: paraquat 10 µM, or H_2O_2: 0.5 mM. Cultures were incubated with agitation at 37°C for 20 hours, and then diluted and plated on MH agar plates supplemented with X-gal. Plates were incubated overnight at 37°C and the number of blue and white CFUs was assessed. Competitive index was calculated by dividing the number of blue CFUs (*lacZ*+ strain) by the number of white CFUs (*lacZ*- strain) and normalizing this ratio to the T0 initial ratio. When a plasmid was present, antibiotic was added to maintain selection: kanamycin 50 µg/ml for pSEVA.

Construction of complementation and overexpression plasmids in pSEVA238

Genes were amplified on *V. cholerae* genomic DNA using primers listed in Table S4 and cloned into pSEVA238 (30) under the dependence of the *Pm* promoter(31), by restriction digestion with XbaI+EcoRI and ligation using T4 DNA ligase. Sodium benzoate 1 mM was added in the medium as inducer.

Survival/tolerance tests were performed on early exponential phase cultures. The overnight stationary phase cultures were diluted 1000x and grown until OD 600 nm = 0.35 to 0.4, at 37°C with shaking, in Erlenmeyers containing 25 mL fresh MH medium. Appropriate dilutions were plated on MH plates to determine the total number of CFUs in time zero untreated cultures. 5 mL of cultures were collected into 50 mL Falcon tubes and treated with lethal doses of desired antibiotics (5 or 10 times the MIC: tobramycin 5 or 10 µg/mL, carbenicillin 50 µg/mL, ciprofloxacin 0.025 µg/mL) for 30 min, 1 hour, 2 hours and 4 hours if needed, at 37°C with shaking in order to guarantee oxygenation. Appropriate dilutions were then plated on MH agar without antibiotics and proportion of growing CFUs were calculated by doing a ratio with total CFUs at time zero. Experiments were performed 3 to 8 times.

151 **MIC determination**
152 Stationary phase cultures grown in MH were diluted 20 times in PBS, and 300 µL were plated on MH
153 plates and dried for 10 minutes. Etest straps (Biomérieux) were placed on the plates and incubated
154 overnight at 37°C.
155
156 **Quantification of fluorescent neomycin uptake** was performed as described(32). Neo-Cy5 is the
157 neomycin aminoglycoside coupled to the fluorophore Cy5, and has been shown to be active against
158 Gram- bacteria(33,34). Briefly, overnight cultures were diluted 100-fold in rich MOPS (Teknova EZ rich
159 defined medium). When the bacterial strains reached an OD 600 nm of ~0.25, they were incubated
160 with 0.4 µM of Cy5 labeled neomycin for 15 minutes at 37°C. 10 µl of the incubated culture were then
161 used for flow cytometry, diluting them in 250 µl of PBS before reading fluorescence. WT *V. cholerae*,
162 was incubated simultaneously without neo-Cy5 as a negative control. Flow cytometry experiments
163 were performed as described(35) and repeated at least 3 times. For each experiment, 100,000 events
164 were counted on the Miltenyi MACSquant device.
165
166 **PMF measurements**
167 Quantification of PMF was performed using the Mitotracker Red CMXRos dye (Invitrogen) as
168 described(36), in parallel with the neo-Cy5 uptake assay, using the same bacterial cultures. 50 µL of
169 each culture were mixed with 60 µL of PBS. Tetrachlorosalicylanilide TCS (Thermofischer), a
170 protonophore, was used as a negative control with a 500 µM treatment applied for 10 minutes at room
171 temperature. Then, 25 nM of Mitotracker Red were added to each sample and let at room temperature
172 for 15 minutes under aluminium foil. 20 µL of the treated culture were then used for flow cytometry,
173 diluted in 200 µL of PBS before reading fluorescence.
174
175 **tRNA overexpressions**
176 Synthetic fragments carrying the P*trc* promoter, the desired tRNA sequence and the natural
177 transcriptional terminator sequence of VCt002 were ordered from IDT as double stranded DNA
178 gBlocks, and cloned into pTOPO plasmid. Sequences are indicated in Table S4.
179
180 **mRNA purification**
181 For RNA extraction, overnight cultures were diluted 1:1000 in MH medium and grown with agitation
182 at 37°C until an OD600 of 0.3-0.4 (exponential phase). 0.5 mL of these cultures were centrifuged and
183 supernatant removed. Pellets were homogenized by resuspension with 1.5 mL of room temperature
184 TRIzol Reagent. Next, 300 µL chloroform were added to the samples following mix by vortexing.
185 Samples were then centrifuged at 4°C for 10 minutes. Upper (aqueous) phase was transferred to a new
186 2mL tube and mixed with 1 volume of 70% ethanol. From this point, the homogenate was loaded into
187 a RNeasy Mini kit (Qiagen) column and RNA purification proceeded according to the manufacturer's
188 instructions. Samples were then subjected to DNase treatment using TURBO DNA-free Kit (Ambion)
189 according to the manufacturer's instructions.
190
191 **mRNA quantifications by digital-RT-PCR**
192 qRT-PCR reactions were prepared with 1 µL of diluted RNA samples using the qScript XLT 1-Step RT-
193 qPCR ToughMix (Quanta Biosciences, Gaithersburg, MD, USA) within Sapphire chips. Digital PCR was
194 conducted on a Naica Geode programmed to perform the sample partitioning step into droplets,
195 followed by the thermal cycling program suggested in the user's manual. Primer and probe sequences
196 used in digital qRT-PCR reaction are listed in Table S4. Image acquisition was performed using the Naica
197 Prism3 reader. Images were then analyzed using Crystal Reader software (total droplet enumeration

198 and droplet quality control) and the Crystal Miner software (extracted fluorescence values for each
199 droplet). Values were normalized against expression of the housekeeping gene *gyrA* as previously
200 described(37).
201
202 **tRNA level quantification by qRT-PCR**
203 First-strand cDNA synthesis and quantitative real-time PCR were performed with KAPA SYBR® FAST
204 Universal (CliniSciences) on the QuantStudio Real-Time PCR (Thermo Fischer) using the primers
205 indicated in Table S4. Transcript levels of each gene were normalized to *gyrA* as the reference gene
206 control(37). Gene expression levels were determined using the $2^{-\Delta\Delta Cq}$ method (Bustin et al., 2009; Livak
207 and Schmittgen, 2001) in respect to the MIQE guidelines. Relative fold-difference was expressed either
208 by reference to antibiotic free culture or the WT strain in the same conditions. All experiments were
209 performed as three independent replicates with all samples tested in duplicate. Cq values of technical
210 replicates were averaged for each biological replicate to obtain the ΔCq. After exponential
211 transformation of the ΔCq for the studied and the normalized condition, medians and upper/lower
212 values were determined.
213
214 **Construction of *gfp* reporters with codon stretches**
215 The positive control was *gfp*mut3 (stable *gfp*)(38) under the control of P*trc* promoter, the transcription
216 start site, *rbs* and ATG start codon are indicated in bold and underlined.
217 TTGACAATTAATCATCCGGCTCGTATAATGTGTGG**A**ATTGTGAGCGGATAACAATTTCACAC**AGGAAAC**AGCG
218 CCGC**ATG**CGTAAAGGAGAAGAACTTTTCACTGGAGTTGTCCCAATTCTTGTTGAATTAGATGGTGATGTTAATG
219 GGCACAAATTTTCTGTCAGTGGAGAGGGTGAAGGTGATGCAACATACGGAAAACTTACCCTTAAATTTATTTG
220 CACTACTGGAAAACTACCTGTTCCATGGCCAACACTTGTCACTACTTTCGGTTATGGTGTTCAATGCTTTGCGAG
221 ATACCCAGATCATATGAAACAGCATGACTTTTTCAAGAGTGCCATGCCCGAAGGTTATGTACAGGAAAGAACT
222 ATATTTTTCAAAGATGACGGGAACTACAAGACACGTGCTGAAGTCAAGTTTGAAGGTGATACCCTTGTTAATA
223 GAATCGAGTTAAAAGGTATTGATTTTAAAGAAGATGGAAACATTCTTGGACACAAATTGGAATACAACTATAA
224 CTCACACAATGTATACATCATGGCAGACAAACAAAAGAATGGAATCAAAGTTAACTTCAAAATTAGACACAAC
225 ATTGAAGATGGAAGCGTTCAACTAGCAGACCATTATCAACAAAATACTCCAATTGGCGATGGCCCTGTCCTTTT
226 ACCAGACAACCATTACCTGTCCACACAATCTGCCCTTTCGAAAGATCCCAACGAAAAGAGAGACCACATGGTCC
227 TTCTTGAGTTTGTAACAGCTGCTGGGATTACACATGGCATGGATGAACTATACAAATAA
228 For the tested codon stretches, 6 repeats of the desired codon were added just after the ATG start
229 codon of *gfp*. The DNA fragments were ordered as double stranded *eblocks* from Integrated DNA
230 technologies (IDT), and cloned into pTOPO-Blunt using kanamycin resistance, following the
231 manufacturer's instructions.
232 For tests of sequence context surrounding tyrosine codons of *rsxA*, DNA was ordered from IDT and
233 cloned into pTOPO as described for codon stretches above, based on the following amino acid
234 sequences (tested sequences in bold):
235 VC1017RsxA *V. cholerae*
236 MLLLWQSRIMPGSEANIYITM**TEYLLL**LIGTVLVNNFVLVKFLGLCPFMGVSKKLETAIGMGLATTFVLTLASVCAYL
237 VESYVLRPLGI**EYLR**TMSFILVIAVVVQFTEMVVHKTSPT**LYRLL**GIFLPLITTNCAVLGVALLNINENHNFIQSIIYGFG
238 AAVGFSLVLILFASMRERIHVADVPAPFKGASIAMITAGLMSLAFMGFTGLVKL
239 RsxA *E. coli*
240 M**TDYLLL**FVGTVLVNNFVLVKFLGLCPFMGVSKKLETAMGMGLATTFVMTLASICAWLIDTWILIPLNLIYLRTLAFIL
241 VIAVVVQFTEMVVRKTSPV**LYRLL**GIFLPLITTNCAVLGVALLNINLGHNFLQSALYGFSAAVGFSLVMVLFAAIRERL
242 AVADVPAPFRGNAIALITAGLMSLAFMGFSGLVKL
243
244 **Quantification of *gfp* fusion expression by fluorescent flow cytometry**
245 Flow cytometry experiments were performed as described(35) on overnight cultures and repeated at
246 least 3 times. For each experiment, 50,000 to 100,000 events were counted on the Miltenyi
247 MACSquant device. The mean fluorescence per cell was measured at the FITC channel for each

248 reporter in both WT and *Δtgt* strains, and the relative fluorescence was calculated as the ratio of the
249 mean fluorescence of a given reporter in *Δtgt* over the mean fluorescence of the same reporter in the
250 WT. Native *gfp* (*gfpmut3*) was used as control.
251 Transcriptional fusion: *rsxA* promoter sequence was amplified using primers ZIP796/ZIP812. gfp was
252 amplified from pZE1-*gfp*(39) using primers ZIP813/ZIP200. The two fragments were PCR assembled
253 into *PrsxA-gfp* using ZIP796/ZIP200 and cloned into pTOPO-TA cloning vector. The *PrsxA-gfp* fragment
254 was then extracted using *EcoRI* and cloned into the low copy plasmid pSC101 (1 to 5 copies per cell).
255 The plasmid was introduced into desired strains, and fluorescence was measured on indicated
256 conditions, by counting 100,000 cells on the Miltenyi MACSquant device. Likewise, the control plasmid
257 *Pc-gfp* (constitutive) was constructed using primers ZIP513/ZIP200 and similarly cloned in pSC101.
258 For translational fusions, the constitutive P*trc* promoter, the *rsxA* gene (without stop codon) with
259 desired codon usage fused to *gfp* (without ATG start codon) was ordered from IDT in the pUC-IDT
260 vector (carbenicillin resistant).
261 Native sequence of *V. cholerae rsxA* gene, called $rsxA^{TAT}gfp$ in this manuscript is shown below. For
262 $rsxA^{TAC}gfp$, all tyrosine TAT codons were replaced with TAC.
263 ATGACCGAA**TAT**CTTTTGTTGTTAATCGGCACCGTGCTGGTCAATAACTTTGTACTGGTGAAGTTTTTGGGCTT
264 ATGTCCTTTTATGGGCGTATCAAAAAAACTAGAGACCGCCATTGGCATGGGGTTGGCGACGACATTCGTCCTC
265 ACCTTAGCTTCGGTGTGCGCT**TAT**CTGGTGGAAAGT**TAC**GTGTTACGTCCGCTCGGCATTGAG**TAT**CTGCGCA
266 CCATGAGCTTTATTTTGGTGATCGCTGTCGTAGTACAGTTCACCGAAATGGTGGTGCACAAAACCAGTCCGACA
267 CTC**TAT**CGCCTGCTGGGCATTTTCCTGCCACTCATCACCACCAACTGTGCGGTATTAGGGGTTGCGCTGCTCAA
268 CATCAACGAAAATCACAACTTTATTCAATCGATCATT**TAT**GGTTTTGGCGCTGCTGTTGGCTTCTCGCTGGTGCT
269 CATCTTGTTCGCTTCAATGCGTGAGCGAATCCATGTAGCCGATGTCCCCGCTCCCTTTAAGGGCGCATCCATTG
270 CGATGATCACCGCAGGTTTAATGTCTTTGGCCTTTATGGGCTTTACCGGATTGGTGAAACTGGCTAGC
271 gfp^{TAC} and gfp^{TAT} (tyrosine 11 TAT instead of 11 TAC) were ordered from IDT as synthetic genes under
272 the control of P*trc* promoter in the pUC-IDT plasmid (carbenicillin resistant). The complete sequence
273 of ordered fragments is indicated in Table S4, tyrosine codons are underlined.
274
275 **Construction of *bla* reporters**
276 Point mutations for codon replacements were performed using primer pairs where the desired
277 mutations were introduced and by whole plasmid PCR amplification on circular pTOPO-TA plasmid.
278 Primers are listed Table S4.
279
280 **Growth on microtiter plate reader for *bla* reporter assays**
281 Overnight cultures were diluted 1:500 in fresh MH medium, on 96 well plates. Each well contained 200
282 µL. Plates were incubated with shaking on TECAN plate reader device at 37°C, OD 600 nm was
283 measured every 15 min. Tobramycin was used at sub-MIC: TOB 0.2 µg/mL. Kanamycin and carbenicillin
284 were used at selective concentration: CRB 100 µg/mL, KAN 50 µg/mL.
285
286 **Protein extraction**
287 Overnight cultures of *V. cholerae* were diluted 1:100 in MH medium and grown with agitation at 37°C
288 until an OD 600 nm of 0.3 (exponential phase). 50 mL of these cultures were centrifuged for 10 min at
289 4°C and supernatant removed. Lysis was achieved by incubating cells in the presence of lysis buffer (10
290 mM Tris-HCl pH 8, 150 mM Nacl, 1% triton 100X) supplemented with 0.1 mg/mL lysozyme and
291 complete EDTA-free Protease Inhibitor Cocktail (Roche) for 1 hour on ice. Resuspensions were
292 sonicated 3x50 sec (power: 6, pulser: 90%), centrifuged for 1 h at 4°C at 5000 rpm and supernatants
293 were quantified using Pierce™ BCA Protein Assay Kit (Cat. No 23225) following the manufacturer's
294 instructions. Proteins were then stored at -80°C.
295

296 **Proteomics MS and analysis**

297 *Sample preparation for MS*

298 Tryptic digestion was performed using eFASP (enhanced Filter-Aided Sample Preparation)
299 protocol(40). All steps were done in 30 kDa Amicon Ultra 0.5 mL filters (Millipore). Briefly, the sample
300 was diluted with a 8M Urea, 100 mM ammonium bicarbonate buffer to obtain a final urea
301 concentration of 6 M. Samples were reduced for 30 min at room temperature (RT) with 5 mM TCEP.
302 Subsequently, proteins were alkylated in 5 mM iodoacetamide for 1 hour in the darkness at RT and
303 digested overnight at 37°C with 1 µg trypsin (Trypsin Gold Mass Spectrometry Grade, Promega).
304 Peptides were recovered by centrifugation, concentrated to dryness and resuspended in 2%
305 acetonitrile (ACN)/0.1% FA just prior to LC-MS injection.

306 *LC-MS/MS analysis*

307 Samples were analyzed on a high-resolution mass spectrometer, Q Exactive™ Plus Hybrid Quadrupole-
308 Orbitrap™ Mass Spectrometer (Thermo Scientific), coupled with an EASY 1200 nLC system (Thermo
309 Fisher Scientific, Bremen). One µg of peptides was injected onto a home-made 50 cm C18 column (1.9
310 µm particles, 100 Å pore size, ReproSil-Pur Basic C18, Dr. Maisch GmbH, Ammerbuch-Entringen,
311 Germany). Column equilibration and peptide loading were done at 900 bars in buffer A (0.1% FA).
312 Peptides were separated with a multi-step gradient from 3 to 22 % buffer B (80% ACN, 0.1% FA) in 160
313 min, 22 to 50 % buffer B in 70 min, 50 to 90 % buffer B in 5 min at a flow rate of 250 nL/min. Column
314 temperature was set to 60°C. The Q Exactive™ Plus Hybrid Quadrupole-Orbitrap™ Mass Spectrometer
315 (Thermo Scientific) was operated in data-dependent mode using a Full MS/ddMS2 Top 10 experiment.
316 MS scans were acquired at a resolution of 70,000 and MS/MS scans (fixed first mass 100 m/z) at a
317 resolution of 17,500. The AGC target and maximum injection time for the survey scans and the MS/MS
318 scans were set to 3E6, 20ms and 1E6, 60ms, respectively. An automatic selection of the 10 most intense
319 precursor ions was activated (Top 10) with a 35 s dynamic exclusion. The isolation window was set to
320 1.6 m/z and normalized collision energy fixed to 27 for HCD fragmentation. We used an underfill ratio
321 of 1.0 % corresponding to an intensity threshold of 1.7E5. Unassigned precursor ion charge states as
322 well as 1, 7, 8 and >8 charged states were rejected and peptide match was disable.

323 *Data analysis*

324 Acquired Raw data were analyzed using MaxQuant 1.5.3.8 version(41) using the Andromeda search
325 engine(42) against *Vibrio cholerae* Uniprot reference proteome database (3,782 entries, download
326 date 2020-02-21) concatenated with usual known mass spectrometry contaminants and reversed
327 sequences of all entries. All searches were performed with oxidation of methionine and protein N-
328 terminal acetylation as variable modifications and cysteine carbamidomethylation as fixed
329 modification. Trypsin was selected as protease allowing for up to two missed cleavages. The minimum
330 peptide length was set to 5 amino acids. The false discovery rate (FDR) for peptide and protein
331 identification was set to 0.01. The main search peptide tolerance was set to 4.5 ppm and to 20 ppm
332 for the MS/MS match tolerance. One unique peptide to the protein group was required for the protein
333 identification. A false discovery rate cut-off of 1 % was applied at the peptide and protein levels. All
334 mass spectrometry proteomics data have been deposited at ProteomeXchange Consortium via the
335 PRIDE partner repository with the dataset identifier PXD035297.

336 The statistical analysis of the proteomics data was performed as follows: three biological replicates
337 were acquired per condition. To highlight significantly differentially abundant proteins between two
338 conditions, differential analyses were conducted through the following data analysis pipeline: (1)
339 deleting the reverse and potential contaminant proteins; (2) keeping only proteins with at least two
340 quantified values in one of the three compared conditions to limit misidentifications and ensure a
341 minimum of replicability; (3) log2-transformation of the remaining intensities of proteins; (4)

342 normalizing the intensities by median centering within conditions thanks to the normalizeD function
343 of the R package DAPAR(43), (5) putting aside proteins without any value in one of both compared
344 conditions: as they are quantitatively present in a condition and absent in another, they are considered
345 as differentially abundant proteins and (6) performing statistical differential analysis on them by
346 requiring a minimum fold-change of 2.5 between conditions and by using a LIMMA t test(44) combined
347 with an adaptive Benjamini-Hochberg correction of the *p*-values thanks to the adjust.p function of the
348 R package cp4p(45). The robust method of Pounds and Cheng was used to estimate the proportion of
349 true null hypotheses among the set of statistical tests(46). The proteins associated with an adjusted *p*-
350 value inferior to an FDR level of 1% have been considered as significantly differentially abundant
351 proteins. Finally, the proteins of interest are therefore the proteins that emerge from this statistical
352 analysis supplemented by those being quantitatively absent from one condition and present in
353 another. The mass spectrometry proteomics data have been deposited to the ProteomeXchange
354 Consortium via the PRIDE partner repository with the dataset identifier PXD035297.
355
356 **RNA purification for RNA-seq**
357 Cultures were diluted 1000X and grown in triplicate in MH supplemented or not with 0.6 µg/ml of
358 tobramycin, corresponding to 50% of the MIC in liquid cultures, to an OD 600nm of 0.4. RNA was
359 purified with the RNAeasy mini kit (Qiagen) according to manufacturer's instructions. Briefly, 4 ml of
360 RNA-protect (Qiagen) reagent were added on 2 ml of bacterial cultures during 5 minutes. After
361 centrifugation, the pellets were conserved at -80°C until extraction. Protocol 2 of the RNA protect
362 Bacteria Reagent Handbook was performed, with the addition of a proteinase K digestion step, such
363 as described in the protocol 4. Quality of RNA was controlled using the Bioanalyzer. Sample collection,
364 total RNA extraction, library preparation, sequencing and analysis were performed as previously
365 described (47). The data for this RNA-seq study has been submitted in the GenBank repository under
366 the project number GSE214520.

367 **Gene Ontology (GO) enrichment analysis**
368 GO enrichment analyses were performed on http://geneontology.org/ as follows: Binomial test was
369 used to determine whether a group of genes in the tested list was more or less enriched than expected
370 in a reference group. The annotation dataset used for the analysis was GO biological process complete.
371 The analyzed lists were for each condition (MH/TOB), genes (**Table S3**) with at least 2-fold change in
372 RNA-seq data of WT strain compared to *Δtgt*, and with an adjusted p-value <0,05. The total number of
373 uploaded gene list to be analyzed were 53 genes for MH and 60 genes for TOB. The reference gene list
374 was *Vibrio cholerae* (all genes in database), 3782 genes. Annotation Version: PANTHER
375 Overrepresentation Test (Released 20220712). GO Ontology database DOI: 10.5281/zenodo.6399963
376 Released 2022-03-22
377
378 **Stringent response measurement**
379 *P1rrnB-gfp* fusion was constructed using *gfp* ASV(48), and cloned into plasmid pSC101. *P1rrnB-GFPasv*
380 transcriptional fusion was amplified from strain R438 (E. coli MG1655 *attB::P1rrnB gfp-ASV::kan*
381 provided by Ivan Matic) using primers AFC060 and AFC055, thus including 42 bp upstream of *rrnB*
382 transcription initiation site. PCR product was then cloned in pTOPOblunt vector and subcloned to
383 pSC101 by *EcoRI* digestion and ligation. The final construct was confirmed by Sanger sequencing. The
384 plasmid was then introduced by electroporation into the tested strains. Overnight cultures were
385 performed in MH + carbenicillin 100 µg/mL and diluted 500x in 10 mL fresh MH or MH+ TOB 0.4 µg/mL,
386 in an Erlenmeyer. At time points 0 min, and every 30 during 3 hours, the OD 600 nm was measured

387 and fluorescence was quantified in flow cytometry. For each experiment, 50,000 to 100,000 events
388 were counted on the Miltenyi MACSquant device.
389
390 **tRNA enriched RNA extraction**
391 Overnight cultures of *V. cholerae* were diluted 1:1000 in MH medium and grown in aerobic conditions,
392 with 180 rotations per minute at 37°C until an OD 600 nm of 0.5. tRNA enriched RNA extracts were
393 prepared using room temperature TRIzol™ reagent as described(49) and contaminating DNA were
394 eliminated using TURBO DNA-free Kit (Ambion). RNA concentration was controlled by UV absorbance
395 using NanoDrop 2000c (Thermo Fisher Scientific). The profile of isolated tRNA fractions was assessed
396 by capillary electrophoresis using an RNA 6000 Pico chip on Bioanalyzer 2100 (Agilent Technologies).
397
398 **tRNA-enriched sample digestion for quantitative analysis of queuosine by mass spectrometry**
399 Purified tRNA enriched RNA fractions were digested to single nucleosides using the New England
400 BioLabs Nucleoside digestion mix (Cat No. M0649S). 10µl of the RNA samples diluted in ultrapure water
401 to 100 ng/µL were mixed with 1µL of enzyme, 2µl of Nucleoside Digestion Mix Reaction Buffer (10X) in
402 a final volume of 20 µL in nuclease-free 1.5 mL tubes. Tubes were wrapped with parafilm to prevent
403 evaporation and incubated at 37°C overnight.
404
405 **Queuosine quantification by LC-MS/MS**
406 Analysis of global levels of queuosine (Q) was performed on a Q exactive mass spectrometer (Thermo
407 Fisher Scientific). It was equipped with an electrospray ionization source (H-ESI II Probe) coupled with
408 an Ultimate 3000 RS HPLC (Thermo Fisher Scientific). The Q standard was purchased from Epitoire
409 (Singapore).
410 Digested RNA was injected onto a ThermoFisher Hypersil Gold aQ chromatography column (100 mm *
411 2.1 mm, 1.9 µm particle size) heated at 30°C. The flow rate was set at 0.3 mL/min and run with an
412 isocratic eluent of 1% acetonitrile in water with 0.1% formic acid for 10 minutes.
413 Parent ions were fragmented in positive ion mode with 10% normalized collision energy in parallel-
414 reaction monitoring (PRM) mode. MS2 resolution was 17,500 with an AGC target of 2e5, a maximum
415 injection time of 50 ms, and an isolation window of 1.0 m/z.
416 The inclusion list contained the following masses: G (284.1) and Q (410.2). Extracted ion
417 chromatograms of base fragments (±5ppm) were used for detection and quantification (152.0565 Da
418 for G; 295.1028 Da for Q). The secondary base fragment 163.0608 was also used to confirm Q detection
419 but not for quantification.
420 Calibration curves were previously generated using synthetic standards in the ranges of 0.2 to 40 pmol
421 injected for G and 0.01 to 1 pmol for Q. Results are expressed as a percentage of total G.
422
423 **Queuosine detection by sequencing**
424 The detection of queuosine was performed as described in (50). Briefly, 200 ng of total RNA were
425 subjected to oxidation by 45 mM of $NaIO_4$ in 50 mM AcONa pH 5.2 buffer for 1h at 37°C. The reaction
426 was quenched by addition of 36 mM glucose and incubation for 30 min at 37°C and RNA was
427 precipitated with absolute ethanol. After precipitation and two washes by 80% ethanol, the RNA pellet
428 was resuspended in 3' ligation reaction buffer 1x and subjected to library preparation using the
429 NEBNext® Small RNA Library Prep Set for Illumina® (NEB, #E7330S). Specific primers for *V. cholerae*
430 tRNAAsn_GUU1, tRNAAsn_GUU2, tRNAAsp_GUC, tRNATyr_GUA and tRNAHis_GUG were hybridized
431 instead of RT primer used in NEBNext® Small RNA Library Prep kit, under the same hybridization
432 conditions. The 5'-SR adaptor was ligated, and reverse transcription was performed for 1h at 50°C
433 followed by 10 min at 80°C using Superscript IV RT (instead of Protoscript II used in the kit). PCR

434 amplification was performed as described in the manufacturer's protocol. Libraries were qualified
435 using Tapestation 4150 and quantified using Qubit fluorometer. Libraries were multiplexed and
436 sequenced in a 50 bp single read mode using NextSeq2000 (Illumina, San Diego).

437 Bioinformatic analysis was performed by trimming of raw reads using trimmomatic v0.39 to remove
438 adapter sequences as well as very short and low-quality sequencing reads. Alignment was done by
439 bowtie2 (v2.4.4) in End-to-End mode with *--mp 2 --rdg 0,2* options to favor retention of reads with
440 deletions, only non-ambiguously mapped reads were taken for further analysis. Coverage file was
441 created with *samtools mpileup* and deletion signature extracted for every position using custom R
442 script. Deletion score was calculated as number of deletions divided by number of matching
443 nucleotides at a given position. Analysis of Q tRNA modification in *V. cholerae* strains was performed
444 in triplicate for biological replicates with technical duplicate for each sample.

445

446 **Analysis of Queuosine tRNA Modification Using APB Northern Blot Assay**

447 Quantification of queuosine in tRNA-Tyr from purified tRNA-enriched RNA fractions was performed
448 using a non-radioactive Northern blot method: the procedure for pouring and running N-acryloyl-3-
449 aminophenylboronic acid (APB) gels was based on the method detailed in (51). tRNA-Tyr were
450 detected using the following 3'-end digoxigenin (DIG)-labeled probe: 5' -
451 CTTTGGCCACTCGGGAACCCCTCC - 3'DIG.
452 For 1 gel, ABP gel buffer was prepared by mixing 4.2g urea, 50mg 3-(Acrylamido) phenylboronic acid
453 (Sigma Aldrich Cat No. 771465), 1ml 10X RNase-free TAE, 3.2ml 30% acrylamide and bis-acrylamide
454 solution 37.5:1 and adding water to adjust the final volume to 10ml. After stirring to facilitate
455 dissolution and right before pouring, 10µl TEMED and 60 µL 10% APS were added to the 10ml ABP
456 buffer to catalyze and initiate polymerization respectively. Gels were casted using the Mini-PROTEAN®
457 Bio-Rad handcast system, short plates (70x100 mm), 0.75 mm spacers and 10-well gel combs. Gels
458 were left to polymerize at room temperature for 50 minutes.
459 Alkaline hydrolysis in 100mM of Tris-HCl pH 9 of our tRNA-enriched RNA extracts was carried out at
460 37°C for 30 min to break the ester bonds between tRNAs and their cognate amino acids. 10µl of the
461 deacylated tRNA-enriched RNA samples were mixed with 8 µl of 2X RNA loading dye (Thermo
462 Scientific™ Cat No. R0641), denatured for 3 min at 72°C and the whole volume was loaded onto the
463 gel. Electrophoresis of the gels were carried out in the Mini-PROTEAN® Tetra Vertical Electrophoresis
464 Cell for 30 min at 85V at room temperature followed by 1h30 at 140 V at 4°C. Gels were incubated at
465 room temperature for 15 min with shaking in 50 ml 1X RNAse-free TAE mixed with 10 µl of 10000X
466 SYBR Gold nucleic acid staining solution (Invitrogen™ S11494) and nucleic acids were visualized using
467 a transilluminator. Transfers of the nucleic acids to positively charged nylon membranes were
468 performed at 5 V/gel for 40 min at room temperature using a semi dry blotting system. RNAs were
469 crosslinked to the membrane surface through exposure to 254 nm UV light at a dose of 1.2 Joules.
470 Membranes were transferred into glass bottles containing 5ml of pre-warmed hybridization buffer and
471 incubated for 1 hour at 42°C at a constant rotation in a hybridization oven. Hybridization buffer was
472 obtained by mixing 12.3 ml of 20X SSX, 1ml of 1M Na2HPO4 pH7.2, 17.5ml of 20% SDS, 2ml of 50X
473 Denhardt's solution and 17ml RNase-free H2O. 3µl of the DIG-labeled probe solution at 100 pmol/µl
474 were then added into the 5ml hybridization buffer and the bottles were rotated in the hybridization
475 oven at 42°C overnight. Membranes were washed 2 time with 2X SSC/5% SDS for 15 min at 42°C and
476 1 time with 1X SSC/1% SDS for 15min at 42°C.
477 Nucleic acids wash and immunological detection of the DIG-labeled probes were performed using the
478 DIG Wash and Block Buffer Set (Roche, Cat No. 11585762001) according to the manufacturer's
479 protocols. Membranes were placed in a plastic container filled with 15ml of the blocking solution for
480 nonspecific binding sites blocking. After 30min incubation at room temperature with rotation, 3µl of

481 the alkaline phosphatase-coupled anti-DIG antibody (Fab fragments, Roche, Cat No. 11093274910)
482 were added to the buffer and incubation at room temperature on a belly-dancer was allowed for 30
483 more min. Next, membranes were washed 3 times 15 min with DIG-wash buffer and once with DIG-
484 detection buffer for 5min. For chemiluminescence visualization of the probe, 1ml of CDP-Star®
485 Chemiluminescent Substrate (Disodium 2-chloro-5-(4-methoxyspiro[1,2-dioxetane-3,2'-(5-
486 chlorotricyclo[3.3.1.13.7]decan])-4-yl]-1-phenyl phosphate) (Roche, Cat No. 11685627001) was added
487 to 9ml of DIG-detection buffer and membranes were then incubated with the substrate for 5 min. The
488 chemiluminescent signal was detected with the iBright Imaging Systems.
489
490 **Ribosome profiling (Ribo-seq)**
491 Pellet from 200 ml of *Vibrio cholerae* at 0.25 OD_{600nm} WT or mutant *Δtgt* in triplicates, with or without
492 tobramycin were flash frozen in liquid nitrogen and stored at -80°C. The polysomes were extracted
493 with 200 µl of extraction buffer (20 mM Tris pH8-150 mM $Mg(CH_3COO)_2$-100 mM NH_4Cl, 5 mM $CaCl_2$-
494 0,4% Triton X100-1% Nonidet P40) added of 2x cocktail anti proteases Roche and 60U RNase Inhibitor
495 Murine to the buffer, DNase I and glass beads (diameter <106 micrometers), vortexed during 30 min
496 at 4°C. The supernatant of this crude extract was centrifugated 10 min at 21 krcf at +4°C. The
497 absorbance was measured at 260nm on 1 µl from 1/10 extract. After 1 hour of digestion at 25°C with
498 0.75 U MNase/0.025 UA_{260nm} of crude extract, the reaction was stopped by the addition of 3 µl 0.5 M
499 EGTA pH8. The monosomes generated by digestion were purified through a 24% sucrose cushion
500 centrifuged 90 min at 110 krpm on a TLA110 rotor at +4°C. The monosomes pellet was rinsed with 200
501 µl of resuspension buffer (20 mM Tris-HCl pH 7,4 - 100 mM NH_4Cl - 15 mM $Mg(CH_3COO)_2$ - 5 mM $CaCl_2$
502) and then recovered with 100 µl. RNA were extracted by acid phenol at 65°C, $CHCL_3$ and precipitated
503 by Ethanol with 0.3M CH_3COONa pH 5.2. Resuspended RNA was loaded on 17% polyacrylamide (19 :1);
504 7 M urea in 1x TAE buffer at 100 V during 6 hours and stained with SYBRgold. RNA fragments
505 corresponding to 28-34 nt were retrieved from gel and precipitated in ethanol with 0.3 M CH_3COONa
506 pH 5.2 in presence of 100 µg glycogen. rRNA were depleted using MicrobExpress Bacterial mRNA
507 Enrichment kit from Invitrogen. The supernatant containing the ribosome footprints were recovered
508 and RNA were precipitated in ethanol in presence of glycogen overnight at -20°C. The RNA
509 concentration was measured by Quant-iT microRNA assay kit (Invitrogen). The RNA was
510 dephosphorylated in 3' and then phosphorylated in 5' to generate cDNA libraries using the NebNext
511 Small RNA Sample Prep kit with 3' sRNA Adapter (Illumina) according to the manufacturer's protocol
512 with 12 cycles of PCR amplification in the last step followed by DNA purification with Monarch PCR
513 DNA cleanup kit (NEB). Library molarity was measured with the Qubit DNAds HS assay kit from
514 Invitrogen and the quality was analyzed using Bioanalyzer DNA Analysis kit (Agilent) and an equimolar
515 pool of the 12 libraries was sequenced by the High-throughput sequencing facility of I2BC with NextSeq
516 500/550 High output kit V2 (75 cycles) (Illumina) with 10 % PhiX.
517 Sequencing data is available at GSE231087.
518
519 **Analysis of ribosome profiling data**
520 RiboSeq analysis was performed using the RiboDoc package (52) for statistical analysis of differential
521 gene expression (DEseq2). Sequencing reads are first trimmed to remove adaptors then aligned to the
522 two *V. cholerae* chromosomes (NC_002505 and NC_002506). Reads aligned uniquely are used to
523 perform the differential gene expression analysis. MNase shows significant sequence specificity at A
524 and T (53). Due to this specificity and A-T biases in *V. cholerae* genome, ribosome profiling data exhibit
525 a high level of noise that prevents the obtention of a resolution at the nucleotide level.
526
527 **UV sensitivity measurements**
528 Overnight cultures were diluted 1:100 in MH medium and grown with agitation at 37°C until an OD
529 600 nm of 0.5-0.7. Appropriate dilutions were then plated on MH agar. The proportion of growing CFUs

530 after irradiation at 60 Joules over total population before irradiation was calculated, doing a ratio with
531 total CFUs. Experiments were performed 3 to 8 times.
532
533 **Quantification and statistical analysis**
534 For comparisons between 2 groups, first an F-test was performed in order to determine whether
535 variances are equal or different between comparisons. For comparisons with equal variance, Student's
536 t-test was used. For comparisons with significantly different variances, we used Welch's t-test. For
537 multiple comparisons, we used ANOVA. We used GraphPad Prism to determine the statistical
538 differences (*p*-value) between groups. **** means $p<0.0001$, *** means $p<0.001$, ** means $p<0.01$, *
539 means $p<0.05$. For survival tests, data were first log transformed in order to achieve normal
540 distribution, and statistical tests were performed on these log-transformed data. The number of
541 replicates for each experiment was $3<n<6$. Means and geometric means for logarithmic values were
542 also calculated using GraphPad Prism.
543
544 **Bioinformatic analysis for whole genome codon bias determinations**
545 *Data.* Genomic data (fasta files containing CDS sequences and their translation, and GFF annotations)
546 for *Vibrio cholerae* (assembly ASM674v1) were downloaded from the NCBI FTP site
547 (ftp://ftp.ncbi.nlm.nih.gov).
548 *Codon counting.* For each gene, the codons were counted in the CDS sequence, assuming it to be in-
549 frame. This step was performed using Python 3.8.3, with the help of the Mappy 2.20 (54) and Pandas
550 1.2.4 (55,56) libraries.
551 *Gene filtering.* Genes whose CDS did not start with a valid start codon were excluded from further
552 computations. A valid start codon is one among ATA, ATC, ATG, ATT, CTG, GTG, TTG, according to the
553 genetic code for bacteria, archaea and plastids (translation table 11 provided by the NCBI at
554 ftp://ftp.ncbi.nlm.nih.gov/entrez/misc/data/gc.prt). Further computations were performed on 3590
555 genes that had a valid start codon.
556 *Codon usage bias computation.* The global codon counts were computed for each codon by summing
557 over the above selected genes. For each gene as well as for the global total, the codons were grouped
558 by encoded amino acid. Within each group, the proportion of each codon was computed by dividing
559 its count by the sum of the counts of the codons in the group. The codon usage bias for a given codon
560 and a given gene was then computed by subtracting the corresponding proportion obtained from the
561 global counts from the proportion obtained for this gene. Codon usage biases were then standardized
562 by dividing each of the above difference by the standard deviation of these differences across all genes,
563 resulting in standardized codon usage biases "by amino acid" ("SCUB by aa" in short). All these
564 computations were performed using the already mentioned Pandas 1.2.4 Python library.
565 *Associating genes to their preferred codon.* For each codon group, genes were associated to the codon
566 for which they had the highest "SCUB by aa" value. This defined a series of gene clusters denoted using
567 the "aa_codon" pattern. For instance, "*_TAT" contains the genes for which TAT is the codon with the
568 highest standardized usage bias among tyrosine codons.
569 *Extracting most positively biased genes from each cluster.* Within each cluster, the distribution of
570 "SCUB by aa" values for each codon was represented using violin plots. Visual inspections of these
571 violin plots revealed that in most cases, the distribution was multi-modal. An automated method was
572 devised to further extract from a given cluster the genes corresponding to the sub-group with the
573 highest "SCUB by aa" for each codon. This was done by estimating a density distribution for "SCUB by
574 aa" values using a Gaussian Kernel Density Estimate and finding a minimum in this distribution. The
575 location of this minimum was used as a threshold above which genes were considered to belong to
576 the most positively biased genes. This was done using the SciPy 1.7.0 (57) Python library. Violin plots
577 were generated using the Matplotlib 3.4.2 (58) and Seaborn 0.11.1 (59) Python libraries.
578 *Code availability.* All codes to perform these analyses were implemented in the form of Python scripts,
579 Jupyter notebooks (60) and Snakemake(61) workflows, and are available in the following git repository:
580 https://gitlab.pasteur.fr/bli/17009_only. Data are available for whole genome codon usage of *V.*

cholerae in excel sheet and *V. cholerae* codon usage biased gene lists at zenodo public repository with the following doi: 10.5281/zenodo.6875293.

Results

Tobramycin tolerance is decreased in *Δtgt* without any difference in uptake

We confirmed *V. cholerae Δtgt* strain's growth defect in sub-MIC tobramycin (TOB) (**Fig. 1A**) and that expression of *tgt* in trans restores growth in these conditions (**Fig. 1B**). We further tested tolerance to lethal antibiotic concentrations by measuring survival after antibiotic treatment during 15 minutes to 4 hours. As expected, *Δtgt* is less tolerant than WT to TOB (**Fig. 1CD**), but had no impact in ciprofloxacin (CIP) or carbenicillin (CRB) (**Fig. 1EF**). In specific cases, the levels of a given tRNA modification can depend on the presence of other ones(62). One example is the m^5C38 modification of $tRNA^{Asp}$ which is favored by the presence of Q in eukaryotes(22,63). However, bacterial tRNAs do not harbor m^5C and neither do they harbor mal-Q or gal-Q hypermodifications, unlike in eukaryotes (64). In *E. coli*, $tRNA^{Tyr}$ is modified by RluF which introduces a pseudouridine (Ψ) at position 35 of the anticodon, next to the G/Q at position 34 (65). We tested whether the presence or absence of this second modification has an impact on Q-dependent fitness phenotypes. Competition experiments showed no effect of the *rluF* deletion in any condition **(Sup. Fig. S1**), showing that the effect of *tgt* is not linked to an effect of a Ψ modification possibly made by RluF in *V. cholerae*.

We asked whether the growth defect of *Δtgt* is due to increased aminoglycoside entry and/or a change in proton-motive force (PMF) (32,66). We used a *ΔtolA* strain as a positive control for disruption of outer membrane integrity and aminoglycoside uptake(67). No changes either in PMF (**Fig. 1G**), nor in uptake of the fluorescent aminoglycoside molecule neo-Cy5 (**Fig. 1H**)(33) were detected in the *Δtgt* strain, indicating that the increased susceptibility of *Δtgt* to TOB is not due to increased aminoglycoside entry into the *V. cholerae* cell.

Overexpression of the canonical $tRNA^{Tyr}_{GUA}$ rescues growth of *Δtgt* in TOB

We next investigated whether all four tRNAs with GUN anticodon modified to QUN by Tgt, are equally important for the TOB sensitivity phenotype of the *Δtgt* mutant: Aspartate (Asp)/Asparagine (Asn)/Tyrosine (Tyr)/Histidine (His). The absence of Q could have direct effects at the level of codon decoding but also indirect effects such as influencing tRNAs' degradation(68). qRT-PCR analysis of $tRNA^{Tyr}$ levels showed no major differences between WT and *Δtgt* strains, making it unlikely that the effect of Q modification on codon decoding is caused by altered synthesis or degradation of $tRNA^{Tyr}$ (**Sup. Fig. S2A**). The levels of the other three tRNAs modified by Tgt also remained unchanged (**Sup. Fig. S2A**). These results do not however exclude a more subtle or heterogeneous effect of Q modification on tRNA levels, which would be below the detection limits of the technique in a bacterial whole population.

We next adopted a tRNA overexpression strategy from a high copy plasmid. The following tRNAs-$_{GUN}$ are the canonical tRNAs which are present in the genome: Tyr_{GUA} (codon TAC), His_{GUG} (codon CAC), two isoforms of Asn_{GUU} (codon AAC), Asp_{GUC} (codon GAT). The following tRNAs-$_{AUN}$ are synthetic tRNAs which are not present in the genome: Tyr_{AUA}, His_{AUG}, Asn_{AUU}, Asp_{AUC}. $tRNA^{Phe}_{GAA}$ was also used as non Tgt-modified control. Overexpression of $tRNA^{Tyr}_{GUA}$, but not $tRNA^{Tyr}_{AUA}$ rescues the *Δtgt* mutant's growth defect in sub-MIC TOB (**Fig. 1I**). Overexpression of $tRNA^{His}_{AUG}$ also seemed to confer a benefit compared to empty plasmid (p0), but not as strong as $tRNA^{Tyr}_{GUA}$ (**Sup. Fig. S2B**). We do not observe any major rescue of TOB sensitive phenotypes when the other tRNAs are overexpressed, suggesting that changes in Tyr codon decoding is mostly responsible for the *Δtgt* mutant's TOB-susceptibility phenotype.

Q modification influences amino acid incorporation at tyrosine codons

We decided to measure the efficiency of amino acid incorporation at corresponding codons in *Δtgt*, using *gfp* reporters. First, we confirmed that GFP fluorescence from native GFP (encoded by *gfpmut3*)

633 is not affected in *Δtgt* compared to WT (*gfp+* in **Fig. 2**), indicating that there are no major differences
634 on expression or folding of the GFP in *Δtgt*. We next constructed *gfp* fluorescent reporters by
635 introducing within their coding sequence, stretches of repeated identical codons, for Asp/Asn/Tyr/His.
636 This set of reporters revealed that the absence of Q leads to an increase of amino acid incorporation
637 at Tyr TAT codons, both without and with sub-MIC TOB (**Fig. 2A** NT and TOB). This was not the case for
638 Asp (Fig. 2B), nor for Asn (Fig. 2D), and we observed a slighter and more variable change for His (Fig.
639 2C). No significant effect of *tgt* was observed for 2nd near-cognate codons obtained by changing 1 base
640 of the triplet for TAC and TAT codons (Fig. 2E): Phe TTC/TTT, Cys TGT/TGC, Ser TCT/TCC (the 3rd near-
641 cognate stop codons TAA and TAG were not tested in this setup). Thus, Q modification strongly impacts
642 the decoding of Tyr codons, and to a lesser extent His codons in this reporter system.
643
644 **The absence of Q decreases misincorporation at Tyr TAT**
645 GFP reporters tested above with codon stretches were pivotal for the identification of codons for
646 which decoding efficiency differs between WT and *Δtgt*, even though it's not a natural setup. We next
647 developed a biologically relevant β-lactamase reporter tool to assess differences in the decoding of
648 the tyrosine codons in WT and *Δtg*t strains. The amino acid Tyr103 of the β-lactamase, was previously
649 shown to be important for its function in resistance to β-lactam antibiotics, such as carbenicillin (69-
650 71). We replaced the native Tyr103 TAC with the synonymous codon Tyr103 TAT (**Fig. 3**). While in the
651 WT, both versions of β-lactamase conferred similar growth in carbenicillin with or without sub-MIC
652 TOB (Fig. 3AB), in the *Δtgt* strain the Tyr-TAT version grows better than the Tyr-TAC version upon
653 exposure to TOB stress (Fig. 3CD). This suggests a more efficient translation of the Tyr103-TAT β-
654 lactamase mRNA, compared to the native Tyr103-TAC version, in stressed *Δtgt* strain.
655 Presence or absence of a modification could also affect aminoacylation of the tRNA. Both TAT and
656 TAC codons are decoded by the same and only one tRNA, $tRNA^{TYR}_{GUA}$. In this case, a defect in
657 aminoacylation of this tRNA would impact the decoding of both codons. Our results do not support
658 such an aminoacylation problem, because the efficiency of decoding of TAT but not TAC increases in
659 *Δtgt*, and the difference is clearer in TOB. These results are also consistent with rescue of TOB-sensitive
660 phenotype by $tRNA^{Tyr}_{GUA}$ but not $tRNA^{Tyr}_{AUA}$ overexpression in *Δtgt*.
661 Altogether, results suggest that in the presence of sub-MIC TOB stress, the absence of Q
662 namely leads to better translation of the TAT vs TAC codon, leading to differential translation of
663 proteins with codon usage biases towards TAC or TAT codons.

664 **Proteomics study identifies RsxA among factors for which translation is most impacted in *Δtgt***
665 These observations show a link between Q modification of tRNA, differential decoding of Tyr
666 codons (among others) and susceptibility to aminoglycosides. We hypothesized that proteins that are
667 differentially translated according to their Tyr codon usage could be involved in the decreased
668 efficiency of the response to aminoglycoside stress in *Δtgt.* We conducted a proteomics study
669 comparing WT vs *Δtgt,* in the absence and presence of sub-MIC TOB (proteomics T**able S1 and Fig. 4**).
670 Loss of Q results in generally decreased detection of many proteins in TOB (shift towards the left in the
671 volcano plot **Fig. 4AB**), and in increases in the levels of 96 proteins. Among those, RsxA (encoded by
672 VC1017) is 13-fold more abundant in the *Δtgt* strain compared to WT in TOB. RsxA is part of an anti-
673 SoxR complex. SoxR is an oxidative stress response regulator(29) that controls *sodA* (VC2694,
674 superoxide dismutase) and *acrA* (VC0913, efflux), among other genes of the regulon. The Rsx complex
675 reduces and inactivates SoxR, preventing the induction of the regulon. Consistently, we find that the
676 levels of SodA and AcrA proteins are decreased in *Δtgt* compared to WT in TOB (indicated in **Fig. 4B**).
677 With 83% of Tyr-TAT codons, instead of the expected 53% average, RsxA has a clear codon usage bias.
678 To test whether some of the differentially abundant protein groups in the Q deficient mutant show
679 similar biases, the Tyr codon usage was calculated for the 96 more abundant and 195 less abundant
680 proteins expressed in TOB. More abundant proteins in *Δtgt* TOB with a codon usage bias towards TAT
681 vs TAC are represented as light blue dots in **Fig. 4AB**. No statistically significant difference was detected
682 for TAT codon usage in neither sets of proteins. Thus, one cannot draw conclusions or infer predictions

683 about codon decoding efficiencies in a tRNA modification mutant such as *Δtgt* from the proteomics
684 data alone.
685 We thus performed Ribo-seq (ribosome profiling) analysis on extracts from WT and *Δtgt* strains
686 grown in presence of sub-MIC TOB. Unlike for eukaryotes, technical limitations (e.g. the RNase which
687 is used displays significant sequence specificity), do not allow to obtain codon resolution in bacteria
688 (72). However, we determined 159 transcripts with increased and 197 with decreased translation in
689 *Δtgt* and we plotted their standardized codon usage bias for codons of interest (Fig. 4DEFG). The
690 calculation of this value is explained in details in the materials and methods section, and shown for
691 *rsxA* as example in **Fig 4C**. Briefly, we took as reference the mean proportion of the codons of interest
692 in the genome (e.g. for tyrosine: TAT= 0.53 and TAC= 0.47, meaning that for a random *V. cholerae*
693 gene, 53% of tyrosine codons are TAT). For each gene, we calculated the proportion of each codon
694 (e.g. for *rsxA*: TAT=0.83 and TAC=0.17). We next calculated the codon usage bias as the difference
695 between a given gene's codon usage and the mean codon usage (e.g. for *rsxA*, the codon usage bias
696 for TAT is 0.83-0.53=+0.30). Finally, in order to consider the codon distribution on the genome and
697 obtain statistically significant values, we calculated standardized bias by dividing the codon usage bias
698 by standard deviation for each codon (e.g. for *rsxA*, 0.30/0.25 = +1.20). This is done to adjust standard
699 deviation to 1, and thus to get comparable (standardized) values, for each codon.
700 Ribo-seq data **(Table S2**) shows that TAT (and GAT) codon usage was decreased in the list of
701 transcripts with decreased translation in *Δtgt*, while it was increased in the list of transcripts with
702 increased translation (**Fig. 4DE**). No difference was detected for AAT and CAT (**Fig. 4FG**). Data is thus
703 consistent with more efficient translation of TAT codons in *Δtgt.*
704 In addition to mistranslation and codon decoding efficiency, other factors also influence
705 detected protein levels, such as transcription, degradation, etc. Moreover, the localization and
706 sequence context of the codons for which the efficiency of translation is impacted, may be important.
707 Nevertheless, as translation of proteins with a codon usage bias towards TAC or TAT may be impacted
708 in *Δtgt*, and as the most abundant protein RsxA in *Δtgt* in TOB shows a strong TAT bias, we decided to
709 evaluate whether RsxA is post-transcriptionally regulated by the Q modification and whether it may
710 affect fitness in the presence of TOB.
711
712 **RsxA is post-transcriptionally upregulated in *Δtgt* due to more efficient decoding of tyrosine TAT**
713 **codons in the absence of Q modification**
714 Transcriptomic analysis comparing at least 2-fold differentially expressed genes between *V.*
715 *cholerae Δtgt* and WT strains (**Table S3**) showed that, respectively, 53 and 26 genes were significantly
716 downregulated in MH and sub-MIC TOB, and 34 were up in sub-MIC TOB. Gene ontology (GO)
717 enrichment analysis showed that the most impacted GO categories were bacteriocin transport and
718 iron import into the cell (45- and 40-fold enriched) in MH, and proteolysis and response to heat (38-
719 and 15-fold enriched) in TOB. In both conditions, the levels of *rsxA* transcript remained unchanged.
720 RsxA carries 6 tyrosine codons among which the first 5 are TAT and the last one is TAC. RsxA is
721 13-fold more abundant in *Δtgt* than WT, but transcript levels measured by digital RT-PCR are
722 comparable in both strains **(Fig. 5A**), consistent with RNA-seq data. We constructed transcriptional and
723 translational *gfp* fusions in order to evaluate the expression of *rsxA* in WT and *Δtgt* strains. As expected
724 from digital RT-PCR results, no significant differences in fluorescence were observed for the
725 transcriptional fusion of the *rsxA* promoter with *gfp* (**Fig. 5B**), excluding transcriptional regulation of
726 *rsxA* in this context. For translational fusions, we used either the native *rsxA* sequence bearing 5 TAT +
727 1 TAC codons, or a mutant *rsxA* allele carrying all 6 TAC codons (hereafter called respectively $RsxA^{TAT}$
728 and $RsxA^{TAC}$). Confirming the proteomics results, the $RsxA^{TAT}$-GFP fusion was more fluorescent in the
729 *Δtgt* mutant, but not the $RsxA^{TAC}$-GFP one (**Fig. 5C** and detailed flow cytometry data in **Sup. Fig. S3ABC**).
730 Since increased *rsxA* expression appeared to be somewhat toxic for growth, and in order to test
731 translation on a reporter which confers no growth defect, we chose to test directly the translation of
732 *gfp*, which originally carries 4 TAT (36%) and 7 TAC (64%) codons in its native sequence. We constructed
733 two synonymous versions of the GFP protein, with all 11 tyrosine codons either changed to TAT or to
734 TAC. Similar to what we observed with *rsxA*, the GFP^{TAT} version, but not the GFP^{TAC} one, generated

more fluorescence in the *Δtgt* background, (**Fig. 5C** and detailed flow cytometry data in **Sup. Fig. S3DEF**).

Since not all TAT biased proteins are found to be enriched in *Δtgt* proteomics data, the sequence context surrounding TAT codons could affect their decoding. Overall, our results demonstrate that RsxA is upregulated in the *Δtgt* strain at the translational level, and that proteins with a codon usage bias towards tyrosine TAT are prone to be more efficiently translated in the absence of Q modification, but this is also dependent on the sequence context.

Increased expression of RsxA hampers growth in sub-MIC TOB

We asked whether high levels of RsxA could be responsible of *Δtgt* strain's increased sensitivity to TOB. *rsxA* cannot be deleted since it is essential in *V. cholerae* (see our TN-seq data (1,73)). We overexpressed *rsxA* from an inducible plasmid in WT strain (**Fig. 5D** and **Sup. Fig. S4ABCD**). In the presence of sub-MIC TOB, overexpression of *rsxA* in the WT strain strongly reduces growth (**Sup. Fig. S4B, black curve compared to blue**), while overexpression of *tgt* restores growth of the *Δtgt* strain (**Sup. Fig. S4D, green curve**)**.** This shows that increased *rsxA* levels can be toxic during growth in sub-MIC TOB and is consistent with decreased growth of the *Δtgt* strain.

Unlike for *V. cholerae*, *rsxA* is not an essential gene in *E. coli*, and does not bear a TAT bias. It has however the same function. In order to confirm that the presence of RsxA can be toxic during growth in sub-MIC TOB, we additionally performed competition experiments in *E. coli* with simple and double mutants of *tgt* and *rsxA*. Since *Δtgt* strain's growth is more affected than WT at TOB 0.5 µg/ml (indicated with an arrow in **Sup. Fig. S4E)**, we chose this concentration for competition and growth experiments. The results confirm that inactivation of *rsxA* in *Δtgt* restores fitness in sub-MIC TOB (**Sup. Fig. S4F**), and that overproduction of RsxA decreases growth in TOB.

tgt* transcription is repressed by CRP and induced by tobramycin in *V. cholerae

tgt was previously observed to be upregulated in *E. coli* isolates from urinary tract infection(74) and in *V. cholerae* after mitomycin C treatment (through indirect SOS induction(47)). We measured *tgt* transcript levels using digital RT-PCR in various transcriptional regulator deficient mutants (iron uptake repressor Fur, general stress response and stationary phase sigma factor RpoS and carbon catabolite control regulator CRP), as well as upon exposure to antibiotics, particularly because *tgt* is required for growth in sub-MIC TOB. We also tested the iron chelator dipyridyl (DP), the oxidant agent paraquat (PQ) and serine hydroxamate (SHX) which induces the stringent response.

Among all tested conditions, we found that sub-MIC TOB and the stringent response increase *tgt* transcript levels, while the carbon catabolite regulator CRP appears to repress it (**Fig. 6A**). We found a sequence between ATG -129 to -114: TTC**G**C^{AGGGAA}A**C**GCG which shows some similarity (in blue) to the *V. cholerae* CRP binding consensus $(^{T}/_{A})_{1}(^{G}/_{T})_{2}(^{T}/_{C})_{3}\mathbf{G}_{4}(^{A}/_{C})_{5}{}^{NNNNNN}(^{T}/_{G})_{12}\mathbf{C}_{13}(^{A}/_{G})_{14}(^{C}/_{A})_{15}(^{T}/_{A})_{16}$. However, CRP binding was not previously detected by ChIP-seq in the promoter region of *tgt* in *V. cholerae*(75). CRP binding could be transitory or the repression of *tgt* expression by CRP could be an indirect effect.

Regarding induction by sub-MIC TOB, the mechanism remains to be determined. We previously showed that sub-MIC TOB induces the stringent response(1,76). Since induction of *tgt* expression by SHX and by TOB seems to be in the same order of magnitude, we hypothesized that sub-MIC TOB could induce *tgt* through the activation of the stringent response. Using a *P1rrnB-gfp* fusion (1), which is down-regulated upon stringent response induction(77) (**Fig. 6B**), we found that the stringent response is significantly induced by sub-MIC TOB, both in WT and *Δtgt*. This indicates that sub-MIC TOB possibly induces *tgt* expression through the stringent response activation.

Q modification levels can be dynamic and are directly influenced by *tgt* transcription levels

We have identified conditions regulating *tgt* expression. We next addressed whether up/down-regulation of *tgt* affects the actual Q modification levels of tRNA. We measured Q levels by mass spectrometry in WT and the *Δcrp* strain, where the strongest impact on *tgt* expression was observed

786 (**Fig. 6C**). We find a significant 1.6-fold increase in Q levels in *Δcrp*. We also tested the effect of sub-
787 MIC TOB, but smaller differences are probably not detected using our approach of mass spectrometry
788 in bulk cultures.
789 In order to get deeper insight into modification level of *V. cholerae* tRNAs potentially having Q34
790 modification, we decided to adapt a recently published protocol for the detection and quantification
791 of queuosine by deep sequencing (50). This allowed us to validate the presence of Q34 modification in
792 the *V. cholerae* tRNAs Asp, His and Asn_GTT2 and precisely measure its level and modulation under
793 different growth conditions (**Fig. 6D**). We also showed that Q34 detection is robust and reproducible,
794 and reveals increased Q34 content for $tRNA^{His}$ and $tRNA^{Asn}$ in *Δcrp* strain where *tgt* expression was
795 induced, while for $tRNA^{Asp}$ Q34 level remains relatively constant. *V. cholerae* $tRNA^{Asn}$_GTT1 is very low
796 expressed and likely contains only sub-stoichiometric amounts of Q34, while analysis of $tRNA^{Tyr}$ is
797 impeded by the presence of other modifications in the anticodon loop (namely i^6A37 or its derivatives),
798 which prevents the correct mapping and quantification of Q34 modifications using deletion signature.
799 In order to evaluate Q34 levels in $tRNA^{Tyr}$ more specifically, we performed APB northern blots allowing
800 visualization and quantification of Q-modified and unmodified tRNAs (51). As anticipated from
801 increased *tgt* expression, Q-modified tRNA levels were strongly increased in *Δcrp* strain. Sub-MIC TOB
802 also increases the proportion of Q containing $tRNA^{Tyr}$ compared to the non-treated condition (**Fig. 6E**).
803 However, this result was variable suggesting a subtle fine-tuning of the Q levels depending on growth
804 state (optical density) and TOB concentration. These results show that tRNA Q modification levels are
805 dynamic and correlate with variations in *tgt* expression, depending on the tRNA.
806
807
808
809 **DNA repair genes are TAT-biased**
810 We further analyzed *in silico* the codon usage of *V. cholerae* genome, and for each gene, we
811 assigned a codon usage value to each codon (**Fig. 4C and doi:10.5281/zenodo.6875293**). This allowed
812 the generation of lists of genes with divergent codon usage, for each codon.
813 For genes with a tyrosine codon usage bias towards TAT in *V. cholerae,* gene ontology
814 enrichment analysis (**Sup. Fig. S5CDE)** highlights the DNA repair category with a *p-value* of 2.28×10^{-2}
815 **(Sup. Fig. S5C.)**. Fig. 7A shows Tyr codon usage of *V. cholerae* DNA repair genes. We hypothesized that
816 translation of DNA repair transcripts could be more efficient in *Δtgt*, and that such basal pre-induction
817 would be beneficial during genotoxic treatments as UV irradiation (single stranded DNA breaks). UV
818 associated DNA damage is repaired through RecA, RecFOR and RuvAB dependent homologous
819 recombination. Five of these genes, *recO, recR, recA* and *ruvA-ruvB*, are biased towards TAT in *V.*
820 *cholerae* (Fig. 7A, red arrows), while their repressor LexA bears a strong bias towards TAC. DNA repair
821 genes (e.g. *ruvA* with 80% TAT, *ruvB* with 83% TAT, *dinB* with 75% TAT) were also found to be up for
822 Δ*tgt* in the Ribo-seq data, with unchanged transcription levels. *V. cholerae Δtgt* appears to be 4 to 9
823 times more resistant to UV irradiation than the WT strain (**Fig. 7B**). This is consistent with increased
824 DNA repair efficiency in the *V. cholerae Δtgt* strain.
825 We also analyzed tyrosine codon usage for the DNA repair genes in *E. coli*, and did not observe
826 the same bias (**Fig. 7C**), with 51% TAT bias, i.e. the expected level for a random group of genes of the
827 *E coli* genome, and with a TAC bias for *recOR* and *recA* (red arrows) and strong TAT bias for *lexA* (blue
828 arrow) (**Sup. Fig.S 5B**, whole genome *E. coli*). These genes thus show the exact opposite bias in *E. coli*
829 (**Fig. 7C**). Strikingly, unlike for *V. cholerae*, *E. coli Δtgt* mutant did not show increased UV resistance
830 (**Fig. 7D**). This is consistent with the hypothesis that modification-tuned translation of codon biased
831 transcripts can be an additional means of regulation building upon already described and well
832 characterized transcriptional regulation pathways.
833
834 **Discussion**
835 We show here that Q modification levels can be dynamic in bacteria and respond to external
836 conditions; and that Q levels on *V. cholerae* $tRNA^{Tyr}$ correlate with *tgt* expression. This is clearer in
837 conditions where *tgt* transcription is highly induced (*Δcrp*), and more variable in conditions where this

838 induction is intermediate (sub-MIC TOB). As summarized in **Fig. 8**, we propose that exposure to sub-
839 MIC aminoglycosides increases *tgt* expression in *V. cholerae*, and impacts the decoding of tyrosine
840 codons. The TAT biased transcripts RsxA is an anti-SoxR factor. SoxR controls a regulon involved in
841 oxidative stress response and sub-MIC aminoglycosides trigger oxidative stress in *V. cholerae*(78). A
842 link between Q and oxidative stress has also been previously found in eukaryotic organisms (24). Better
843 decoding at TAT versus TAC codons in the absence of Q observed here in *V. cholerae* is also consistent
844 with recent findings in human tRNAs, where the presence of Q increases translation of transcripts
845 biased in C-ending codons (79). Our findings are in accordance with the concept of the so-called
846 modification tunable transcripts (MoTTs)(20). We thus show that a proteins' codon content can
847 influence its translation in a Q modification dependent way, and that this can also impact the
848 translation of antibiotic resistance genes (here β-lactamase). Note that, our results do not exclude the
849 involvement of additional Q-regulated MoTTs in the response to sub-MIC TOB, since Q modification
850 leads to reprogramming of the whole proteome. Finally, we show that we can predict *in silico*,
851 candidates for which translation can be modulated by the presence or absence of Q modification (e.g.
852 DNA repair genes), which was confirmed using phenotypic tests (UV resistance).
853 Essential/housekeeping genes are generally TAC biased (**Sup. Fig. S5AB**), as well as ribosomal
854 proteins, which carry mostly tyrosine TAC codons both in *V. cholerae* and *E. coli*. It has been proposed
855 that codon bias corresponding to abundant tRNAs at such highly expressed genes, guarantees their
856 proper expression and avoids titration of tRNAs, allowing for efficient expression of the rest of the
857 proteome(80). Induction of *tgt* by stress could also possibly be a signal for the cell to favor the synthesis
858 of essential factors. Our results are also consistent with the fact that synonymous mutations can
859 influence the expression of genes(81).
860 *V. cholerae* is the model organism for different species of *Vibrio*. We have previously shown that *V.*
861 *cholerae's* response to sub-MIC antibiotic stress is transposable to other Gram-negative pathogens
862 *(78,82),* while there are differences between *E. coli* and *V. cholerae*, in the response to sub-MIC
863 antibiotics and oxidative stress phenotypes (78,82,83). Here, we have also addressed some of the
864 effects of TOB in *E. coli Δtgt* mutant. In *E. coli,* the deletion of *tgt* has a less dramatic effect on the
865 susceptibility to TOB ((1) and **Sup. Fig S4F**). *V. cholerae* and *E. coli* globally show similar tyrosine codon
866 usage in their genomes (**Sup. Fig. S5AB**). However, *E. coli rsxA* does not display a codon bias towards
867 TAT, and neither do DNA repair genes. One can think that in regard to MoTTs, different organisms have
868 evolved according to the environments where they grow, selecting the integration of specific stress
869 response pathways under specific post-transcriptional regulations.
870 It was recently shown that *E. coli Δtgt* strain is more resistant than the WT to nickel toxicity, most
871 certainly because the nickel importer genes *nikABCDE* are less expressed, but the underlying molecular
872 mechanism had not been elucidated(28). As NikR, the repressor of the *nik* operon is enriched in TAT
873 codons (100%), a more efficient translation of the *nikR* gene in the absence of Q would lead to the
874 observed repression phenotype. In addition, the nickel exporter gene *rcnA* is also enriched is TAT
875 (100%), while one of the genes for subunits of the nickel importer *nikD* is enriched in TAC codons
876 (100%). In combination this could explain the clear resistance of the *tgt* strain to high levels of nickel.
877 However, protein levels are not always in line with the codon bias predictions. The positions of the
878 codons of interest and their sequence context may also be important for differential translation. The
879 presence of the codon of interest in the 5'-end vs 3'-end of a transcript could have a bigger impact on
880 the efficiency of translation (84,85). A recent study testing TAC/TAT codons placed between two genes
881 in a translational fusion yielded different results compared to our constructs with the tested codons at
882 the 5' of the transcript(86). Similarly, the distance between two codons of interest, or the identity of
883 the nearby codons may be important. The translation of highly transcribed genes and genes with low
884 levels of mRNAs could be dissimilar. Codon usage may also directly impact gene expression at mRNA
885 levels with an effect on transcription termination(87), especially for constitutive genes. Thus, the
886 search for MoTTs could be facilitated by comparing transcriptomics to proteomics data, and additional
887 experiments need to be performed to elucidate post-transcriptional regulation-related phenotypes,
888 but the differential expression of specific TAT/TAC biased proteins finally allows to propose a model
889 for the pleiotropic phenotype caused by Q deficiency in *E. coli.*

890 Studies, mostly in eukaryotes, reveal that tRNA modifications are dynamic and not static as
891 initially thought (88-90). Modification levels depend on growth (91,92), environmental changes (93)
892 and stress (reviewed in (62)). Stress regulated tRNA modification levels have an impact on the
893 translation of regulators, which in turn trigger translational reprogramming and optimized responses
894 to stress (2,94,95). We show here that *tgt* expression is regulated by sub-MIC TOB, the stringent
895 response and CRP, and that $tRNA^{Tyr}$ Q modification levels increase with *tgt* expression. The fact that
896 such correlation between *tgt* expression and Q levels does not occur for all tRNAs (e.g. $tRNA^{Asp}$),
897 indicates that other parameters also influence Q modification levels. One possibility is that other
898 modifications, such as those on the anticodon loop of $tRNA^{Tyr}$, may influence the way Tgt modifies
899 these tRNAs, as documented for other modification circuits (22,96). Tgt may also bind these tRNAs
900 differently (for a review on modification specificity (62)). Since sub-MIC TOB triggers the stringent
901 response, one hypothesis could be that sub-MIC TOB induces *tgt* through stringent response
902 activation. The stringent response is usually triggered upon starvation, for example when amino acids
903 are scarce. *tgt* expression was also recently shown to be regulated by tyrosine levels and to affect
904 tRNA-Tyr codon choice in *Trypanosoma brucei*(97).
905 Regarding CRP, the carbon catabolite regulator, it represses transcription of *tgt*. Interestingly, *V.*
906 *cholerae crp* carries only TAC codons for tyrosine, and is strongly down-regulated in *Δtgt* in our Ribo-
907 seq data, while its transcription levels remain unchanged. The downregulation of CRP translation when
908 Q modifications are low (as in the *Δtgt* strain), could be a way to de-repress *tgt* and increase Q
909 modification levels. Note that CRP is involved in natural competence of *V. cholerae*, during growth on
910 crustacean shells where horizontal gene transfer occurs. One can thus speculate that during exogenous
911 DNA uptake, *tgt* repression by CRP could lead to better decoding of AT rich (i.e. TAT biased) mRNAs.
912 Thus, modulation of *tgt* levels during natural transformation may modulate the expression of
913 horizontally transferred genes, which by definition may bear different GC content and codon usage.
914 Moreover, if *tgt* expression is repressed by CRP during competence state, this would favor the
915 translation of TAT-biased DNA repair genes and possibly recombination of incoming DNA into the
916 chromosome. Translational reprogramming in response to DNA damage can thus be an advantageous
917 property selected during evolution.
918 Our results also demonstrate that we can identify other Q-dependent MoTT candidates using *in*
919 *silico* codon usage analysis. In fact, since we now have extensively calculated the codon usage biases
920 at all codons for *V. cholerae* and *E. coli* genes, this approach is readily adaptable to any tRNA
921 modification for which we know the differentially translated codons. Such regulation may be a possible
922 way to tune the expression of essential or newly acquired genes, differing in GC-content. It may also,
923 in some cases, explain antibiotic resistance profiles in bacterial collections with established genome
924 sequences, and for which observed phenotypic resistance does not always correlate with known
925 resistance factors(98). Further studies are needed to characterize the determinants of tRNA
926 modification-dependent translational reprogramming.
927

928 **Acknowledgements**

929 We thank Dr. Francesca Tuorto for sharing the protocol for boronated northern blots. Many thanks to
930 Dr. Paola Arimondo for discussions about setting up the queuosine mass spectrometry experiments.
931 We also thank, for RNA-seq experiments, E. Turc, L. Lemée, T. Cokelaer, Biomics Platform, C2RT,
932 Institut Pasteur, Paris, France, supported by France Génomique (ANR-10-INBS-09) and IBISA. We would
933 like to acknowledge Valérie Bourguignon (IMoPA, UMR7365 CNRS-UL) for her help in validation of
934 queuosine modification protocol.
935 This research was funded by the Institut Pasteur, the Centre National de la Recherche Scientifique
936 (CNRS-UMR 3525), ANR ModRNAntibio (ANR-21-CE35-0012), ANR-LabEx [ANR-10-LABX-62-IBEID], the
937 Fondation pour la Recherche Médicale (FRM EQU202103012569), the Institut Pasteur grant PTR 245-
938 19 and by the National Institute of General Medical Sciences (NIGMS) grant GM70641 to V dC-L. AB

was funded by Institut Pasteur Roux-Cantarini fellowship. The authors acknowledge a DIM1Health 2019 grant from the Région Ile de France to the project EpiK for the LCMS equipment.

Author contributions

Conceived and designed the analysis: ZB, DM; Collected the data: ZB, LF, AB, AC, ML, MD, BL, QG-G, FB, CF, GS, IH; Contributed data or analysis tools: BL, ON, CF, MM, MD, QG-G, FB, HA, VdC-L, VM, YM; Performed the analysis: ZB, LF, AB, AC, ML, BL; Wrote the paper: ZB, VdC-L.

945 **References**

946

947 1. Babosan, A., Fruchard, L., Krin, E., Carvalho, A., Mazel, D. and Baharoglu, Z. (2022) Non-essential
948 tRNA and rRNA modifications impact the bacterial response to sub-MIC antibiotic stress. *microLife*.

949 2. Pollo-Oliveira, L. and de Crecy-Lagard, V. (2019) Can Protein Expression Be Regulated by
950 Modulation of tRNA Modification Profiles? *Biochemistry*, **58**, 355-362.

951 3. Suzuki, T. (2021) The expanding world of tRNA modifications and their disease relevance. *Nat Rev*
952 *Mol Cell Biol*.

953 4. Chujo, T. and Tomizawa, K. (2021) Human transfer RNA modopathies: diseases caused by
954 aberrations in transfer RNA modifications. *FEBS J*, **288**, 7096-7122.

955 5. Zhong, W., Koay, A., Ngo, A., Li, Y., Nah, Q., Wong, Y.H., Chionh, Y.H., Ng, H.Q., Koh-Stenta,
956 X., Poulsen, A. *et al.* (2019) Targeting the Bacterial Epitranscriptome for Antibiotic Development:
957 Discovery of Novel tRNA-(N(1)G37) Methyltransferase (TrmD) Inhibitors. *ACS Infect Dis*, **5**, 326-
958 335.

959 6. de Crecy-Lagard, V. and Jaroch, M. (2021) Functions of Bacterial tRNA Modifications: From
960 Ubiquity to Diversity. *Trends Microbiol*, **29**, 41-53.

961 7. Urbonavicius, J., Qian, Q., Durand, J.M., Hagervall, T.G. and Bjork, G.R. (2001) Improvement of
962 reading frame maintenance is a common function for several tRNA modifications. *EMBO J*, **20**,
963 4863-4873.

964 8. Taylor, D.E., Trieber, C.A., Trescher, G. and Bekkering, M. (1998) Host mutations (miaA and rpsL)
965 reduce tetracycline resistance mediated by Tet(O) and Tet(M). *Antimicrob Agents Chemother*, **42**, 59-
966 64.

967 9. Parker, J. (1982) Specific mistranslation in hisT mutants of Escherichia coli. *Mol Gen Genet*, **187**,
968 405-409.

969 10. Bruni, C.B., Colantuoni, V., Sbordone, L., Cortese, R. and Blasi, F. (1977) Biochemical and
970 regulatory properties of Escherichia coli K-12 hisT mutants. *J Bacteriol*, **130**, 4-10.

971 11. Thongdee, N., Jaroensuk, J., Atichartpongkul, S., Chittrakanwong, J., Chooyoung, K., Srimahaeak,
972 T., Chaiyen, P., Vattanaviboon, P., Mongkolsuk, S. and Fuangthong, M. (2019) TrmB, a tRNA
973 m7G46 methyltransferase, plays a role in hydrogen peroxide resistance and positively modulates
974 the translation of katA and katB mRNAs in Pseudomonas aeruginosa. *Nucleic Acids Res*, **47**, 9271-
975 9281.

976 12. Aubee, J.I., Olu, M. and Thompson, K.M. (2016) The i6A37 tRNA modification is essential for
977 proper decoding of UUX-Leucine codons during rpoS and iraP translation. *RNA*, **22**, 729-742.

978 13. Vecerek, B., Moll, I. and Blasi, U. (2007) Control of Fur synthesis by the non-coding RNA RyhB
979 and iron-responsive decoding. *EMBO J*, **26**, 965-975.

980 14. Hou, Y.M., Matsubara, R., Takase, R., Masuda, I. and Sulkowska, J.I. (2017) TrmD: A Methyl
981 Transferase for tRNA Methylation With m(1)G37. *Enzymes*, **41**, 89-115.

982 15. Chionh, Y.H., McBee, M., Babu, I.R., Hia, F., Lin, W., Zhao, W., Cao, J., Dziergowska, A.,
983 Malkiewicz, A., Begley, T.J. *et al.* (2016) tRNA-mediated codon-biased translation in mycobacterial
984 hypoxic persistence. *Nature communications*, **7**, 13302.

985 16. Fleming, B.A., Blango, M.G., Rousek, A.A., Kincannon, W.M., Tran, A., Lewis, A.J., Russell, C.W.,
986 Zhou, Q., Baird, L.M., Barber, A.E. *et al.* (2022) A tRNA modifying enzyme as a tunable regulatory
987 nexus for bacterial stress responses and virulence. *Nucleic Acids Res*.

988 17. Thompson, K.M. and Gottesman, S. (2014) The MiaA tRNA modification enzyme is necessary for
989 robust RpoS expression in Escherichia coli. *J Bacteriol*, **196**, 754-761.

990 18. Kimura, S., Dedon, P.C. and Waldor, M.K. (2020) Comparative tRNA sequencing and RNA mass
991 spectrometry for surveying tRNA modifications. *Nat Chem Biol*, **16**, 964-972.

992 19. Masuda, I., Matsubara, R., Christian, T., Rojas, E.R., Yadavalli, S.S., Zhang, L., Goulian, M., Foster,
993 L.J., Huang, K.C. and Hou, Y.M. (2019) tRNA Methylation Is a Global Determinant of Bacterial
994 Multi-drug Resistance. *Cell Syst*, **8**, 302-314 e308.

995 20. Endres, L., Dedon, P.C. and Begley, T.J. (2015) Codon-biased translation can be regulated by
996 wobble-base tRNA modification systems during cellular stress responses. *RNA Biol*, **12**, 603-614.

997 21. Advani, V.M. and Ivanov, P. (2019) Translational Control under Stress: Reshaping the Translatome.
998 *Bioessays*, **41**, e1900009.

999 22. Ehrenhofer-Murray, A.E. (2017) Cross-Talk between Dnmt2-Dependent tRNA Methylation and
1000 Queuosine Modification. *Biomolecules*, **7**.

1001 23. Meier, F., Suter, B., Grosjean, H., Keith, G. and Kubli, E. (1985) Queuosine modification of the
1002 wobble base in tRNAHis influences 'in vivo' decoding properties. *EMBO J*, **4**, 823-827.

1003 24. Nagaraja, S., Cai, M.W., Sun, J., Varet, H., Sarid, L., Trebicz-Geffen, M., Shaulov, Y., Mazumdar,
1004 M., Legendre, R., Coppee, J.Y. *et al.* (2021) Queuine Is a Nutritional Regulator of Entamoeba
1005 histolytica Response to Oxidative Stress and a Virulence Attenuator. *mBio*, **12**.

1006 25. Manickam, N., Joshi, K., Bhatt, M.J. and Farabaugh, P.J. (2016) Effects of tRNA modification on
1007 translational accuracy depend on intrinsic codon-anticodon strength. *Nucleic Acids Res*, **44**, 1871-
1008 1881.

1009 26. Manickam, N., Nag, N., Abbasi, A., Patel, K. and Farabaugh, P.J. (2014) Studies of translational
1010 misreading in vivo show that the ribosome very efficiently discriminates against most potential
1011 errors. *RNA*, **20**, 9-15.

1012 27. Noguchi, S., Nishimura, Y., Hirota, Y. and Nishimura, S. (1982) Isolation and characterization of
1013 an Escherichia coli mutant lacking tRNA-guanine transglycosylase. Function and biosynthesis of
1014 queuosine in tRNA. *J Biol Chem*, **257**, 6544-6550.

1015 28. Pollo-Oliveira, L., Davis, N., Hossain, I., Ho, P., Yuan, Y., Garcia, P.S., Pereira, C., Byrne, S.R.,
1016 Leng, J., Sze, M. *et al.* (2022) The absence of the Queuosine tRNA modification leads to pleiotropic
1017 phenotypes revealing perturbations of metal and oxidative stress homeostasis in Escherichia coli
1018 K12. *Metallomics*.

1019 29. Koo, M.S., Lee, J.H., Rah, S.Y., Yeo, W.S., Lee, J.W., Lee, K.L., Koh, Y.S., Kang, S.O. and Roe,
1020 J.H. (2003) A reducing system of the superoxide sensor SoxR in Escherichia coli. *EMBO J*, **22**,
1021 2614-2622.

1022 30. Silva-Rocha, R., Martinez-Garcia, E., Calles, B., Chavarria, M., Arce-Rodriguez, A., de Las Heras,
1023 A., Paez-Espino, A.D., Durante-Rodriguez, G., Kim, J., Nikel, P.I. *et al.* (2013) The Standard
1024 European Vector Architecture (SEVA): a coherent platform for the analysis and deployment of
1025 complex prokaryotic phenotypes. *Nucleic Acids Res*, **41**, D666-675.

1026 31. Kessler, B., Timmis, K.N. and de Lorenzo, V. (1994) The organization of the Pm promoter of the
1027 TOL plasmid reflects the structure of its cognate activator protein XylS. *Mol Gen Genet*, **244**, 596-
1028 605.

1029 32. Lang, M.N., Krin, E., Korlowski, C., Sismeiro, O., Varet, H., Coppee, J.Y., Mazel, D. and
1030 Baharoglu, Z. (2021) Sleeping ribosomes: Bacterial signaling triggers RaiA mediated persistence to
1031 aminoglycosides. *Iscience*, **24**.

1032 33. Sabeti Azad, M., Okuda, M., Cyrenne, M., Bourge, M., Heck, M.P., Yoshizawa, S. and Fourmy, D.
1033 (2020) Fluorescent aminoglycoside antibiotics and methods for accurately monitoring uptake by
1034 bacteria. *ACS Infect Dis*.

1035 34. Okuda, M. (2015), Université Paris Sud - Paris XI.

1036 35. Baharoglu, Z., Bikard, D. and Mazel, D. (2010) Conjugative DNA transfer induces the bacterial
1037 SOS response and promotes antibiotic resistance development through integron activation. *PLoS*
1038 *Genet*, **6**, e1001165.

1039 36. El Mortaji, L., Tejada-Arranz, A., Rifflet, A., Boneca, I.G., Pehau-Arnaudet, G., Radicella, J.P.,
1040 Marsin, S. and De Reuse, H. (2020) A peptide of a type I toxin-antitoxin system induces
1041 Helicobacter pylori morphological transformation from spiral shape to coccoids. *Proc Natl Acad Sci*
1042 *U S A*, **117**, 31398-31409.

1043 37. Lo Scrudato, M. and Blokesch, M. (2012) The regulatory network of natural competence and
1044 transformation of Vibrio cholerae. *PLoS Genet*, **8**, e1002778.

1045 38. Cormack, B.P., Valdivia, R.H. and Falkow, S. (1996) FACS-optimized mutants of the green
1046 fluorescent protein (GFP). *Gene*, **173**, 33-38.

1047 39. Elowitz, M.B. and Leibler, S. (2000) A synthetic oscillatory network of transcriptional regulators.
1048 *Nature*, **403**, 335-338.

1049 40. Erde, J., Loo, R.R. and Loo, J.A. (2014) Enhanced FASP (eFASP) to increase proteome coverage
1050 and sample recovery for quantitative proteomic experiments. *J Proteome Res*, **13**, 1885-1895.

1051 41. Cox, J., Neuhauser, N., Michalski, A., Scheltema, R.A., Olsen, J.V. and Mann, M. (2011)
1052 Andromeda: a peptide search engine integrated into the MaxQuant environment. *J Proteome Res*, **10**,
1053 1794-1805.

1054 42. Tyanova, S., Temu, T. and Cox, J. (2016) The MaxQuant computational platform for mass
1055 spectrometry-based shotgun proteomics. *Nat Protoc*, **11**, 2301-2319.

1056 43. Wieczorek, S., Combes, F., Lazar, C., Giai Gianetto, Q., Gatto, L., Dorffer, A., Hesse, A.M., Coute,
1057 Y., Ferro, M., Bruley, C. *et al.* (2017) DAPAR & ProStaR: software to perform statistical analyses
1058 in quantitative discovery proteomics. *Bioinformatics*, **33**, 135-136.

1059 44. Ritchie, M.E., Phipson, B., Wu, D., Hu, Y., Law, C.W., Shi, W. and Smyth, G.K. (2015) limma
1060 powers differential expression analyses for RNA-sequencing and microarray studies. *Nucleic Acids*
1061 *Res*, **43**, e47.

1062 45. Giai Gianetto, Q., Combes, F., Ramus, C., Bruley, C., Coute, Y. and Burger, T. (2016) Calibration
1063 plot for proteomics: A graphical tool to visually check the assumptions underlying FDR control in
1064 quantitative experiments. *Proteomics*, **16**, 29-32.

1065 46. Pounds, S. and Cheng, C. (2006) Robust estimation of the false discovery rate. *Bioinformatics*, **22**,
1066 1979-1987.

1067 47. Krin, E., Pierle, S.A., Sismeiro, O., Jagla, B., Dillies, M.A., Varet, H., Irazoki, O., Campoy, S., Rouy,
1068 Z., Cruveiller, S. *et al.* (2018) Expansion of the SOS regulon of Vibrio cholerae through extensive
1069 transcriptome analysis and experimental validation. *BMC Genomics*, **19**, 373.

1070 48. Andersen, J.B., Sternberg, C., Poulsen, L.K., Bjorn, S.P., Givskov, M. and Molin, S. (1998) New
1071 unstable variants of green fluorescent protein for studies of transient gene expression in bacteria.
1072 *Appl Environ Microbiol*, **64**, 2240-2246.

1073 49. Galvanin, A., Ayadi, L., Helm, M., Motorin, Y. and Marchand, V. (2019) Mapping and
1074 Quantification of tRNA 2'-O-Methylation by RiboMethSeq. *Methods Mol Biol*, **1870**, 273-295.

1075 50. Katanski, C.D., Watkins, C.P., Zhang, W., Reyer, M., Miller, S. and Pan, T. (2022) Analysis of
1076 queuosine and 2-thio tRNA modifications by high throughput sequencing. *Nucleic Acids Res*, **50**,
1077 e99.

1078 51. Cirzi, C. and Tuorto, F. (2021) Analysis of Queuosine tRNA Modification Using APB Northern
1079 Blot Assay. *Methods Mol Biol*, **2298**, 217-230.

1080 52. Francois, P., Arbes, H., Demais, S., Baudin-Baillieu, A. and Namy, O. (2021) RiboDoc: A Docker-
1081 based package for ribosome profiling analysis. *Comput Struct Biotechnol J*, **19**, 2851-2860.

53. Dingwall, C., Lomonossoff, G.P. and Laskey, R.A. (1981) High sequence specificity of micrococcal nuclease. *Nucleic Acids Res*, **9**, 2659-2673.

54. Li, H. (2018) Minimap2: pairwise alignment for nucleotide sequences. *Bioinformatics*, **34**, 3094-3100.

55. McKinney, W. (2010) Data Structures for Statistical Computing in Python. *Stéfan van der Walt, Jarrod Millman, editors.* , **Proceedings of the 9th Python in Science Conference**, 56--61.

56. Reback J, M.W., jbrockmendel, den Bossche JV, Augspurger T, Cloud P, et al. (2021) pandas-dev/pandas: Pandas 1.2.4.

57. Virtanen, P., Gommers, R., Oliphant, T.E., Haberland, M., Reddy, T., Cournapeau, D., Burovski, E., Peterson, P., Weckesser, W., Bright, J. *et al.* (2020) SciPy 1.0: fundamental algorithms for scientific computing in Python. *Nat Methods*, **17**, 261-272.

58. JD., H. (2007) Matplotlib: A 2D Graphics Environment. . *Computing in Science & Engineering*, **9**, 90--95.

59. ML, W. (2021) Seaborn: Statistical Data Visualization. *Journal of Open Source Software*, **6**, :3021.

60. Kluyver T, R.-K.B., Pérez F, Granger B, Bussonnier M, Frederic J, et al. (2016) Jupyter Notebooks -- a publishing format for reproducible computational workflows., **Loizides Fernando, Scmidt Birgit, editors**, 87--90.

61. Molder, F., Jablonski, K.P., Letcher, B., Hall, M.B., Tomkins-Tinch, C.H., Sochat, V., Forster, J., Lee, S., Twardziok, S.O., Kanitz, A. *et al.* (2021) Sustainable data analysis with Snakemake. *F1000Res*, **10**, 33.

62. Barraud, P. and Tisne, C. (2019) To be or not to be modified: Miscellaneous aspects influencing nucleotide modifications in tRNAs. *IUBMB Life*, **71**, 1126-1140.

63. Tuorto, F., Legrand, C., Cirzi, C., Federico, G., Liebers, R., Muller, M., Ehrenhofer-Murray, A.E., Dittmar, G., Grone, H.J. and Lyko, F. (2018) Queuosine-modified tRNAs confer nutritional control of protein translation. *EMBO J*, **37**.

64. Jackman, J.E. and Alfonzo, J.D. (2013) Transfer RNA modifications: nature's combinatorial chemistry playground. *Wiley interdisciplinary reviews. RNA*, **4**, 35-48.

65. Addepalli, B. and Limbach, P.A. (2016) Pseudouridine in the Anticodon of Escherichia coli tRNATyr(QPsiA) Is Catalyzed by the Dual Specificity Enzyme RluF. *J Biol Chem*, **291**, 22327-22337.

66. Carvalho, A., Mazel, D. and Baharoglu, Z. (2021) Deficiency in cytosine DNA methylation leads to high chaperonin expression and tolerance to aminoglycosides in Vibrio cholerae. *Plos Genetics*, **17**.

67. Rivera, M., Hancock, R.E., Sawyer, J.G., Haug, A. and McGroarty, E.J. (1988) Enhanced binding of polycationic antibiotics to lipopolysaccharide from an aminoglycoside-supersusceptible, tolA mutant strain of Pseudomonas aeruginosa. *Antimicrob Agents Chemother*, **32**, 649-655.

68. Kimura, S. and Waldor, M.K. (2019) The RNA degradosome promotes tRNA quality control through clearance of hypomodified tRNA. *Proc Natl Acad Sci U S A*, **116**, 1394-1403.

69. Doucet, N., De Wals, P.Y. and Pelletier, J.N. (2004) Site-saturation mutagenesis of Tyr-105 reveals its importance in substrate stabilization and discrimination in TEM-1 beta-lactamase. *J Biol Chem*, **279**, 46295-46303.

70. Escobar, W.A., Miller, J. and Fink, A.L. (1994) Effects of site-specific mutagenesis of tyrosine 105 in a class A beta-lactamase. *Biochem J*, **303 (Pt 2)**, 555-558.

71. Jacob, F., Joris, B., Lepage, S., Dusart, J. and Frere, J.M. (1990) Role of the conserved amino acids of the 'SDN' loop (Ser130, Asp131 and Asn132) in a class A beta-lactamase studied by site-directed mutagenesis. *Biochem J*, **271**, 399-406.

72. Mohammad, F., Green, R. and Buskirk, A.R. (2019) A systematically-revised ribosome profiling method for bacteria reveals pauses at single-codon resolution. *Elife*, **8**.

1127 73. Negro, V., Krin, E., Aguilar Pierle, S., Chaze, T., Giai Gianetto, Q., Kennedy, S.P., Matondo, M.,
1128 Mazel, D. and Baharoglu, Z. (2019) RadD Contributes to R-Loop Avoidance in Sub-MIC
1129 Tobramycin. *MBio*, **10**.

1130 74. Bielecki, P., Muthukumarasamy, U., Eckweiler, D., Bielecka, A., Pohl, S., Schanz, A., Niemeyer, U.,
1131 Oumeraci, T., von Neuhoff, N., Ghigo, J.M. *et al.* (2014) In vivo mRNA profiling of uropathogenic
1132 Escherichia coli from diverse phylogroups reveals common and group-specific gene expression
1133 profiles. *mBio*, **5**, e01075-01014.

1134 75. Manneh-Roussel, J., Haycocks, J.R.J., Magan, A., Perez-Soto, N., Voelz, K., Camilli, A., Krachler,
1135 A.M. and Grainger, D.C. (2018) cAMP Receptor Protein Controls Vibrio cholerae Gene
1136 Expression in Response to Host Colonization. *MBio*, **9**.

1137 76. Carvalho, A., Krin, E., Korlowski, C., Mazel, D. and Baharoglu, Z. (2021) Interplay between
1138 Sublethal Aminoglycosides and Quorum Sensing: Consequences on Survival in V. cholerae. *Cells*,
1139 **10**.

1140 77. Kolmsee, T., Delic, D., Agyenim, T., Calles, C. and Wagner, R. (2011) Differential stringent control
1141 of Escherichia coli rRNA promoters: effects of ppGpp, DksA and the initiating nucleotides.
1142 *Microbiology (Reading)*, **157**, 2871-2879.

1143 78. Baharoglu, Z., Krin, E. and Mazel, D. (2013) RpoS Plays a Central Role in the SOS Induction by
1144 Sub-Lethal Aminoglycoside Concentrations in Vibrio cholerae. *Plos Genetics*, **9**.

1145 79. Huber, S.M., Begley, U., Sarkar, A., Gasperi, W., Davis, E.T., Surampudi, V., Lee, M., Melendez,
1146 J.A., Dedon, P.C. and Begley, T.J. (2022) Arsenite toxicity is regulated by queuine availability and
1147 oxidation-induced reprogramming of the human tRNA epitranscriptome. *Proc Natl Acad Sci U S A*,
1148 **119**, e2123529119.

1149 80. Frumkin, I., Lajoie, M.J., Gregg, C.J., Hornung, G., Church, G.M. and Pilpel, Y. (2018) Codon
1150 usage of highly expressed genes affects proteome-wide translation efficiency. *Proc Natl Acad Sci U*
1151 *S A*, **115**, E4940-E4949.

1152 81. Kudla, G., Murray, A.W., Tollervey, D. and Plotkin, J.B. (2009) Coding-sequence determinants of
1153 gene expression in Escherichia coli. *Science*, **324**, 255-258.

1154 82. Gutierrez, A., Laureti, L., Crussard, S., Abida, H., Rodriguez-Rojas, A., Blazquez, J., Baharoglu, Z.,
1155 Mazel, D., Darfeuille, F., Vogel, J. *et al.* (2013) beta-lactam antibiotics promote bacterial mutagenesis
1156 via an RpoS-mediated reduction in replication fidelity. *Nature communications*, **4**, 1610.

1157 83. Baharoglu, Z. and Mazel, D. (2011) Vibrio cholerae Triggers SOS and Mutagenesis in Response to
1158 a Wide Range of Antibiotics: a Route towards Multiresistance. *Antimicrobial Agents and Chemotherapy*,
1159 **55**, 2438-2441.

1160 84. Osterman, I.A., Chervontseva, Z.S., Evfratov, S.A., Sorokina, A.V., Rodin, V.A., Rubtsova, M.P.,
1161 Komarova, E.S., Zatsepin, T.S., Kabilov, M.R., Bogdanov, A.A. *et al.* (2020) Translation at first
1162 sight: the influence of leading codons. *Nucleic Acids Res*, **48**, 6931-6942.

1163 85. Boel, G., Letso, R., Neely, H., Price, W.N., Wong, K.H., Su, M., Luff, J., Valecha, M., Everett, J.K.,
1164 Acton, T.B. *et al.* (2016) Codon influence on protein expression in E. coli correlates with mRNA
1165 levels. *Nature*, **529**, 358-363.

1166 86. Kimura, S., Srisuknimit, V., McCarty, K.L., Dedon, P.C., Kranzusch, P.J. and Waldor, M.K. (2022)
1167 Sequential action of a tRNA base editor in conversion of cytidine to pseudouridine. *Nature*
1168 *communications*, **13**, 5994.

1169 87. Zhao, F., Zhou, Z., Dang, Y., Na, H., Adam, C., Lipzen, A., Ng, V., Grigoriev, I.V. and Liu, Y.
1170 (2021) Genome-wide role of codon usage on transcription and identification of potential regulators.
1171 *Proc Natl Acad Sci U S A*, **118**.

1172 88. Chan, C.T., Dyavaiah, M., DeMott, M.S., Taghizadeh, K., Dedon, P.C. and Begley, T.J. (2010) A
1173 quantitative systems approach reveals dynamic control of tRNA modifications during cellular
1174 stress. *PLoS Genet*, **6**, e1001247.

1175 89. Torrent, M., Chalancon, G., de Groot, N.S., Wuster, A. and Madan Babu, M. (2018) Cells alter their
1176 tRNA abundance to selectively regulate protein synthesis during stress conditions. *Sci Signal*, **11**.

1177 90. Chan, C.T., Pang, Y.L., Deng, W., Babu, I.R., Dyavaiah, M., Begley, T.J. and Dedon, P.C. (2012)
1178 Reprogramming of tRNA modifications controls the oxidative stress response by codon-biased
1179 translation of proteins. *Nature communications*, **3**, 937.

1180 91. Keith, G., Rogg, H., Dirheimer, G., Menichi, B. and Heyham, T. (1976) Post-transcriptional
1181 modification of tyrosine tRNA as a function of growth in Bacillus subtilis. *FEBS Lett*, **61**, 120-123.

1182 92. Moukadiri, I., Garzon, M.J., Bjork, G.R. and Armengod, M.E. (2014) The output of the tRNA
1183 modification pathways controlled by the Escherichia coli MnmEG and MnmC enzymes depends
1184 on the growth conditions and the tRNA species. *Nucleic Acids Res*, **42**, 2602-2623.

1185 93. Frey, B., McCloskey, J., Kersten, W. and Kersten, H. (1988) New function of vitamin B12:
1186 cobamide-dependent reduction of epoxyqueuosine to queuosine in tRNAs of Escherichia coli and
1187 Salmonella typhimurium. *J Bacteriol*, **170**, 2078-2082.

1188 94. Persson, B.C. (1993) Modification of tRNA as a regulatory device. *Mol Microbiol*, **8**, 1011-1016.

1189 95. Galvanin, A., Vogt, L.M., Grober, A., Freund, I., Ayadi, L., Bourguignon-Igel, V., Bessler, L., Jacob,
1190 D., Eigenbrod, T., Marchand, V. *et al.* (2020) Bacterial tRNA 2'-O-methylation is dynamically
1191 regulated under stress conditions and modulates innate immune response. *Nucleic Acids Res*, **48**,
1192 12833-12844.

1193 96. Han, L. and Phizicky, E.M. (2018) A rationale for tRNA modification circuits in the anticodon
1194 loop. *RNA*, **24**, 1277-1284.

1195 97. Dixit, S., Kessler, A.C., Henderson, J., Pan, X., Zhao, R., D'Almeida, G.S., Kulkarni, S., Rubio,
1196 M.A.T., Hegedusova, E., Ross, R.L. *et al.* (2021) Dynamic queuosine changes in tRNA couple
1197 nutrient levels to codon choice in Trypanosoma brucei. *Nucleic Acids Res*, **49**, 12986-12999.

1198 98. Oprea, M., Njamkepo, E., Cristea, D., Zhukova, A., Clark, C.G., Kravetz, A.N., Monakhova, E.,
1199 Ciontea, A.S., Cojocaru, R., Rauzier, J. *et al.* (2020) The seventh pandemic of cholera in Europe
1200 revisited by microbial genomics. *Nature communications*, **11**, 5347.

1201
1202

Figure legends

Figure 1. *V. cholerae Δtgt* shows decreased aminoglycoside tolerance. A. Competition experiments between WT and *Δtgt* with the indicated antibiotic or oxidant at sub-MIC concentration*. NT: non-treated.* TOB: tobramycin 0.6 µg/ml; CIP: ciprofloxacin 0.01 µg/ml; CRB: carbenicillin 2.5 µg/ml; PQ: paraquat 10 µM; H_2O_2: 2mM. **B.** Competition experiments between WT and *Δtgt* carrying the indicated plasmids. MH: *non-treated*. **CDEF**. Survival of exponential phase cultures after various times of incubation (indicated in minutes on the X-axis) with the indicated antibiotic at lethal concentration: 5MIC: 5 times the MIC; 10MIC: 10 times the MIC. **G.** PMF measurement of exponential phase cultures using fluorescent Mitotracker dye, measured using flow cytometry. **H**. Neomycin uptake measurement by flow cytometry using fluorescent Cy5 coupled neomycin. **I.** Competition experiments between WT and *Δtgt* carrying either empty plasmid (p0), or a plasmid overexpressing tRNA-Tyr with the native GUA anti-codon, or with the synthetic AUA anticodon. The anticodon sequence is indicated (e.g. tRNATyrAUA decodes the TAT codon). *NT: non-treated.* TOB: tobramycin 0.6 µg/ml. For multiple comparisons, we used one-way ANOVA. **** means p<0.0001, *** means p<0.001, ** means p<0.01, * means p<0.05. ns: non-significant. Number of replicates for each experiment: 3<n<8.

Figure 2. Codon decoding differences for *V. cholerae* WT and *Δtgt*. A. to E. Codon specific translation efficiency in WT and *Δtgt* using 6xcodon stretches inserted in GFP. Y axis represents the relative fluorescence of a given GFP in Δtgt over the same construct in WT. NT: non-treated; TOB: tobramycin at 0.4 µg/ml. Each specified codon is repeated 6x within the coding sequence of the GFP (e.g. TACTACTACTACTACTAC). For multiple comparisons, we used one-way ANOVA. **** means p<0.0001, *** means p<0.001, ** means p<0.01, * means p<0.05. ns: non-significant. Number of replicates for each experiment: 3<n, each dot represents one replicate.

Figure 3. Differential translation at tyrosine codons evaluated by growth on carbenicillin of mutated β-lactamase reporters. The catalytic tyrosine at position 103 was tested in its native sequence (TAC), or with the synonymous TAT mutation. **A to D.** Growth on microtiter plates. Growth was followed by measuring the OD 620 nm every 15 minutes during 800 minutes. CARB was used at 100 µg/ml. A and C: not TOB. B and D: TOB at 0.2 µg/ml (20% of MIC).

Figure 4. Post-transcriptional regulation in *Δtgt* and Tyr codon usage bias. A. and B. Volcano plots showing less and more abundant proteins in proteomics analysis (performed in triplicates) in *Δtgt* compared to WT during growth without antibiotics (A. where MH is the growth medium), or in sub-MIC TOB at 0.4 µg/ml (B.). **C.** Codon usage bias calculation example with VC1017 *rsxA* tyrosine TAC and TAT codons. **D. to G.** Plots showing codon usage bias for genes lists that are up or down in ribosome profiling analysis (performed in triplicates), for codons decoded by tRNAs with Q modification. Each dot represents one gene of the lists.

Figure 5. Post-transcriptional upregulation of RsxA in *Δtgt* due to a Tyr codon bias towards TAT and toxicity in sub-MIC TOB. A. *rsxA* mRNA levels measured by digital RT-PCR. **B.** Transcriptional expression levels from the *rsxA* promoter measured by flow cytometry. **C.** Translational fusion of *rsxA* to *gfp* and *gfp* alone, with differences in codon usage. *** means p<0.001, ** means p<0.01. ns: non-significant. **D.** Relative OD 620 nm of WT strain carrying either empty plasmid or plasmid overexpressing RsxA comparing growth in sub-MIC TOB divided by growth in the absence of treatment.

Figure 6. Regulation of *tgt* expression and tRNA Q levels. A: *tgt* transcript levels measured by digital-RT-PCR. Y-axis represents relative abundance compared to the non-treated (NT) condition in WT. For multiple comparisons, we used one-way ANOVA (for A. C. E.). **** means *p*<0.0001, *** means *p*<0.001, ** means *p*<0.01. Only significant differences are shown. **B.** Stringent response induction measured with *P1rrn-gfp* reporter shown as fluorescence (Y-axis) as a function of growth (X-axis: OD 600 nm). **C.** Q levels in tRNA enriched RNA extracts, measured by mass spectrometry**. D**. Q detection and quantification by $IO4^-$ oxidation coupled to deep sequencing. The Y-axis represents deletion score, which correlates with the Q34 level in tRNA. Results for tRNAs His, AsnGUU2 and Asp are shown. Analysis was performed for three biological replicates (shown as colored dots) and at least two technical replicates for each strain (only mean of technical replicates is shown). p-values are calculated by two-tailed T-test, error bars correspond to standard error of the mean. **E.** Northern blot and quantification of Q levels in $tRNA^{Tyr}$. The lower band in the gel corresponds to unmodified $tRNA^{Tyr}$. The upper band corresponds to Q-modified tRNA-Tyr. *Δtgt* is the negative control without modification of $tRNA^{Tyr}$. Histograms show the quantification of Q-modified $tRNA^{Tyr}$ over total $tRNA^{Tyr}$**,** as follows: Q-modified $tRNA^{Tyr}$/(Q-modified $tRNA^{Tyr}$ + $tRNA^{Tyr}$ without Q)= upper band/(upper band + lower band). 2.5 µg of in tRNA enriched RNA extracts were deposited in lanes WT NT, WT TOB and *Δcrp*. 0.9 µg was deposited in lanes *Δtgt.* Number of replicates for each experiment: 3

1256 **Figure 7. DNA repair after UV irradiation is more efficient in *V. cholerae Δtgt*. A and C**. Tyrosine codon usage of
1257 DNA repair genes A: in *V. cholerae. C: in E. coli.* Red indicates positive codon usage bias, i.e. TAT bias. Blue
1258 indicates negative codon usage bias for TAT, i.e. TAC bias. **B and D.** Survival of *Δtgt* relative to WT after UV
1259 irradiation (linear scale) B: in *V. cholerae. D: in E. coli.* For multiple comparisons, we used one-way ANOVA. ****
1260 means p<0.0001, ns: non-significant.

1261 **Figure 8. Model.** Upon exposure to sub-MIC aminoglycosides, the expression of *tgt* is up-regulated in *V. cholerae*
1262 and influences the decoding of tyrosine TAC vs TAT codons. This leads to differential translation from transcripts
1263 bearing a codon usage bias for tyrosine codons. The *rsxA* transcript bears a tyrosine codon bias and its translation
1264 can be tuned by tRNA Q modification. RsxA is an anti-SoxR factor. SoxR controls a regulon involved in oxidative
1265 stress response. When RsxA levels are high, SoxR is increasingly inactivated and oxidative stress response
1266 efficiency decreases. It has been previously shown that sub-MIC aminoglycosides trigger oxidative stress in *V.*
1267 *cholerae*(78). Increasing RsxA levels thus reduces fitness in TOB by hampering efficient oxidative stress response.
1268 As a corollary, decreased RsxA would lead to increased expression of the SoxR regulon, which would allow for
1269 more efficient response to oxidative stress, and increased fitness in the presence of sub-MIC TOB. We propose
1270 that when Tgt/Q levels in tRNA increase, RsxA synthesis is low and active SoxR levels are high, facilitating the
1271 bacterial response to aminoglycoside dependent oxidative stress.

1272

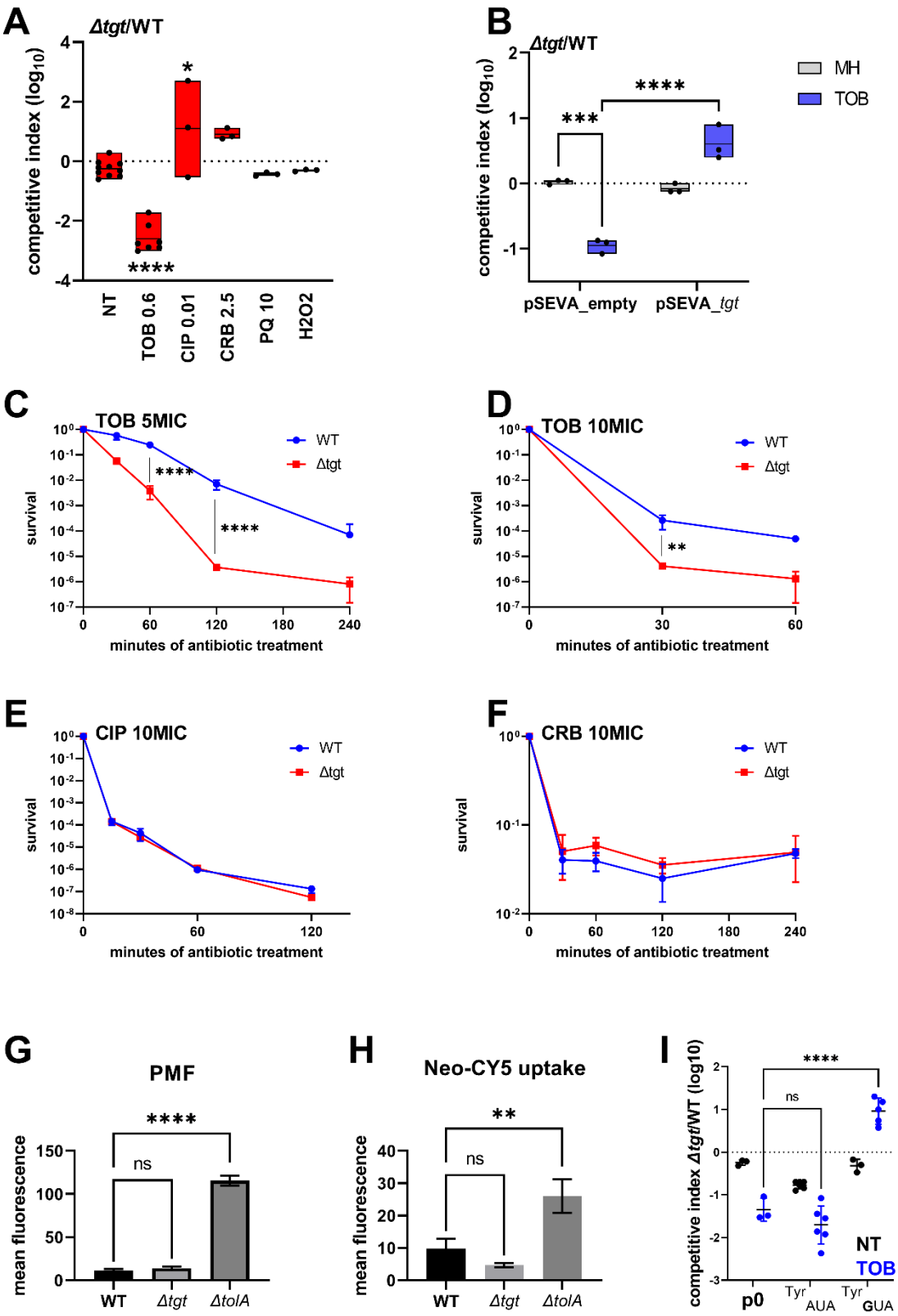

Figure 1. *V. cholerae Δtgt* shows decreased aminoglycoside tolerance. A. Competition experiments between WT and *Δtgt* with the indicated antibiotic or oxidant at sub-MIC concentration. *NT: non-treated.* TOB: tobramycin 0.6 µg/ml; CIP: ciprofloxacin 0.01 µg/ml; CRB: carbenicillin 2.5 µg/ml; PQ: paraquat 10 µM; H_2O_2: 2mM. **B.** Competition experiments between WT and *Δtgt* carrying the indicated plasmids. MH: *non-treated*. **CDEF**. Survival of exponential phase cultures after various times of incubation (indicated in minutes on the X-axis) with the

indicated antibiotic at lethal concentration: 5MIC: 5 times the MIC; 10MIC: 10 times the MIC. **G.** PMF measurement of exponential phase cultures using fluorescent Mitotracker dye, measured using flow cytometry. **H**. Neomycin uptake measurement by flow cytometry using fluorescent Cy5 coupled neomycin. **I.** Competition experiments between WT and *Δtgt* carrying either empty plasmid (p0), or a plasmid overexpressing tRNA-Tyr with the native GUA anti-codon, or with the synthetic AUA anticodon. The anticodon sequence is indicated (e.g. tRNATyrAUA decodes the TAT codon). *NT: non-treated.* TOB: tobramycin 0.6 µg/ml. For multiple comparisons, we used one-way ANOVA on GraphPad Prism. **** means p<0.0001, *** means p<0.001, ** means p<0.01, * means p<0.05. ns: non-significant. Number of replicates for each experiment: 3<n<8.

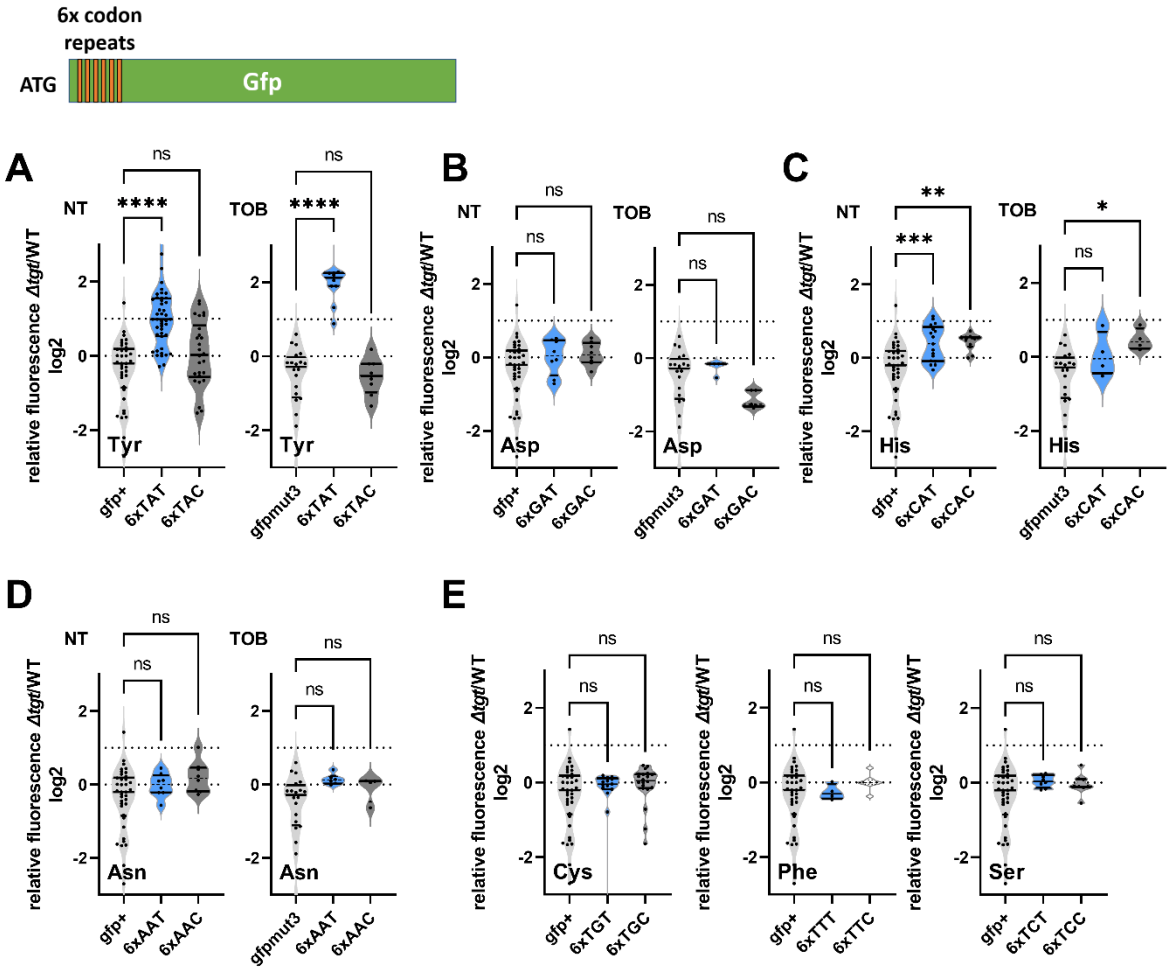

Figure 2. Codon decoding differences for *V. cholerae* WT and *Δtgt*. A. to E. Codon specific translation efficiency in WT and *Δtgt* using 6xcodon stretches inserted in GFP. Y axis represents the relative fluorescence of a given GFP in *Δtgt* over the same construct in WT. NT: non-treated; TOB: tobramycin at 0.4 µg/ml. Each specified codon is repeated 6x within the coding sequence of the GFP (e.g. TACTACTACTACTACTAC). "*gfp+*" is the native *gfp* gene without stretch. For multiple comparisons, we used one-way ANOVA on GraphPad Prism. **** means p<0.0001, *** means p<0.001, ** means p<0.01, * means p<0.05. ns: non-significant. Number of replicates for each experiment: 3<n, each dot represents one replicate.

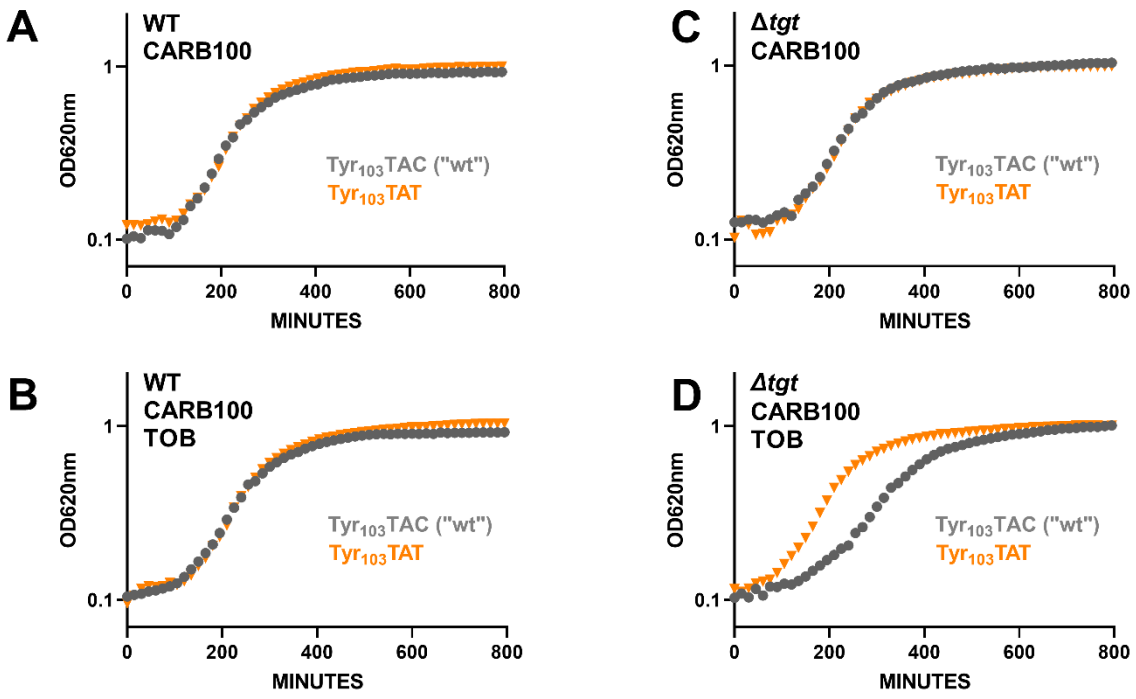

Figure 3. Differential translation at tyrosine codons evaluated by growth on carbenicillin of mutated β-lactamase reporters. The catalytic tyrosine at position 103 was tested in its native sequence (TAC), or with the synonymous TAT mutation. **A to D.** Growth on microtiter plates. Growth was followed by measuring the OD 620 nm every 15 minutes during 800 minutes. CARB was used at 100 µg/ml. A and C: not TOB. B and D: TOB at 0.2 µg/ml (20% of MIC).

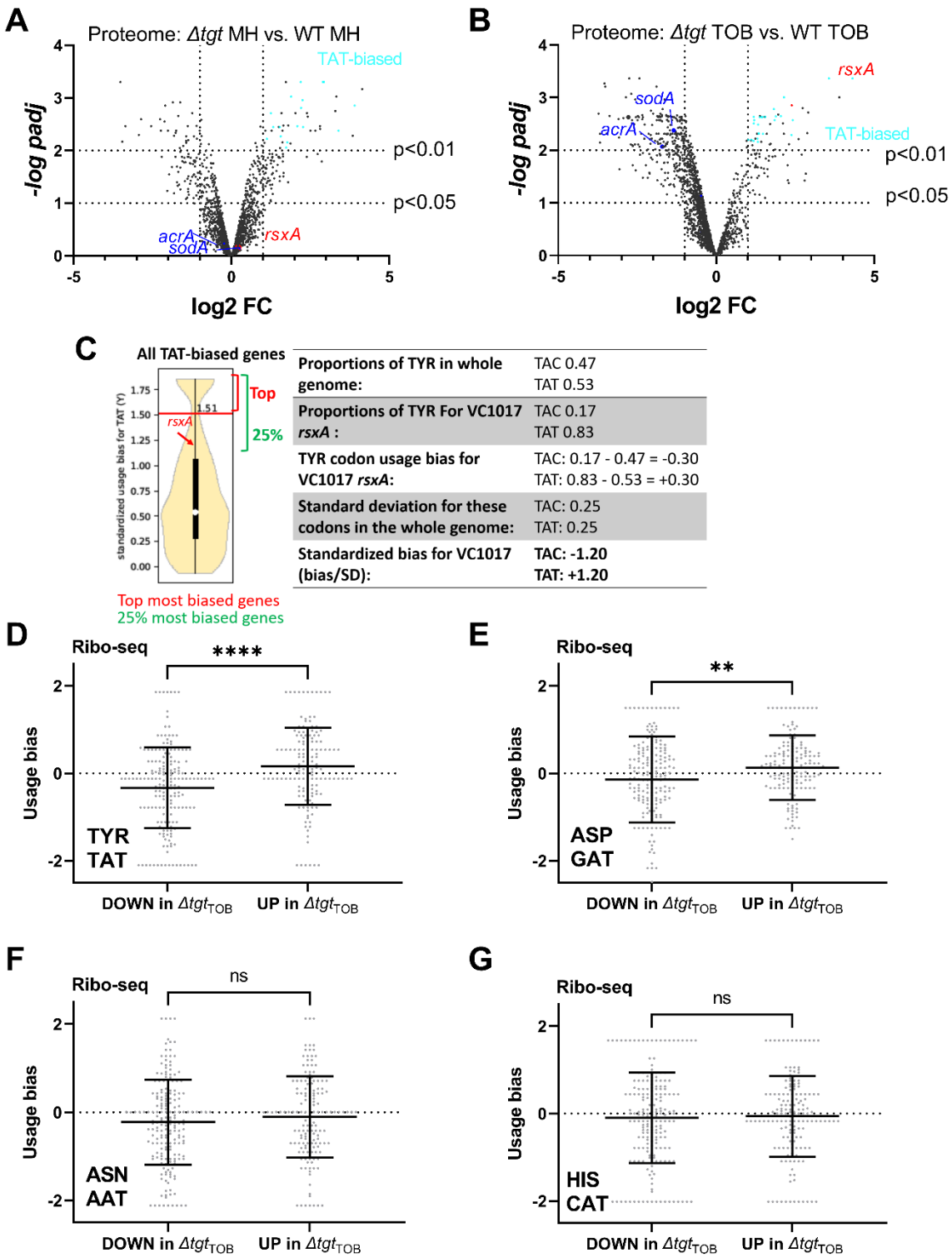

Figure 4. Post-transcriptional regulation in *Δtgt* and Tyr codon usage bias. A. and B. Volcano plots showing less and more abundant proteins in proteomics analysis (performed in triplicates) in *Δtgt* compared to WT during growth without antibiotics (A. where MH is the growth medium), or in sub-MIC TOB at 0.4 µg/ml (B.). **C.** Codon usage bias calculation example with VC1017 *rsxA* tyrosine TAC and TAT codons. **D. to G.** Plots showing codon usage bias for genes lists that are up or down in ribosome profiling analysis (performed in triplicates), for codons decoded by tRNAs with Q modification. Each dot represents one gene of the lists.

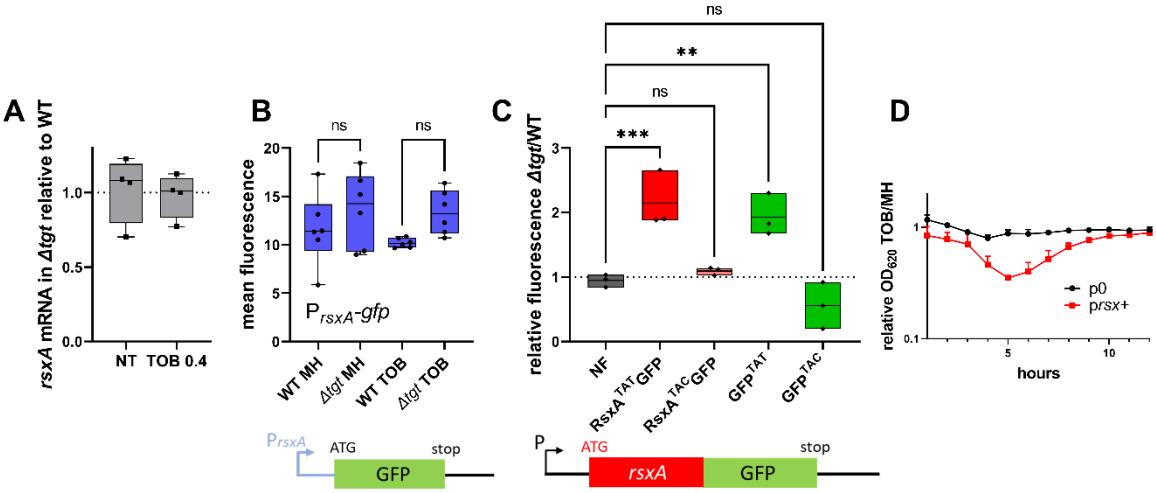

Figure 5. Post-transcriptional upregulation of RsxA in *Δtgt* due to a Tyr codon bias towards TAT and toxicity in sub-MIC TOB. A. *rsxA* mRNA levels measured by digital RT-PCR. **B.** Transcriptional expression levels from the *rsxA* promoter measured by flow cytometry. **C.** Translational fusion of *rsxA* to *gfp* and *gfp* alone, with differences in codon usage. *** means p<0.001, ** means p<0.01. ns: non-significant. **D.** Relative OD 620 nm of WT strain carrying either empty plasmid or plasmid overexpressing RsxA comparing growth in sub-MIC TOB divided by growth in the absence of treatment.

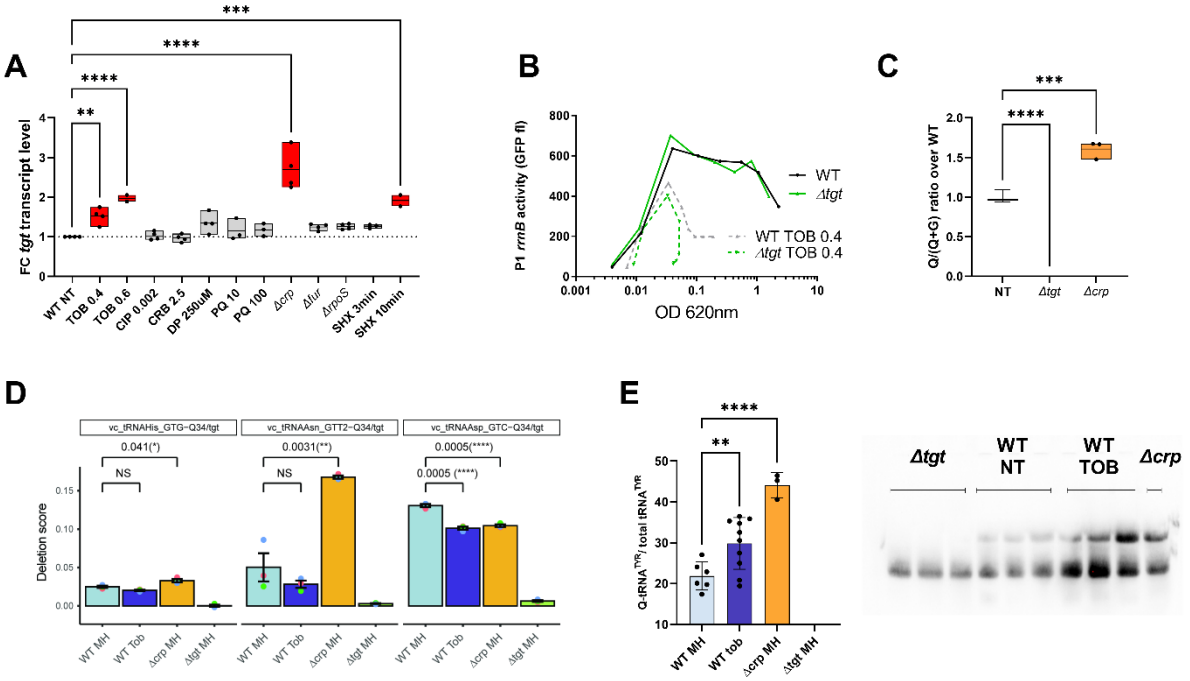

Figure 6. Regulation of *tgt* expression and tRNA Q levels. A: *tgt* transcript levels measured by digital-RT-PCR. Y-axis represents relative abundance compared to the non-treated (NT) condition in WT. For multiple comparisons, we used one-way ANOVA on GraphPad Prism. **** means $p<0.0001$, *** means $p<0.001$, ** means $p<0.01$. Only significant differences are shown. **B.** Stringent response induction measured with *P1rrn-gfp* reporter shown as fluorescence (Y-axis) as a function of growth (X-axis: OD 600 nm). **C.** Q levels in tRNA enriched RNA extracts, measured by mass spectrometry**. D**. Q detection by sequencing. The Y-axis represents deletion score, where "deletion" corresponds to the presence of Q after chemical treatment. Results for tRNAs His, Asn and Asp are shown. **E.** Northern blot and quantification of Q levels in tRNA-Tyr. The lower band in the gel corresponds to unmodified tRNA-Tyr. The upper band corresponds to Q-modified tRNA-Tyr. Δtgt is the negative control without modification of tRNA-Tyr. Histograms show the quantification of Q-modified tRNA tyr over total tRNA. **** means p<0.0001, *** means p<0.001, * means p<0.05. Number of replicates for each experiment: 3

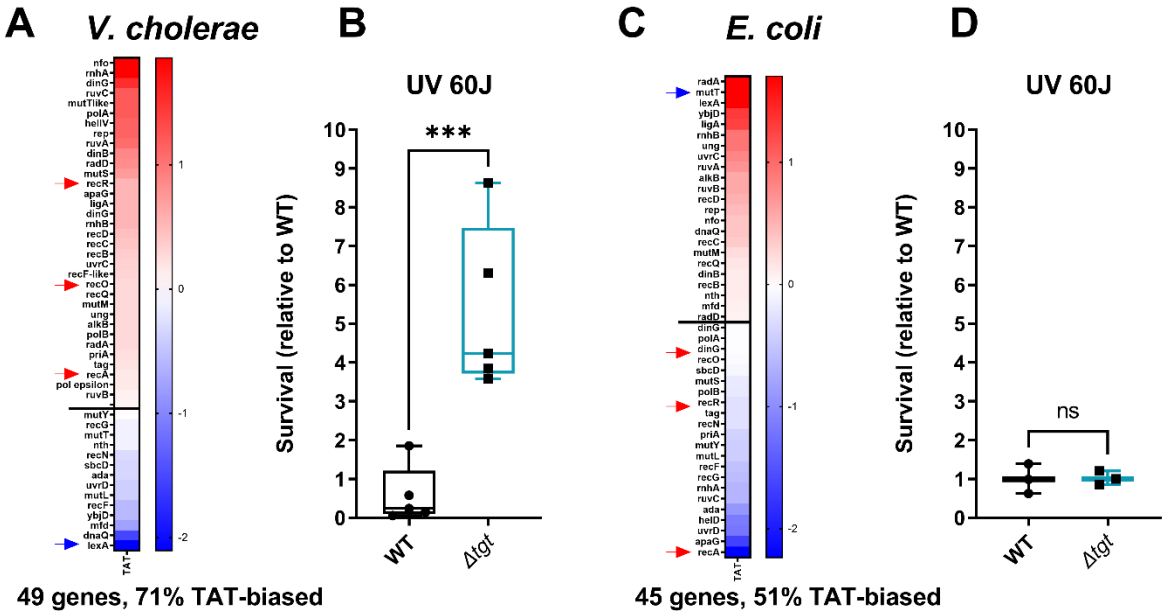

Figure 7. DNA repair after UV irradiation is more efficient in *V. cholerae Δtgt*. A and C. Tyrosine codon usage of DNA repair genes A: in *V. cholerae. C: in E. coli.* Red indicates positive codon usage bias, i.e. TAT bias. Blue indicates negative codon usage bias for TAT, i.e. TAC bias. **B and D.** Survival of *Δtgt* relative to WT after UV irradiation (linear scale) B: in *V. cholerae. D: in E. coli.* For multiple comparisons, we used one-way ANOVA on GraphPad Prism. **** means p<0.0001, ns: non-significant.

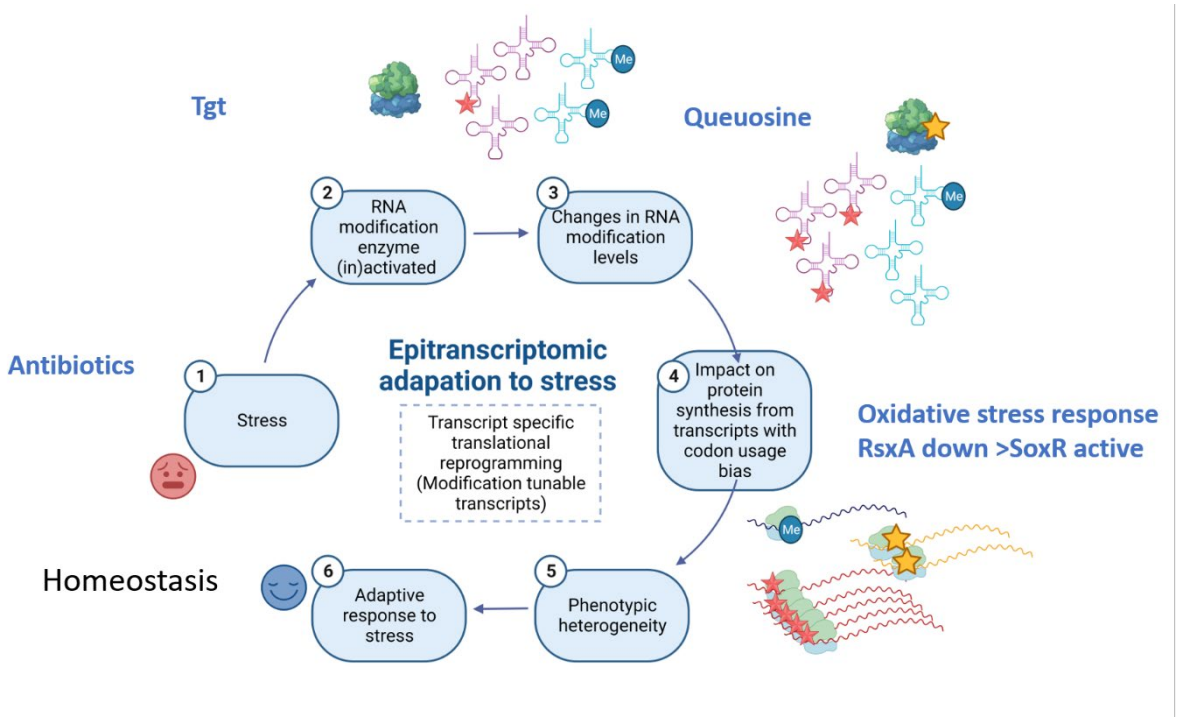

Figure 8. Model. Upon exposure to sub-MIC aminoglycosides, the expression of *tgt* is up-regulated in *V. cholerae* and influences the decoding of tyrosine TAC vs TAT codons. This leads to differential translation from transcripts bearing a codon usage bias for tyrosine codons. The *rsxA* transcript bears a tyrosine codon bias and its translation can be tuned by tRNA Q modification. RsxA is an anti-SoxR factor. SoxR controls a regulon involved in oxidative stress response. When RsxA levels are high, SoxR is increasingly inactivated and oxidative stress response efficiency decreases. It has been previously shown that sub-MIC aminoglycosides trigger oxidative stress in *V. cholerae.* We propose that when Tgt/Q levels in tRNA increase, RsxA synthesis is low and active SoxR levels are high, facilitating the bacterial response to aminoglycoside dependent oxidative stress.

Supplementary figure legends

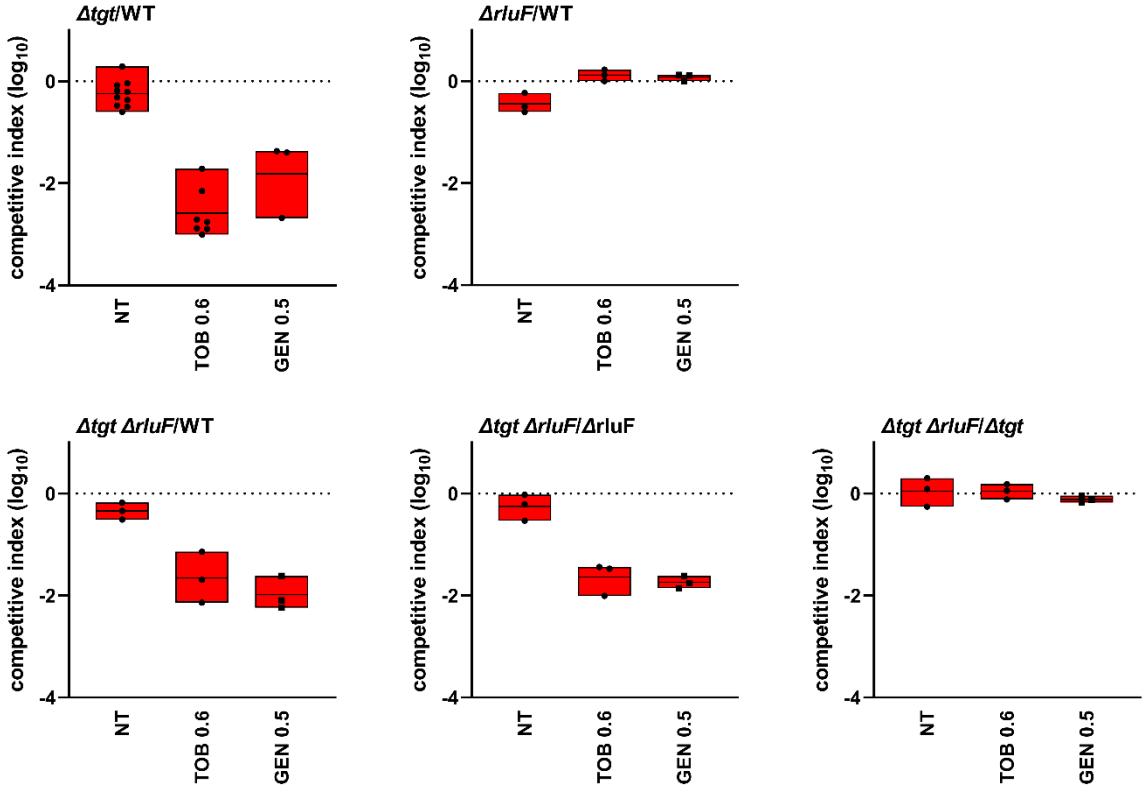

Figure S1. No effect of *rluF* deletion on fitness in *V. cholerae* WT and *Δtgt* strains. In vitro competition experiments of *V. cholerae* WT and mutant strains in the absence or presence of sub-MIC aminoglycosides tobramycin TOB and gentamicin (GEN) (50% of the MIC, TOB 0.6 µg/ml, GEN 0.5 µg/ml). MH: no antibiotic treatment. The Y-axis represents $\log_{10}$ of competitive index calculated as described in the methods. A competitive index of 1 indicates equal growth of both strains. The X-axis indicates growth conditions. For multiple comparisons, we used one-way ANOVA on GraphPad Prism. **** means $p<0.0001$, * means $p<0.05$. Number of replicates for each experiment: $3<n<10$.

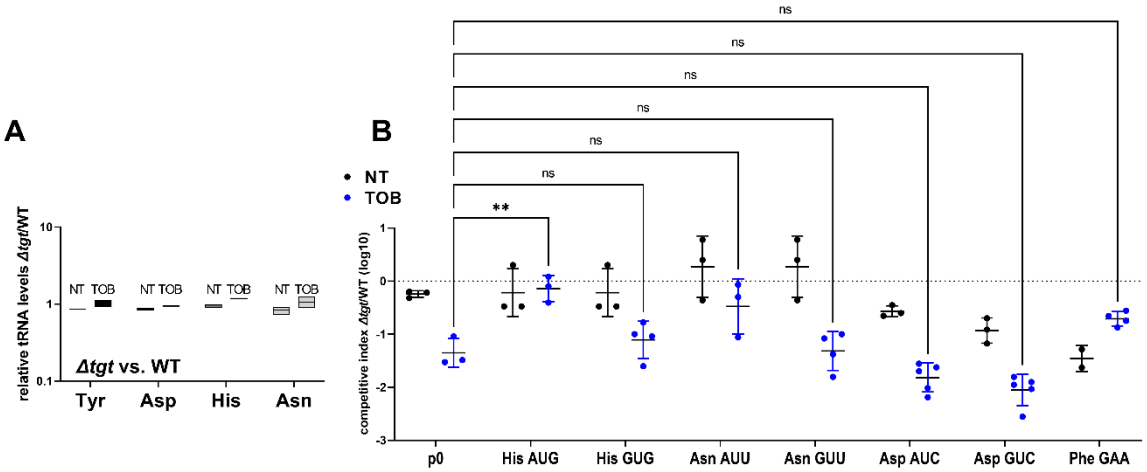

Figure S2. Impact of tRNA overexpression on fitness during growth in sub-MIC TOB. A. Absence of *tgt* does not visibly affect endogenous tRNA-GUN levels. qRTPCR. A: relative tRNA abundance in *Δtgt* compared to WT strain in the absence of treatment (NT) and in the presence of sub-MIC tobramycin (TOB). **B.** In vitro competition experiments between *V. cholerae* WT and *Δtgt* strains, carrying a plasmid overexpressing the indicated tRNA; in the absence (NT) or presence of sub-MIC tobramycin (50% of the MIC, TOB 0.6 µg/ml). NT: no antibiotic treatment. The Y-axis represents $\log_{10}$ of competitive index calculated as described in the methods. A competitive index of 1 indicates equal growth of both strains. The X-axis indicates which tRNA is overexpressed, from the high copy pTOPO plasmid. The anticodon sequence is indicated (e.g. $tRNA^{Tyr}_{AUA}$ decodes the TAT codon). The following tRNAs-GUN are the canonical tRNAs which are present in the genome, and modified by Tgt: Tyr_{GUA}, His_{GUG}, Asn_{GUU}, Asp_{GUC}. The following tRNAs-AUN are synthetic tRNAs which are not present in the genome: Tyr_{AUA}, His_{AUG}, Asn_{AUU}, Asp_{AUC}. $tRNA^{Phe}_{GAA}$ is used as non Tgt-modified control. p0 is the empty plasmid. For multiple comparisons, we used one-way ANOVA on GraphPad Prism. **** means $p<0.0001$, * means $p<0.05$. Number of replicates for each experiment: $3<n<8$. In A, only significant differences are indicated. ns means non-significant.

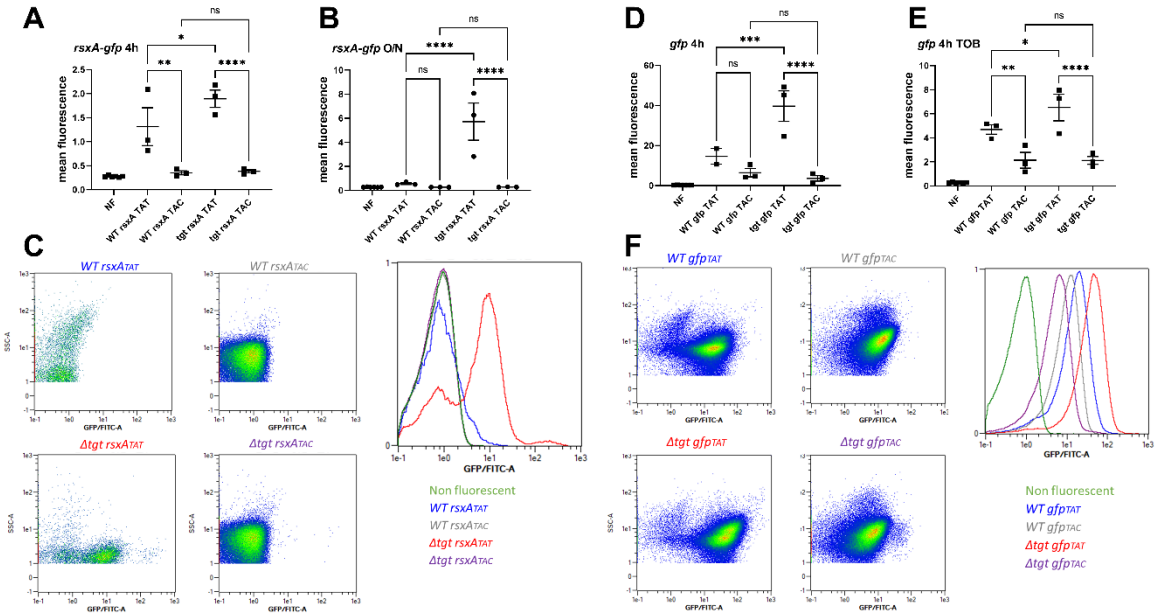

Figure S3. Post-transcriptional upregulation of RsxA in *Δtgt* due to a Tyr codon bias towards TAT and toxicity in sub-MIC TOB. ABC. Translational fusion of TAC and TAT versions of *rsxA* to *gfp* (A. 4 hours exponential phase cultures, B. overnight stationary phase cultures). **DEF**. TAC and TAT versions of *gfp* alone (C. 4 hours exponential phase cultures without antibiotics, D. in the presence of sub-MIC TOB), measured by flow cytometry. Y-axis represents mean fluorescence. **C and F** show representative examples of fluorescence observed with indicated reporters.

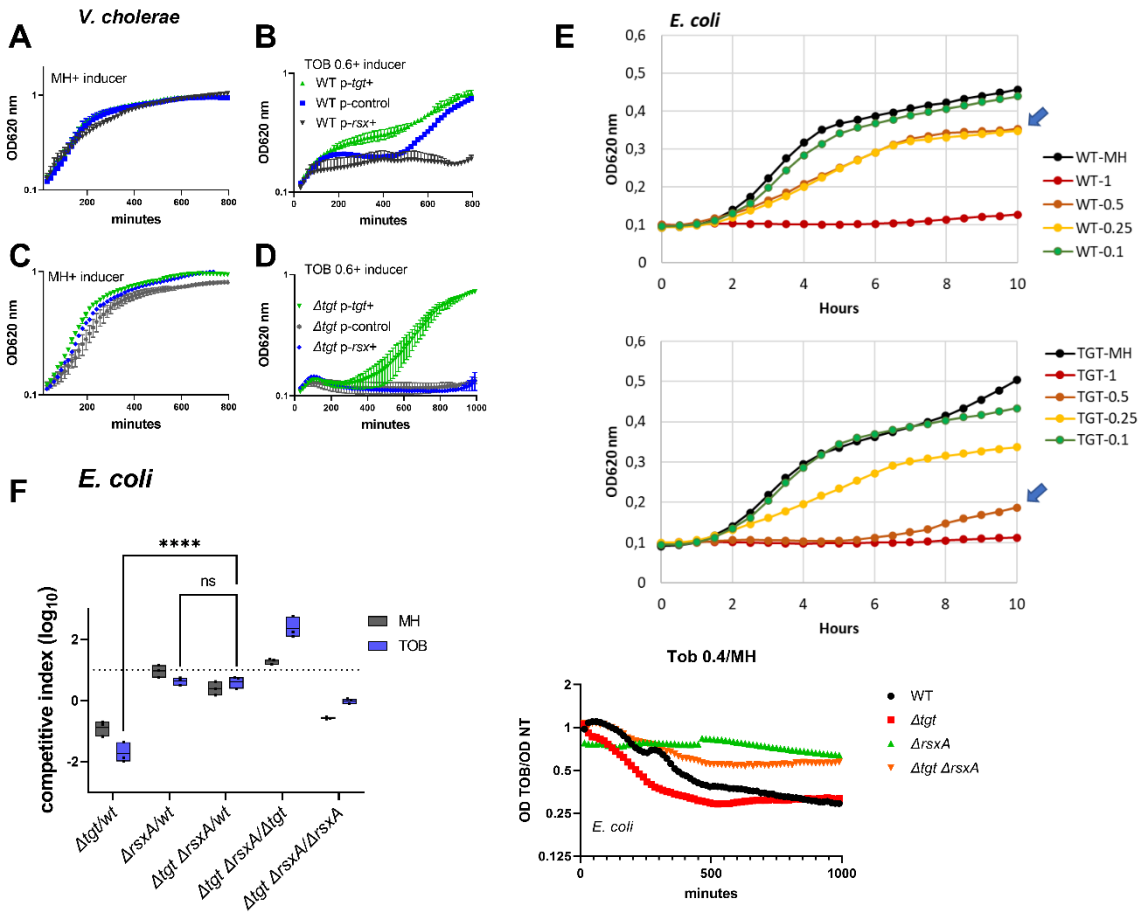

Figure S4. *rsxA* levels impact growth in the presence of sub-MIC TOB. ABCD. Growth curves in microtiter plate reader, in *V. cholerae* in indicated conditions**.** P-tgt+: pSEVA expressing *tgt*. P-rsx+: pSEVA expressing *rsxA*. P-control: empty pSEVA. **E**. Growth curves in microtiter plate reader, in *E. coli* WT and *Δtgt* in MH or in the presence of tobramycin at the indicated concentrations (in µg/mL). **F.** Left: Competition experiments in *E. coli*, with indicated strains. Right: Relative OD 620 nm of indicated strain comparing growth in TOB (0.4 µg/ml) divided by growth in the absence of treatment.

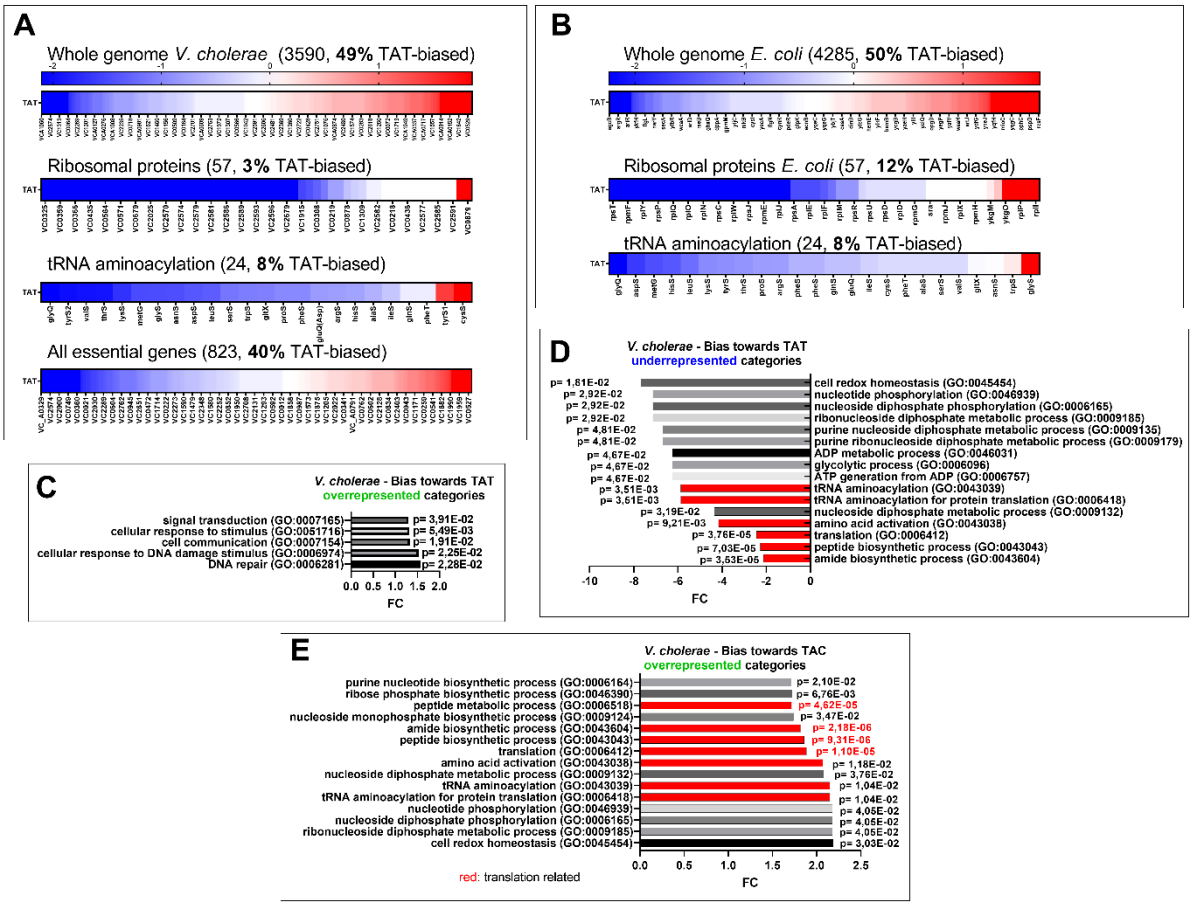

Figure S5. Codon usage. A and B: Tyrosine codon usage in A: *V. cholerae* and B: *E. coli* in the whole genome and selected groups of genes. Red indicates positive codon usage bias, i.e. TAT bias. Blue indicates negative codon usage bias for TAT, i.e. TAC bias. **CDE.** Gene ontology enrichment analysis in *V. cholerae* of **C:** overrepresented gene categories with TAT usage bias**. D:** underrepresented gene categories with TAT usage bias**. E:** overrepresented gene categories with TAC usage bias.

Table S1: Proteomics identify differentially abundant proteins

Uniprot	Gene Name	Fasta headers
		I - More abundant in WT
		I – 1. PresentF606WT_AbsentJ420tgt
Q9KTY9	tgt	Queuine tRNA-ribosyltransferase
Q9KNM6	VC_2706	queuosine precursor transporter
Q9KNH8	VC_2761	Bcr/CflA family efflux transporter
Q9KMV7	VC_A0211	Sensory box sensor histidine kinase
Q9KN55	VC_A0110	Uncharacterized protein
Q9KP41	VC_2538	Thiamine ABC transporter, permease protein,
Q9KTU0	VC_0798	Citrate lyase, beta subunit
Q9KSB8	VC_1340	PrpE protein
Q9KRW0	VC_1524	ABC transporter, permease protein
Q9KMB6	VC_A0457	Uncharacterized protein
Q9KUU0	VC_0425	lacZ
Q9KND5	VC_A0030	Uncharacterized protein
Q9KNP5	zapB	Cell division protein ZapB
Q9KUS6	VC_0439	ThrE_2 domain-containing protein
Q9KLK9	VC_A0734	Uncharacterized protein
Q9KRP8	VC_1588	Transcriptional regulator, LysR family
Q9KRB9	VC_1723	TVP38/TMEM64 family membrane protein
Q9KNT7	argB	Acetylglutamate kinase
Q9KRX3	VC_1510	Uncharacterized protein
Q9KPM7	VC_2340	HD-GYP domain-containing protein
Q9KL36	VC_A0913	Hemin ABC transporter, periplasmic hemin-binding protein HutB
Q9KVY3	VC_0005	Putative membrane protein insertion efficiency factor
Q9KQV1	VC_1897	Hit family protein
Q9KMY2	VC_A0184	cspE Cold shock DNA-binding domain protein
Q9KL45	VC_A0903	Uncharacterized protein glycertae kinase
Q9KRM7	VC_1609	Uncharacterized protein ABC-2 type transport system permease
Q9KSC1	VC_1337	Citrate synthase
Q9KLD9	VC_A0807	ABC transporter, periplasmic substrate-binding protein
Q9KT63	VC_1042	Long-chain fatty acid transport protein
Q9KN12	VC_A0154	Uncharacterized protein Na+:H+ antiporter subunit E
Q9KN05	tnaA	Tryptophanase
Q9KS94	queE	7-carboxy-7-deazaguanine synthase
Q9KQI2	tmk	Thymidylate kinase
Q9KVP6	ubiC	Probable chorismate pyruvate-lyase
Q9KMP2	VC_A0281	Integrase
Q9KUW3	VC_0396	Transcriptional regulator, LuxR family
Q9KUK3	VC_0515	Uncharacterized protein
Q9KSC8	VC_1330	Uncharacterized protein
Q9KUQ7	VC_0458	UPF0235 protein yggU

I – 2. MoreF606wt_ThanJ420tgt			log2FC WT/tgt	p value	Adjusted p value
Q9KTJ4	gmhB	D-glycero-beta-D-manno-heptose-1,7-bisphosphate 7-phosphatase	3,51	0,0001	0,0005
Q9KTU3	VC_0795	Citrate/sodium symporter	3,46	0,0085	0,0068
Q9KSB4	VC_1345	Putative dioxygenase	3,35	0,0024	0,0034
Q9KS61	cheR2	Chemotaxis protein methyltransferase	2,93	0,0053	0,0050
Q9KN74	VC_A0091	UPF0251 protein VC_A0091	2,86	0,0013	0,0025
Q9KR81	VC_1762	EH_Signature domain-containing protein	2,54	0,0023	0,0034
Q9KM90	VC_A0491	Uncharacterized protein	2,26	0,0013	0,0025
Q9KQ10	VC_2197	Flagellar hook protein FlgE	2,23	0,0036	0,0042
Q9KVI7	murI	Glutamate racemase	2,11	0,0015	0,0028
Q9KV46	VC_0312	NAD(P)H-flavin reductase	2,10	0,0004	0,0014
Q9KL60	VC_A0888	Transcriptional regulator malT , LuxR family	2,01	0,0038	0,0042
Q9KSV5	VC_1151	Uncharacterized protein lysO	1,85	0,0003	0,0012
Q9KUR5	VC_0450	Membrane-bound lytic murein transglycosylase C	1,81	0,0057	0,0052
Q9KVM8	VC_0113	ubiG? Methyltransferase-related protein	1,76	0,0047	0,0046
Q9KPC7	VC_2445	gspA General secretion pathway protein A	1,75	0,0039	0,0042
Q9KNL2	nfuA	Fe/S biogenesis protein NfuA	1,68	0,0010	0,0022
Q9KVI5	VC_0161	Transcriptional activator IlvY	1,63	0,0128	0,0090
Q9KL10	VC_A0940	Transcriptional regulator, DeoR family	1,62	0,0003	0,0012
Q9KR73	VC_1770	Uncharacterized protein	1,52	0,0112	0,0082
Q9KKR5	VC_A1037	Amino acid ABC transporter, ATP-binding protein	1,43	0,0080	0,0065
H9L4R1	VC_0412	MshO Uncharacterized protein	1,43	0,0094	0,0071
Q9KKN4	VC_A1068	LRP Transcriptional regulator, AsnC family	1,43	0,0061	0,0053
P45784	epsN	Type II secretion system protein N	1,38	0,0022	0,0034
Q9KU51	VC_0673	Probable membrane transporter protein	1,37	0,0076	0,0063
Q9KNR9	VC_2662	Uncharacterized protein	1,24	0,0008	0,0019
Q9KRY1	rsmF	Ribosomal RNA small subunit methyltransferase F	1,18	0,0060	0,0053
Q9KLX1	VC_A0620	Thiosulfate sulfurtransferase SseA, putative	1,10	0,0020	0,0034
Q9KV88	VC_0268	ygaJ Uncharacterized protein	1,09	0,0070	0,0060
Q9KPI7	VC_2380	Cobalamin biosynthesis protein CbiB, putative	1,00	0,0042	0,0042
I – 3. PresentF606TOB_AbsentJ420TOB					
P0C6D1	irgB	Iron-regulated virulence regulatory protein IrgB			
P0C6D6	tcpN	TCP pilus virulence regulatory protein			
Q56632	vibA	Vibriobactin-specific 2,3-dihydro-2,3-dihydroxybenzoate dehydrogenase			
Q9KKP3	VC_A1059	Putative pseudouridine methyltransferase			
Q9KL40	hutX	Intracellular heme transport protein HutX			
Q9KLG0	fabV2	Enoyl-[acyl-carrier-protein] reductase [NADH] 2			
Q9KLJ6	glpB	Anaerobic glycerol-3-phosphate dehydrogenase subunit B			
Q9KLR1	VC_A0681	33-cGAMP-specific phosphodiesterase 1			
Q9KMY6	pepT	Peptidase T			
Q9KNL4	bioH	Pimeloyl-[acyl-carrier protein] methyl ester esterase			
Q9KPE3	coaE	Dephospho-CoA kinase			
Q9KRQ1	VC_1585	Catalase			

Q9KS61	cheR2	Chemotaxis protein methyltransferase 2
Q9KSB4	VC_1345	Putative dioxygenase
Q9KSW7	hisI	Histidine biosynthesis bifunctional protein HisIE
Q9KTY9	tgt	Queuine tRNA-ribosyltransferase
Q9KU27	VC_0702	Inosine/xanthosine triphosphatase
H9L4T3	VC_2212	Uncharacterized protein
Q9K2M8	VC_A0348	Uncharacterized protein
Q9KKK0	VC_A1105	DNA-binding response regulator
Q9KKX8	VC_A0972	MFS domain-containing protein
Q9KL71	VC_A0876	D-serine deaminase activator
Q9KLB3	VC_A0833	Transcriptional regulator, LysR family
Q9KLG6	VC_A0778	AHS2 domain-containing protein
Q9KLK5	VC_A0738	Uncharacterized protein
Q9KLK9	VC_A0734	Uncharacterized protein
Q9KLQ1	VC_A0691	Acetoacetyl-CoA reductase
Q9KM02	VC_A0587	PPC domain-containing protein
Q9KM77	VC_A0511	Anaerobic ribonucleoside-triphosphate reductase
Q9KM86	VC_A0496	Glutathione S-transferase, putative
Q9KM98	VC_A0483	Uncharacterized protein
Q9KMX3	VC_A0193	Na+/H+ antiporter, putative
Q9KN01	VC_A0165	GGDEF family protein
Q9KN09	VC_A0157	NADH dehydrogenase, putative
Q9KN25	VC_A0141	C4-dicarboxylate transport sensor protein, putative
Q9KN46	VC_A0119	ImpA_N domain-containing protein
Q9KN85	VC_A0080	GGDEF family protein
Q9KN89	VC_A0076	Gate domain-containing protein
Q9KN99	VC_A0066	Uncharacterized protein
Q9KNA1	VC_A0064	TonB system receptor, putative
Q9KNA2	VC_A0063	Protease II
Q9KNB4	VC_A0051	Uncharacterized protein
Q9KNE3	VC_A0022	Glutathione S-transfersae-related protein
Q9KNF6	VC_A0008	Methyl-accepting chemotaxis protein
Q9KNM6	VC_2706	Probable queuosine precursor transporter
Q9KNN0	VC_2702	Transcriptional regulator, LuxR family
Q9KPD7	cpdA	3,5-cyclic adenosine monophosphate phosphodiesterase CpdA
Q9KPJ7	VC_2370	Sensory box/GGDEF family protein
Q9KPR2	VC_2304	Uncharacterized protein
Q9KPY8	VC_2224	GGDEF family protein
Q9KQ04	VC_2203	Flagellar protein, putative
Q9KQ78	fliP	Flagellar biosynthetic protein FliP
Q9KQN1	VC_1967	Methyl-accepting chemotaxis protein
Q9KQQ9	VC_1939	Uncharacterized protein
Q9KQW7	VC_1880	DUF2062 domain-containing protein
Q9KR48	VC_1798	Eha protein
Q9KRH6	VC_1666	VIBCH ABC transporter, ATP-binding protein, putative

Q9KRJ6	VC_1644	Uncharacterized protein
Q9KRL9	VC_1617	Transcriptional regulator, LysR family
Q9KRN2	VC_1604	Transcriptional regulatory protein
Q9KRW9	VC_1515	Chaperone, formate dehydrogenase-specific, putative
Q9KSC1	VC_1337	Citrate synthase
Q9KSC6	VC_1332	Uncharacterized protein
Q9KSC9	VC_1329	Opacity protein-related protein
Q9KSE2	VC_1315	Sensor histidine kinase
Q9KSP0	VC_1216	GGDEF family protein
Q9KSV5	VC_1151	Uncharacterized protein
Q9KT20	VC_1085	Sensor histidine kinase
Q9KT74	VC_1031	Inosine monophosphate dehydrogenase-related protein
Q9KTC3	VC_0979	Oxidoreductase, short-chain dehydrogenase/reductase family
Q9KTI4	VC_0918	UDP-N-acetyl-D-mannosaminuronic acid dehydrogenase
Q9KTV0	VC_0787	Transcriptional regulator, LysR family
Q9KU51	VC_0673	Probable membrane transporter protein
Q9KUQ1	VC_0464	Transcriptional regulator, LuxR family
Q9KUW6	VC_0393	Uncharacterized protein
Q9KV54	VC_0303	Sensor histidine kinase
Q9KVM2	VC_0119	Uroporphyrinogen-III synthase
Q9KVM8	VC_0113	Methyltransferase-related protein
Q9KVP4	VC_0097	Flagellar protein FliL
Q9KVS6	VC_0063	ThiF protein

I – 4. MoreF606TOB_ThanJ420TOB			**log2 FC WT/tgt**	**p value**	**Adjusted p value**
Q9KMV8	VC_A0210	33-cGAMP-specific phosphodiesterase 2	5,21	0,00000	0,00005
Q9KSR2	VC_1194	J domain-containing protein	3,68	0,00929	0,00488
Q9KKY6	VC_A0964	Glycine cleavage operon activator, putative	5,30	0,00002	0,00043
Q9KKL6	VC_A1087	Anti-sigma F factor antagonist, putative	3,72	0,00060	0,00202
Q9KSK7	VC_1249	ACT domain-containing protein	2,37	0,00973	0,00488
Q9KS89	VC_1370	GGDEF family protein	3,51	0,00007	0,00062
Q9KNA0	VC_A0065	P/Homo B domain-containing protein	3,48	0,00876	0,00488
Q9KT21	VC_1084	Sensory box sensor histidine kinase	1,77	0,00183	0,00235
Q9KRA1	VC_1741	Transcriptional regulator, TetR family	1,71	0,01423	0,00606
Q9KU00	cutC	Copper homeostasis protein CutC	1,85	0,01810	0,00696
Q9KTH7	VC_0925	Polysaccharide biosynthesis protein, putative	3,09	0,00236	0,00256
Q9KSD3	VC_1325	Galactoside ABC transporter, periplasmic D-galactose/D-glucose-binding protein SV=1"	1,77	0,02018	0,00745
Q9KUU2	arcA	ARCA_VIBCH Arginine deiminase	2,78	0,00191	0,00235
Q9KLB8	phhA	PH4H_VIBCH Phenylalanine-4-hydroxylase	2,16	0,03098	0,00967
Q9KPI7	VC_2380	Cobalamin biosynthesis protein CbiB, putative	1,83	0,00973	0,00488
Q9KSE3	VC_1314	Transporter, putative	2,64	0,02472	0,00834
Q9KQX3	VC_1874	Uncharacterized protein	2,66	0,00403	0,00309
Q9KMJ2	VC_A0356	Uncharacterized protein	2,60	0,00439	0,00321
Q9KRW3	VC_1521	Sensor histidine kinase	2,69	0,00011	0,00085

Q9KN34	rbsK	Ribokinase	2,49	0,00270	0,00269
Q9KQX5	VC_1872	AAA_PrkA domain-containing protein	2,94	0,00216	0,00245
Q9KS12	rtxA	Multifunctional-autoprocessing repeats-in-toxin	3,68	0,01920	0,00716
Q9KQ01	VC_2206	Uncharacterized protein	2,76	0,00003	0,00043
P45774	epsH	Type II secretion system protein H	2,58	0,02202	0,00772
Q9KU02	VC_0728	PPK2 domain-containing protein	3,08	0,01270	0,00574
Q9KKL7	VC_A1086	Response regulator	2,65	0,02350	0,00806
Q9KSG5	VC_1291	Uncharacterized protein	3,38	0,00096	0,00223
Q9KSV0	VC_1156	Sensor histidine kinase	2,48	0,00113	0,00224
Q9KN48	VC_A0117	Sigma-54 dependent transcriptional regulator	1,56	0,00974	0,00488
Q9KRG0	VC_1682	Peptide ABC transporter, permease protein	2,56	0,00020	0,00109
Q9KRG1	VC_1681	Peptide ABC transporter, permease protein	2,86	0,00015	0,00099
Q9KSD1	mglA	Galactose/methyl galactoside import ATP-binding protein MglA	2,08	0,02068	0,00754
Q9KLT8	VC_A0653	PTS system, sucrose-specific IIBC component	2,43	0,00003	0,00043
P0C6Q8	dam	DNA adenine methylase	2,26	0,00448	0,00324
P0C6D3	vibB	Vibriobactin-specific isochorismatase	2,32	0,00194	0,00235
Q9KLF1	VC_A0795	Resolvase, putative	2,33	0,00078	0,00215
Q9KNN7	VC_2694	Superoxide dismutase	1,34	0,00647	0,00419
Q9KNW3	VC_2617	Arginine N-succinyltransferase OS=Vibrio cholerae serotype	1,27	0,02884	0,00915
Q9KUA1	VC_0622	Histidine kinase	1,89	0,00950	0,00488
Q9KQX9	VC_1868	Methyl-accepting chemotaxis protein	2,27	0,01417	0,00606
Q9KS63	VC_1397	Chemotaxis protein CheA	2,42	0,02557	0,00852
Q9KR16	VC_1831	Sensor histidine kinase	2,54	0,00188	0,00235
Q9KKR5	VC_A1037	Amino acid ABC transporter, ATP-binding protein	1,56	0,02096	0,00754
Q9KPK6	grcA	GRCA_VIBCH Autonomous glycyl radical cofactor	2,66	0,00332	0,00269
Q9KQX4	VC_1873	UPF0229 protein VC_1873	2,70	0,02180	0,00770
Q9KTI9	VC_0913	HlyD_D23 domain-containing protein	1,71	0,02570	0,00852
Q9KTC7	VC_0975	NfeD domain-containing protein	2,07	0,00048	0,00177
Q9KU65	VC_0658	C-di-GMP phosphodiesterase A-related protein	2,14	0,00930	0,00488
Q9KNB6	VC_A0049	GGDEF family protein	2,45	0,00175	0,00235
Q9KNY0	VC_2600	Uncharacterized protein	1,81	0,00123	0,00224
Q9KTF2	mrdA	Peptidoglycan D,D-transpeptidase MrdA	1,65	0,01002	0,00488
Q9KQY2	VC_1865	Uncharacterized protein	1,78	0,00316	0,00269
Q9KL39	VC_A0909	Oxygen-independent coproporphyrinogen III oxidase, putative	2,04	0,01389	0,00602
Q9KVF6	VC_0190	DNA helicase uvrD	1,94	0,01686	0,00663
Q9KUM9	VC_0486	Transcriptional regulator, DeoR family	1,92	0,03066	0,00961
Q9KRI2	VC_1659	Uncharacterized protein	2,10	0,01469	0,00612
Q9KNJ0	VC_2748	Nitrogen regulation protein	1,87	0,00126	0,00224
Q9KP22	VC_2557	Uncharacterized protein OS	1,81	0,00291	0,00269
Q9KRV1	VC_1533	DTW domain-containing protein	1,83	0,00205	0,00235
Q9KQC8	VC_2072	Peptidase, insulinase family	1,58	0,00893	0,00488
Q9KUM3	VC_0492	Uncharacterized protein	2,34	0,00243	0,00259
Q9KQI3	VC_2015	DNA polymerase III, delta prime subunit	1,77	0,00063	0,00202
Q9KPT7	crl	Sigma factor-binding protein Crl	1,58	0,00088	0,00219

Q9KS69	VC_1390	Transcriptional regulator, LysR family	1,89	0,00007	0,00062
Q9KSC3	VC_1335	Transcriptional regulator, GntR family	1,55	0,00321	0,00269
Q9KRL1	VC_1629	Uncharacterized protein	1,89	0,00322	0,00269
Q9KLS5	VC_A0666	L-serine dehydratase	1,71	0,00079	0,00215
Q9KM52	VC_A0537	Uncharacterized protein	1,27	0,01088	0,00511
Q9KRI6	VC_1655	Magnesium transporter MgtE	1,72	0,00363	0,00282
Q9KTJ1	VC_0911	Trehalose-6-phosphate hydrolase	1,70	0,00042	0,00166
Q9KPZ9	VC_2208	Uncharacterized protein	1,79	0,01534	0,00629
Q9KM32	VC_A0557	GGDEF family protein	1,37	0,02135	0,00762
Q9KSA6	VC_1353	GGDEF family protein	1,52	0,00156	0,00231
Q9KUC2	VC_0600	AB hydrolase-1 domain-containing protein	1,72	0,00123	0,00224
Q9KM15	VC_A0574	N-acetyltransferase domain-containing protein	1,39	0,01767	0,00683
Q9KS83	VC_1376	GGDEF family protein	1,51	0,00363	0,00282
Q9KPT2	VC_2280	Uncharacterized protein	1,45	0,00471	0,00331
Q9KVN8	VC_0103	Uncharacterized protein	1,55	0,00249	0,00262
Q9KT24	VC_1081	Response regulator	1,65	0,02632	0,00861
Q9KRJ1	VC_1649	Trypsin, putative	1,54	0,00092	0,00220
Q9KLP6	VC_A0697	Sensory box/GGDEF family protein	1,63	0,00022	0,00109
Q9KQ23	ispE	ISPE_VIBCH 4-diphosphocytidyl-2-C-methyl-D-erythritol kinase ispE	1,57	0,00119	0,00224
H9L4T1	VC_A0450	Uncharacterized protein	1,76	0,00290	0,00269
Q9KU16	VC_0714	Uncharacterized protein	1,60	0,02409	0,00820
Q9KRS6	katG	KATG_VIBCH Catalase-peroxidase katG	1,39	0,01256	0,00571
P29485	tcpP	Toxin coregulated pilus biosynthesis protein P tcpP	1,56	0,00124	0,00224
Q9KU53	rppH	RPPH_VIBCH RNA pyrophosphohydrolase rppH	2,03	0,00467	0,00331
Q9KKX3	VC_A0977	ABC transporter, ATP-binding protein	1,84	0,02092	0,00754
Q9KQL5	VC_1983	Peptidase, putative	2,47	0,02205	0,00772
Q9KSG0	VC_1296	Phosphomethylpyrimidine kinase	3,54	0,00005	0,00054
Q9KPJ4	VC_2373	Glutamate synthase, large subunit	1,53	0,00120	0,00224
Q9KS96	VC_1363	Siroheme synthase component enzyme	1,31	0,00930	0,00488
Q9KP89	VC_2484	Long-chain-fatty-acid--CoA ligase, putative	1,53	0,00535	0,00367
Q9KSM2	VC_1234	Exodeoxyribonuclease I	1,59	0,02087	0,00754
Q9KSX5	VC_1131	Na_H_antiporter domain-containing protein	2,07	0,01089	0,00511
Q9KTJ2	VC_0910	PTS system, trehalose-specific IIBC component	1,33	0,00205	0,00235
Q9KKZ7	VC_A0953	Peptidyl-prolyl cis-trans isomerase C	1,30	0,00997	0,00488
Q9KUU7	VC_0418	dTTP/UTP pyrophosphatase	1,24	0,00258	0,00267
Q9KV39	birA	Bifunctional ligase/repressor BirA	1,47	0,00649	0,00419
Q9KS28	VC_1433	Uncharacterized protein	1,23	0,00965	0,00488
Q9KMM4	VC_A0307	HNHc domain-containing protein	1,46	0,00110	0,00224
Q9KUJ8	VC_0522	Beta-ketoadipate enol-lactone hydrolase, putative	1,37	0,00202	0,00235
Q9KVT7	purE	N5-carboxyaminoimidazole ribonucleotide mutase	1,45	0,00886	0,00488
Q9KRU5	VC_1539	Probable ketoamine kinase VC_1539	1,09	0,01619	0,00652
Q9KSU7	serC	Phosphoserine aminotransferase	1,41	0,00147	0,00231
Q9KQU2	VC_1906	Methyltranfer_dom domain-containing protein	2,00	0,00065	0,00202
Q9KRW4	VC_1520	ABC transporter, ATP-binding protein	1,17	0,00887	0,00488
Q9KU52	VC_0672	Phosphoenolpyruvate-protein phosphotransferase	1,41	0,00145	0,00231
Q9KLI6	VC_A0758	Arginine ABC transporter, permease protein	1,24	0,01152	0,00534

Q9KPQ9	panE	2-dehydropantoate 2-reductase	1,32	0,02013	0,00745
Q9KNW7	VC_2613	Phosphoribulokinase	1,22	0,00346	0,00278
Q9KT18	VC_1087	Response regulator	1,12	0,00908	0,00488
Q9KPP6	recB	RecBCD enzyme subunit RecB	1,24	0,00085	0,00218
Q9KQK1	VC_1997	Uncharacterized protein	1,16	0,00200	0,00235
Q9KUN3	argP	ARGP_VIBCH HTH-type transcriptional regulator ArgP	1,53	0,00885	0,00488
Q9KMW8	VC_A0198	Site-specific DNA-methyltransferase, putative	1,15	0,00300	0,00269
Q9KVB8	VC_0228	Uncharacterized protein	1,27	0,00223	0,00248
Q9KVE7	VC_0199	Hemolysin secretion ATP-binding protein, putative	1,29	0,00999	0,00488
Q9KQM5	menB	1,4-dihydroxy-2-naphthoyl-CoA synthase menB	1,40	0,00328	0,00269
Q9KR89	VC_1753	Paraquat-inducible protein A	1,11	0,00739	0,00467
Q9KQJ7	VC_2001	Putative glucose-6-phosphate 1-epimerase	1,57	0,01040	0,00501
P57070	lolB	Outer-membrane lipoprotein LolB	1,04	0,01285	0,00577
Q9KL63	VC_A0884	Uncharacterized protein	1,15	0,02695	0,00863
H9L4P1	VC_0259	Lipopolysaccharide biosynthesis protein RfbV	1,21	0,00560	0,00377
Q9KMU4	VC_A0225	Glutamine amidotransferase type-2 domain-containing protein	1,14	0,00164	0,00235
Q9KKU5	VC_A1005	Transcriptional regulator, MarR family	1,14	0,02484	0,00834
Q9KVK1	VC_0142	DUF4145 domain-containing protein	1,20	0,01451	0,00609
Q9KVB5	VC_0231	Uncharacterized protein	1,09	0,00932	0,00488
Q9KKS4	VC_A1026	Uncharacterized protein	1,31	0,00883	0,00488
Q9KUU0	VC_0425	Uncharacterized protein	1,54	0,01872	0,00702
Q9KTA5	VC_0998	Uncharacterized protein	1,15	0,00530	0,00367
Q9KNC4	gltS	Sodium/glutamate symporter	1,21	0,02667	0,00862
Q9KRS8	VC_1558	6-phospho-beta-glucosidase	1,37	0,00196	0,00235
Q9KMT9	VC_A0230	Iron(III) ABC transporter, ATP-binding protein	1,08	0,01196	0,00547
Q9KPZ0	VC_2222	Smr domain-containing protein	1,04	0,02562	0,00852
Q9KQE2	VC_2058	Uncharacterized protein	1,05	0,00651	0,00419
P57066	lolD	LOLD_VIBCH Lipoprotein-releasing system ATP-binding protein LolD	1,01	0,00981	0,00488
Q9KLE5	VC_A0801	Q9KLE5_VIBCH Inosine-guanosine kinase	1,00	0,02622	0,00861
Q9KS35	VC_1426	Spermidine/putrescine ABC transporter, permease protein	1,11	0,00158	0,00231
Q9KSV4	VC_1152	HDOD domain-containing protein	1,07	0,00926	0,00488
Q9KUM2	VC_0493	Q9KUM2_VIBCH Uncharacterized protein	1,76	0,01375	0,00600
Q9KNA9	VC_A0056	Q9KNA9_VIBCH Transcriptional regulator, MerR family	1,07	0,01454	0,00609
Q9KQ71	VC_2130	Flagellum-specific ATP synthase FliI	1,15	0,00357	0,00282
Q9KLD8	VC_A0808	NodN-related protein	1,27	0,00802	0,00488
Q9KP78	VC_2497	HD-GYP domain-containing protein	1,09	0,00149	0,00231
Q60153	tcpA	TCPA_VIBCH Toxin coregulated pilin	1,01	0,02653	0,00862
Q9KRU1	VC_1543	Uncharacterized protein	1,09	0,00268	0,00269
Q9KQ38	VC_2166	Trp repressor-binding protein	1,46	0,01086	0,00511
Q9KQN3	VC_1965	TetR_C_33 domain-containing protein	1,28	0,00698	0,00445
Q9KN86	VC_A0079	Uncharacterized protein	1,23	0,00556	0,00377
Q9KRD3	VC_1709	Zinc protease, insulinase family	1,25	0,00993	0,00488
Q9KKS7	VC_A1023	Uncharacterized protein	1,16	0,00537	0,00367

Q9KVB7	VC_0229	Uncharacterized protein	1,66	0,01838	0,00696
Q9KNR2	VC_2669	5-carboxymethyl-2-hydroxymuconate delta isomerase, putative	1,22	0,01524	0,00628
Q9KUI6	mutS	MUTS_VIBCH DNA mismatch repair protein MutS	1,07	0,00298	0,00269
Q9KVF0	VC_0196	ATP-dependent DNA helicase RecQ	1,04	0,00303	0,00269
Q9KTJ3	VC_0909	Trehalose operon repressor	1,03	0,00981	0,00488
Q9KVH1	VC_0175	Deoxycytidylate deaminase-related protein	1,28	0,01307	0,00584
Q9KR77	VC_1766	Uncharacterized protein	1,01	0,01408	0,00606
Q9KTL4	truC	tRNA pseudouridine synthase C truC	1,09	0,00416	0,00310
Q9KUM4	VC_0491	Uncharacterized protein	1,10	0,00571	0,00379
P52022	dnaE	DNA polymerase III subunit alpha	1,07	0,00324	0,00269
Q9KP97	VC_2476	UPF0149 protein VC_2476	1,70	0,02715	0,00865
Q9KS92	VC_1367	GGDEF family protein	1,19	0,00957	0,00488
Q9KU08	ppx	Exopolyphosphatase ppx	1,04	0,01694	0,00663
Q9KSI6	VC_1270	Glyoxylase II family protein	1,32	0,01645	0,00653
Q9KRA6	bpt	Aspartate/glutamate leucyltransferase bpt	1,04	0,01838	0,00696
Q9KQF5	topB	DNA topoisomerase 3 topB	1,05	0,02938	0,00928
Q9KNF3	malT	HTH-type transcriptional regulator MalT	1,10	0,00227	0,00249
Q9KPE8	VC_2420	Flavodoxin	1,39	0,00897	0,00488
Q9KNT4	ppc	Phosphoenolpyruvate carboxylase ppc	1,05	0,00302	0,00269
Q9KU29	VC_0700	Soluble lytic murein transglycosylase	1,07	0,00291	0,00269
Q9KQV0	VC_1898	Methyl-accepting chemotaxis protein	1,01	0,00574	0,00379
Q9KPE7	VC_2421	ampD protein	1,04	0,02430	0,00824
Q9KU20	rluD	Ribosomal large subunit pseudouridine synthase D rluD	1,03	0,00290	0,00269
Q9KNQ5	VC_2676	Cell division protein FtsN, putative	1,20	0,01452	0,00609
H9L4T5	VC_0847	Integrase, phage family	1,28	0,02687	0,00863
Q9KQ28	VC_2176	UPF0162 protein VC_2176	1,04	0,00311	0,00269
Q9KUC0	mrcB	PBPB_VIBCH Penicillin-binding protein 1B	1,15	0,01050	0,00502
Q9KPV6	uppS	UPPS_VIBCH Ditrans,polycis-undecaprenyl-diphosphate synthase	1,03	0,00800	0,00488
Q9KVU5	rsmB	RSMB_VIBCH Ribosomal RNA small subunit methyltransferase B	1,02	0,01178	0,00542
Q9KMC3	VC_A0441	Uncharacterized protein	1,17	0,00930	0,00488
Q9KVL9	VC_0122	Adenylate cyclase	1,23	0,02356	0,00806
Q9KUW9	metH	Methionine synthase	1,28	0,02670	0,00862
Q9KL09	VC_A0941	Acyl-CoA thioester hydrolase-related protein	1,03	0,02584	0,00853
Q9KMY4	VC_A0182	Sigma-54 dependent transcriptional regulator	1,00	0,00859	0,00488
Q9KQ13	flgH	Flagellar L-ring protein	1,06	0,01335	0,00593
Q9KT38	VC_1067	GGDEF domain-containing protein	1,04	0,02971	0,00935
Q9KM78	VC_A0510	Uncharacterized protein	1,01	0,01640	0,00653
P0C6R0	irgA	IRGA_VIBCH Iron-regulated outer membrane virulence protein	1,03	0,02028	0,00745
Q9KPD8	VC_2432	Uncharacterized protein	1,23	0,03115	0,00968
Q9KVS4	thiG	THIG_VIBCH Thiazole synthase	1,50	0,03191	0,00983
Q9KMG4	higA-1	Antitoxin HigA-1	1,30	0,01712	0,00665
Q9KUY5	VC_0373	Uncharacterized protein	1,25	0,02357	0,00806
Q9KMG8	VC_A0388	Uncharacterized protein	1,58	0,00081	0,00215

Uniprot	Gene Name	Fasta headers			
		II - More abundant in *Δtgt*			
		II – 1. PresentJ420tgt_AbsentF606wt			
O34419	rstR1	Cryptic phage CTXphi transcriptional repressor RstR			
Q9KN37	rbsA	Ribose import ATP-binding protein RbsA			
Q9KT77	moaE	Molybdopterin synthase catalytic subunit			
Q9KVG9	vspR	Transcriptional regulator VspR			
H9L4R3	VC_A0444	RelE protein			
Q9KKW7	VC_A0983	L-lactate permease			
Q9KL14	VC_A0935	Uncharacterized protein			
Q9KLD8	VC_A0808	NodN-related protein			
Q9KLF6	VC_A0788	DnaJ-related protein			
Q9KLJ2	VC_A0752	Thioredoxin 2			
Q9KLV6	VC_A0635	Transcriptional regulator, LysR family			
Q9KM02	VC_A0587	PPC domain-containing protein			
Q9KM27	VC_A0562	Uncharacterized protein			
Q9KMP9	VC_A0271	Uncharacterized protein			
Q9KNC6	VC_A0039	Uncharacterized protein			
Q9KNE3	VC_A0022	Glutathione S-transfersae-related protein			
Q9KNI2	VC_2757	Uncharacterized protein			
Q9KNM7	VC_2705	Sodium/solute symporter, putative			
Q9KPF0	VC_2418	Thiol:disulfide interchange protein			
Q9KQ76	VC_2125	Flagellar motor switch protein FliN			
Q9KQG6	VC_2032	Uncharacterized protein			
Q9KQS3	VC_1925	C4-dicarboxylate transport sensor protein			
Q9KR71	VC_1772	WYL domain-containing protein			
Q9KRG4	VC_1678	Phage shock protein A			
Q9KRH0	VC_1672	DNA-3-methyladenine glycosidase I			
Q9KRM1	VC_1615	Uncharacterized protein			
Q9KRR5	VC_1571	Quinol oxidase, subunit I			
Q9KSM4	VC_1232	Uncharacterized protein			
Q9KSN9	VC_1217	N-acetyltransferase domain-containing protein			
Q9KTS9	VC_0809	SWIM-type domain-containing protein			
Q9KTV0	VC_0787	Transcriptional regulator, LysR family			
Q9KUN2	VC_0483	Uncharacterized protein			
Q9KUW6	VC_0393	Uncharacterized protein			
Q9KVR9	VC_0070	Uncharacterized protein			
		II – 2. MoreJ420tgt_ThanF606wt	**log2 wt/tgt**	**p value**	**Adjusted p value**
Q9KNX3	kefG	Glutathione-regulated potassium-efflux system ancillary protein KefG	-7,30	0,00001	0,00036
Q9KLB8	phhA	Phenylalanine-4-hydroxylase	-4,14	0,00010	0,00068
P09545	hlyA	Hemolysin	-3,90	0,00039	0,00140

Q9KQN1	VC_1967	Methyl-accepting chemotaxis protein	-3,84	0,00567	0,00521
Q9KV16	queG	Epoxyqueuosine reductase	-3,39	0,00416	0,00420
H9L4T3	VC_2212	Uncharacterized protein - putative Fe3+-citrate ABC transporter	-3,32	0,00017	0,00094
Q9KTJ9	syd	Syd	-3,29	0,00057	0,00177
Q9KNW3	VC_2617	Arginine N-succinyltransferase	-2,93	0,00002	0,00050
Q9KU56	mutH	DNA mismatch repair protein MutH	-2,90	0,00004	0,00050
Q9KTZ6	VC_0734	Malate synthase	-2,81	0,00306	0,00389
Q9KKQ7	mtlA	PTS system mannitol-specific EIICBA component	-2,80	0,00214	0,00343
Q9KLB3	VC_A0833	Transcriptional regulator, LysR family	-2,66	0,00379	0,00420
Q9KTM2	VC_0880	Uncharacterized protein	-2,50	0,00364	0,00420
Q9KSQ4	hutH	Histidine ammonia-lyase	-2,42	0,00105	0,00227
Q9KPR5	VC_2301	Transcriptional activator, putative	-2,39	0,00075	0,00195
Q9KNF6	VC_A0008	Methyl-accepting chemotaxis protein	-2,27	0,00264	0,00357
Q9KRF2	VC_1690	Alpha-1,6-galactosidase, putative	-2,25	0,00022	0,00110
Q9KS52	VC_1408	Transcriptional regulator, TetR family	-2,20	0,00047	0,00154
Q9KUN3	argP	HTH-type transcriptional regulator ArgP	-2,20	0,00006	0,00050
Q9KU74	VC_0649	Transcriptional regulator, MarR family	-2,08	0,00232	0,00343
Q9KRA1	VC_1741	Transcriptional regulator, TetR family	-2,03	0,00074	0,00195
Q9KQ71	VC_2130	Flagellum-specific ATP synthase FliI	-1,89	0,00016	0,00094
Q9KUU2	arcA	Arginine deiminase	-1,88	0,00990	0,00732
Q9KM69	VC_A0519	Fructose repressor	-1,80	0,00183	0,00331
Q9KS51	VC_1409	Multidrug resistance protein, putative	-1,77	0,00895	0,00699
Q9KS17	VC_1444	Uncharacterized protein	-1,73	0,01228	0,00882
P0C6Q5	tcpF	Toxin coregulated pilus biosynthesis protein F	-1,72	0,00006	0,00050
Q9KVH8	VC_0168	Cytochrome c5	-1,65	0,00187	0,00331
Q9KP69	VC_2507	PINc domain-containing protein	-1,62	0,00903	0,00699
Q9KM51	VC_A0538	Cytochrome b561, putative	-1,62	0,00417	0,00420
Q9KTY1	VC_0749	Iron-sulfur cluster assembly scaffold protein IscU	-1,59	0,00072	0,00195
Q9KMJ5	VC_A0351	Uncharacterized protein	-1,56	0,00615	0,00534
Q9KS13	VC_1449	Uncharacterized protein	-1,54	0,01266	0,00895
Q9KLM0	VC_A0723	3-hydroxy-3-methylglutaryl CoA reductase	-1,53	0,00266	0,00357
Q9KV51	VC_0306	Thioredoxin	-1,50	0,00255	0,00357
Q9KRR1	VC_1575	Uncharacterized protein	-1,32	0,00274	0,00358
Q9F854	hisD	Histidinol dehydrogenase	-1,28	0,00385	0,00420
Q9KUS1	pdxA	4-hydroxythreonine-4-phosphate dehydrogenase	-1,25	0,00082	0,00195
Q9KSI8	VC_1268	Uncharacterized protein	-1,13	0,00714	0,00600
Q9KPA8	VC_2465	Sigma-E factor regulatory protein RseB	-1,08	0,00400	0,00420
Q9KLG6	VC_A0778	AHS2 domain-containing protein	-1,08	0,00343	0,00420
Q9KVJ1	VC_0153	Uncharacterized protein	-1,05	0,00936	0,00708
	II – 3. PresentJ420tgtTOB_AbsentF606wtTOB				
Q9KNM4	gmk	Guanylate kinase			
Q9KNC1	VC_A0044	Uncharacterized protein put mb protease			
Q9KRS9	VC_1557	Transcriptional regulator, LacI family lipid A biosynthesis acyltransferase			

Q9KQH2	VC_2026	Uncharacterized protein rRNA accumulation protein YceD			
Q9KRR2	VC_1574	Uncharacterized protein put Transmembrane signal peptide protein			
Q9KT04	VC_1101	Uncharacterized protein putative tryptophan/tyrosine transport system substrate-binding protein or T6SS			
Q9KVH8	VC_0168	Cytochrome c5			
Q9KR31	VC_1816	Uncharacterized protein 1 HYP TRANSPORTER			
Q9KQN0	VC_1968	Transcriptional regulator, HTH_3 family sutR regulator utilization of sulfur			
Q9KNT7	argB	Acetylglutamate kinase ornithine and arginine biosynthesis			
Q9KU61	VC_0662	Branched-chain amino acid transport system carrier protein brnQ transport leucine, valine, and isoleucine			
Q9KPR5	VC_2301	Transcriptional activator, putative putative anti-ECFsigma factor, ChrR			
Q9KQ26	prmC	Release factor glutamine methyltransferase			
Q9KM00	VC_A0589	Peptide ABC transporter, permease protein, putative oligopeptide ABC transporter membrane subunit YejE			
Q9KVR7	VC_0072	Sensory box/GGDEF family protein			
II – 4. MoreJ420tgtTOB_ThanF606wtTOB			**log2 wt/tgt**	**p value**	**Adjusted p value**
Q9KSP4	VC_1212	DNA polymerase	-2,38	0,01099	0,00512
Q9KR61	nanK	N-acetylmannosamine kinase	-4,31	0,00003	0,00043
Q9KT86	rnfA/rsxA	Ion-translocating oxidoreductase complex subunit A	-3,56	0,00002	0,00043
Q9KRT1	VC_1555	Uncharacterized protein	-1,48	0,00902	0,00488
Q9KV51	VC_0306	Thioredoxin trxA	-1,69	0,02226	0,00776
Q9KM51	VC_A0538	Cytochrome b561, putative	-2,87	0,00756	0,00474
Q9KNR9	VC_2662	Uncharacterized protein	-1,31	0,03255	0,00995
Q9KR73	VC_1770	Uncharacterized protein	-1,31	0,01849	0,00696
P0C6C8	fur	Ferric uptake regulation protein	-2,39	0,00030	0,00141
Q9KMN5	VC_A0293	Uncharacterized protein	-2,14	0,00017	0,00099
Q9KV88	VC_0268	Uncharacterized protein	-2,11	0,00406	0,00309
Q9KNQ9	rraA	Regulator of ribonuclease activity A	-2,42	0,00310	0,00269
Q9KPZ5	VC_2217	Beta-N-acetylhexosaminidase	-2,91	0,00054	0,00191
Q9KTN7	tadA	tRNA-specific adenosine deaminase	-2,04	0,00110	0,00224
Q9KRP5	VC_1591	Oxidoreductase, short-chain dehydrogenase/reductase family	-2,14	0,00804	0,00488
P0C6C4	flaB	Flagellin B	-1,88	0,00131	0,00228
Q9KTZ8	VC_0732	Transcriptional regulator, LysR family oxyR like	-1,96	0,00070	0,00210
Q9KSV6	VC_1150	Uncharacterized protein	-1,29	0,01007	0,00488
Q9KVM9	VC_0112	Cytochrome c4	-2,60	0,01486	0,00616
Q9KVK6	cdgJ	Cyclic di-GMP phosphodiesterase CdgJ	-3,89	0,00017	0,00099
Q9KR96	VC_1746	Transcriptional regulator, TetR family	-1,85	0,00299	0,00269
P0C6C5	flaC	Flagellin C OS=Vibrio cholerae serotype	-1,82	0,00042	0,00166
Q9KPX7	VC_2235	Methyltransf_11 domain-containing protein	-1,53	0,00144	0,00231
Q9KL76	VC_A0871	Transcriptional regulator, GntR family	-1,20	0,00284	0,00269

Q9KQ58	VC_2146	Uncharacterized protein	-1,38	0,00181	0,00235
Q9KKP2	ribB	3,4-dihydroxy-2-butanone 4-phosphate synthase	-2,73	0,00036	0,00157
Q9KNL7	greB	Transcription elongation factor GreB	-2,29	0,02154	0,00765
Q9KV61	VC_0296	Biotin carboxyl carrier protein of acetyl-CoA carboxylase	-1,70	0,00429	0,00317
Q9KUN2	VC_0483	Uncharacterized protein	-1,46	0,00180	0,00235
P0C6P9	tpx	Thiol peroxidase	-1,42	0,01847	0,00696
Q9KN91	VC_A0074	GGDEF family protein	-1,35	0,00934	0,00488
Q9KV27	nudC	NADH pyrophosphatase	-1,38	0,00104	0,00224
Q9KTF3	mrdB	Peptidoglycan glycosyltransferase	-1,35	0,00766	0,00476
Q9F854	hisD	Histidinol dehydrogenase	-1,60	0,00994	0,00488
Q9KV12	miaA	tRNA dimethylallyltransferase	-1,44	0,00177	0,00235
Q9KT82	VC_1023	Putative gluconeogenesis factor	-1,72	0,02103	0,00754
Q9KKQ1	VC_A1051	Uncharacterized protein	-1,32	0,00452	0,00324
Q9KKZ9	VC_A0951	UPF0145 protein VC_A0951	-1,30	0,01376	0,00600
Q9KLK6	luxP	Autoinducer 2-binding periplasmic protein LuxP	-1,19	0,00413	0,00310
Q9KTX4	ndk	Nucleoside diphosphate kinase	-1,10	0,01640	0,00653
Q9KMJ8	VC_A0345	Uncharacterized protein	-1,18	0,01699	0,00663
Q9KU82	rimP	Ribosome maturation factor RimP	-1,24	0,01367	0,00600
Q9KSF3	VC_1303	Para-aminobenzoate synthase, component I	-1,14	0,02352	0,00806
Q9KS93	queC	7-cyano-7-deazaguanine synthase	-1,01	0,01568	0,00635
Q9KQM0	VC_1978	5-deoxynucleotidase	-1,18	0,00153	0,00231
Q9KST2	trpE	Anthranilate synthase component 1	-1,86	0,03127	0,00968
Q9KN74	VC_A0091	UPF0251 protein	-1,10	0,01555	0,00634
Q9KL95	VC_A0851	HATPase_c domain-containing protein	-1,55	0,00154	0,00231
Q9KNJ9	VC_2739	AsmA domain-containing protein	-1,16	0,03228	0,00991

Table S2. Ribosome profiling.

ID	log2FoldChange	p value adj
Transcripts UP		
VC_RS08405	5,16	2,54E-15
VC_RS08700	4,78	5,99E-03
glpD	4,19	1,40E-25
VC_RS00110	3,89	4,75E-13
VC_RS08400	3,83	3,23E-47
VC_RS07070	3,78	2,77E-05
VC_RS16920	3,64	9,32E-14
iscR	3,56	1,67E-24
VC_RS15320	3,47	4,97E-03
VC_RS16810	3,26	4,95E-04
hscB	3,14	6,58E-29
fadE	3,01	4,79E-14
siaQ	2,98	5,85E-06
VC_RS12540	2,90	2,09E-07
VC_RS15715	2,87	3,51E-03
VC_RS03415	2,76	5,14E-06
pdhR	2,69	4,02E-17
fadB	2,69	3,71E-16
VC_RS05835	2,66	2,21E-11
VC_RS12625	2,63	9,15E-17
VC_RS15780	2,57	3,00E-05
VC_RS06745	2,56	1,00E-03
VC_RS02460	2,53	4,43E-11
VC_RS15675	2,51	1,77E-07
VC_RS03375	2,50	3,27E-13
VC_RS15660	2,50	7,01E-08
VC_RS12840	2,45	1,93E-07
astA	2,43	3,51E-08
VC_RS18335	2,40	4,25E-05
VC_RS18385	2,40	6,53E-07
VC_RS18760	2,38	5,01E-03
VC_RS15265	2,37	1,85E-06
VC_RS15655	2,35	1,32E-08
VC_RS09590	2,34	2,10E-16
VC_RS17980	2,30	2,40E-07
rluC	2,30	3,62E-12
VC_RS08995	2,28	3,72E-05
VC_RS15750	2,25	9,78E-13
VC_RS06650	2,22	2,84E-03
VC_RS06240	2,21	3,77E-07
VC_RS17900	2,20	9,26E-06
dinB	2,19	6,60E-05
VC_RS16075	2,18	1,66E-06

glpK	2,13	5,64E-06
VC_RS03935	2,13	9,02E-06
VC_RS03750	2,13	3,89E-15
VC_RS09530	2,11	1,28E-03
iscA	2,10	7,00E-11
VC_RS18910	2,02	1,35E-03
VC_RS18595	2,00	3,76E-06
VC_RS06645	1,99	5,86E-04
VC_RS17880	1,97	1,27E-06
VC_RS17250	1,96	1,02E-04
VC_RS14235	1,95	7,29E-04
vpsQ	1,94	1,63E-05
VC_RS15795	1,92	3,27E-05
pncB	1,92	2,09E-11
VC_RS14320	1,91	3,76E-03
VC_RS19075	1,89	1,12E-06
VC_RS18065	1,88	2,22E-05
VC_RS05480	1,86	1,03E-03
VC_RS09310	1,86	1,69E-03
VC_RS16025	1,83	1,60E-07
VC_RS05200	1,82	3,76E-03
VC_RS06880	1,81	4,25E-06
VC_RS03615	1,81	9,36E-03
sdhC	1,80	8,98E-06
VC_RS12765	1,80	4,08E-06
vceC	1,77	2,69E-06
VC_RS08690	1,77	1,16E-03
VC_RS18420	1,75	4,95E-06
VC_RS06145	1,75	9,56E-08
VC_RS13705	1,73	3,89E-03
VC_RS09775	1,72	1,29E-05
VC_RS00830	1,72	2,06E-09
VC_RS15990	1,71	4,18E-04
astD	1,69	4,99E-05
rmuC	1,69	3,91E-06
cobA	1,67	6,18E-03
VC_RS06730	1,67	9,56E-03
VC_RS03925	1,67	2,64E-06
rpoE	1,65	3,06E-04
VC_RS13840	1,64	1,26E-06
pspC	1,62	5,50E-04
VC_RS05485	1,61	7,43E-04
VC_RS13775	1,60	2,22E-04
VC_RS13830	1,59	1,63E-05
VC_RS05795	1,59	8,95E-07
VC_RS04070	1,57	1,90E-04

pspA	1,55	6,11E-04
ectB	1,54	6,29E-03
VC_RS18060	1,53	9,22E-06
bioA	1,53	4,28E-03
VC_RS17350	1,50	2,41E-05
VC_RS16055	1,49	3,45E-04
VC_RS03930	1,49	2,68E-05
hppD	1,49	1,68E-03
rmf	1,48	6,04E-03
VC_RS18045	1,48	3,59E-03
pgl	1,47	3,65E-04
VC_RS09410	1,46	1,81E-03
VC_RS15825	1,46	8,01E-04
VC_RS01860	1,46	4,25E-03
VC_RS00045	1,46	2,22E-04
VC_RS08415	1,45	5,19E-05
thiC	1,44	3,32E-05
VC_RS03545	1,43	5,16E-04
VC_RS07590	1,42	2,00E-03
bioF	1,39	3,28E-05
vcrM	1,39	1,90E-03
VC_RS11130	1,38	4,37E-03
VC_RS13575	1,38	3,80E-03
thiD	1,37	1,07E-05
VC_RS17170	1,37	5,86E-04
VC_RS00235	1,37	1,19E-04
VC_RS06940	1,37	1,53E-05
purM	1,37	5,79E-04
emrD	1,35	1,37E-04
rpoS	1,32	9,84E-06
rpsN	1,31	5,86E-04
iscU	1,31	3,91E-04
VC_RS05395	1,30	3,89E-03
purN	1,30	6,54E-05
VC_RS08990	1,29	2,00E-03
truB	1,28	4,26E-04
rnc	1,28	4,81E-03
VC_RS16325	1,28	3,14E-03
miaB	1,25	1,55E-06
VC_RS00525	1,24	1,94E-03
VC_RS00310	1,24	2,05E-03
recN	1,23	1,53E-04
VC_RS00450	1,23	6,52E-03
norR	1,22	7,84E-04
rpmG	1,22	9,32E-03
VC_RS05080	1,20	3,77E-06

VC_RS00360	1,20	7,07E-04
VC_RS17040	1,20	2,06E-03
VC_RS11880	1,20	5,73E-05
zwf	1,19	9,56E-05
rimO	1,18	8,37E-04
xseB	1,18	1,46E-03
fadA	1,17	5,74E-03
pspB	1,17	7,83E-03
nhaA	1,17	2,57E-03
gspI	1,16	3,74E-03
VC_RS00180	1,16	1,52E-03
rluB	1,16	8,17E-05
VC_RS05405	1,15	2,69E-03
queE	1,15	9,97E-03
erpA	1,12	9,42E-03
VC_RS05410	1,11	2,47E-03
dbpA	1,06	7,53E-03
VC_RS15770	1,06	2,50E-03
VC_RS05800	1,06	1,80E-03
VC_RS15765	1,05	4,86E-03
ilvG	1,02	9,03E-04
VC_RS17205	1,02	2,74E-03
cgtA	1,02	2,06E-04
VC_RS08280	1,01	7,16E-04
lepA	0,98	1,30E-03
secD	0,97	1,44E-04
secD	0,97	1,44E-04
thiI	0,95	9,17E-03
yihI	0,94	7,72E-03
nlpD	0,93	6,99E-03
lipB	0,93	3,85E-03
VC_RS03795	0,92	6,44E-03
rpoH	0,91	2,26E-04
VC_RS07895	0,86	9,32E-03
ruvA	0,86	4,66E-03
ruvB	0,83	7,43E-03
mgtE	0,83	2,99E-03
mgtE	0,83	2,99E-03
der	0,82	2,14E-03
lepB	0,77	9,17E-03
Transcripts DOWN		
tgt	-5,96	1,33E-07
treC	-4,79	2,04E-86
VC_RS07220	-4,54	2,03E-02
VC_RS06415	-4,35	1,81E-24
VC_RS08165	-4,34	5,68E-48

VC_RS06535	-4,33	4,12E-20
treB	-4,26	3,95E-77
dcuC	-4,25	5,49E-40
frdD	-4,02	3,04E-05
VC_RS13520	-4,01	8,27E-03
VC_RS12800	-4,01	2,09E-15
VC_RS06405	-3,90	5,49E-40
VC_RS18125	-3,89	1,70E-24
adhE	-3,85	4,00E-38
VC_RS03955	-3,85	1,12E-06
VC_RS03950	-3,76	2,56E-13
frdC	-3,75	2,75E-14
VC_RS03300	-3,73	7,21E-21
VC_RS06410	-3,66	1,68E-19
VC_RS09000	-3,62	6,89E-35
frdA	-3,50	3,01E-12
VC_RS16590	-3,49	2,26E-11
VC_RS18120	-3,45	5,19E-20
VC_RS11425	-3,44	3,82E-18
VC_RS17100	-3,42	5,40E-24
grcA	-3,39	4,67E-14
nrdD	-3,38	6,19E-33
VC_RS14495	-3,36	4,85E-02
pepT	-3,35	8,01E-18
menC	-3,34	2,34E-16
VC_RS03305	-3,30	5,57E-23
VC_RS13030	-3,30	2,56E-03
VC_RS09030	-3,16	1,21E-22
VC_RS10340	-3,13	1,28E-10
VC_RS09395	-3,12	4,11E-18
VC_RS18865	-3,06	6,78E-05
VC_RS09390	-3,06	2,71E-20
menE	-3,05	1,43E-13
yccS	-2,99	1,50E-20
pykF	-2,94	2,21E-27
VC_RS13475	-2,93	4,46E-19
VC_RS04335	-2,90	6,37E-19
nrdG	-2,86	8,31E-09
ompW	-2,82	1,14E-12
VC_RS14490	-2,81	4,01E-02
pfkA	-2,80	1,13E-25
menB	-2,69	5,30E-14
VC_RS16905	-2,69	5,23E-27
VC_RS16240	-2,65	1,77E-14
pflB	-2,55	2,04E-18
VC_RS10735	-2,52	3,50E-09

VC_RS02445	-2,44	3,57E-12
VC_RS10000	-2,42	7,69E-10
vesC	-2,41	4,62E-15
VC_RS14330	-2,41	5,14E-15
VC_RS10325	-2,41	6,01E-11
gap	-2,38	1,72E-13
VC_RS03835	-2,37	3,58E-08
pgi	-2,30	3,04E-18
VC_RS09625	-2,30	4,67E-14
malT	-2,28	1,93E-13
malQ	-2,26	4,59E-15
VC_RS02160	-2,20	1,11E-14
VC_RS05160	-2,19	1,61E-17
VC_RS14510	-2,19	4,33E-04
VC_RS02215	-2,18	1,52E-05
VC_RS17420	-2,18	8,35E-17
glmS	-2,18	3,77E-04
VC_RS14455	-2,16	7,21E-21
bioD	-2,15	2,32E-15
malF	-2,11	7,13E-15
VC_RS06340	-2,07	2,48E-11
VC_RS08370	-2,05	1,61E-03
VC_RS02435	-2,04	7,63E-04
ppc	-2,04	4,69E-17
VC_RS12995	-2,04	5,80E-09
ilvC	-2,01	6,88E-10
gpmM	-2,01	2,13E-13
nhaC	-2,01	5,45E-17
narQ	-2,00	7,24E-04
feoB	-1,95	1,14E-04
VC_RS03315	-1,94	9,33E-10
VC_RS14530	-1,94	1,56E-02
malK	-1,93	4,62E-15
VC_RS03320	-1,92	3,28E-06
raiA	-1,91	6,39E-05
VC_RS08805	-1,90	2,13E-02
malE	-1,90	1,05E-13
VC_RS13960	-1,89	2,50E-04
VC_RS15980	-1,89	2,11E-11
eno	-1,89	3,01E-12
VC_RS14460	-1,89	4,21E-12
edd	-1,88	7,92E-09
VC_RS01665	-1,88	8,78E-06
elbB	-1,88	1,66E-05
malG	-1,88	6,61E-16
tpiA	-1,87	2,63E-10

VC_RS05825	-1,85	4,69E-07
VC_RS05625	-1,84	5,26E-07
VC_RS00575	-1,76	3,28E-04
VC_RS04300	-1,75	9,63E-13
VC_RS08210	-1,73	1,90E-05
VC_RS11965	-1,71	1,10E-07
VC_RS05975	-1,68	4,73E-05
ptsI	-1,68	2,67E-08
VC_RS11420	-1,63	1,01E-05
VC_RS02480	-1,59	4,28E-03
VC_RS18185	-1,58	7,43E-08
folA	-1,58	2,16E-05
VC_RS09155	-1,57	4,41E-05
VC_RS06100	-1,56	7,43E-03
VC_RS13010	-1,55	6,39E-03
tcpP	-1,55	2,45E-06
glgB	-1,55	3,74E-05
VC_RS00620	-1,55	6,37E-09
VC_RS16100	-1,53	1,92E-10
fbaA	-1,52	1,93E-06
VC_RS11495	-1,52	3,89E-04
ushA	-1,51	6,73E-07
hlyA	-1,49	4,31E-08
fdh3B	-1,49	5,16E-06
VC_RS05670	-1,49	1,67E-04
crp	-1,47	5,77E-10
VC_RS07315	-1,46	4,15E-09
VC_RS04785	-1,46	2,40E-07
nagK	-1,44	6,82E-06
lamB	-1,43	7,42E-06
pal	-1,43	2,31E-04
VC_RS02505	-1,42	2,01E-03
VC_RS08795	-1,41	8,87E-03
ccmD	-1,40	4,93E-02
gltB	-1,39	7,58E-08
gltB	-1,39	7,58E-08
VC_RS11435	-1,38	3,62E-05
VC_RS02090	-1,38	1,06E-02
fruA	-1,37	3,76E-10
VC_RS14360	-1,37	6,67E-06
hcp-2	-1,37	1,35E-03
hcp-2	-1,37	1,35E-03
fruB	-1,36	1,89E-07
VC_RS11635	-1,36	1,17E-05
VC_RS16670	-1,35	3,55E-04
VC_RS07305	-1,35	2,69E-06

VC_RS13950	-1,34	1,50E-03
VC_RS08520	-1,34	2,22E-05
menH	-1,33	9,08E-03
VC_RS05665	-1,33	2,65E-03
VC_RS17105	-1,32	1,71E-03
VC_RS02210	-1,32	3,87E-04
ptsG	-1,29	2,17E-06
VC_RS05295	-1,28	1,39E-04
VC_RS01370	-1,27	1,44E-03
pfkB	-1,27	2,74E-05
VC_RS09325	-1,27	4,85E-02
VC_RS02820	-1,25	2,75E-02
galK	-1,24	3,60E-04
VC_RS01625	-1,24	2,75E-03
VC_RS03680	-1,22	2,37E-02
VC_RS18380	-1,21	1,44E-03
katG	-1,21	1,44E-03
pntB	-1,21	1,32E-04
VC_RS07330	-1,21	4,84E-06
VC_RS14215	-1,21	1,92E-02
ccoO	-1,20	4,76E-02
VC_RS01395	-1,20	2,02E-02
tssM	-1,19	6,95E-04
VC_RS01300	-1,19	1,01E-02
asnB	-1,18	3,77E-05
tusB	-1,18	2,69E-03
VC_RS05860	-1,18	4,25E-03
VC_RS14825	-1,18	9,82E-03
VC_RS11350	-1,18	2,09E-03
VC_RS02830	-1,18	3,88E-03
VC_RS14815	-1,17	2,31E-04
VC_RS18835	-1,17	3,09E-02
VC_RS08225	-1,17	2,91E-03
modC	-1,16	3,88E-03
VC_RS16360	-1,16	4,86E-03
VC_RS01390	-1,16	1,96E-04
VC_RS14820	-1,15	3,49E-04
tcpH	-1,15	2,13E-02
VC_RS01790	-1,14	2,16E-05
VC_RS08240	-1,14	1,35E-02
tagO	-1,14	4,81E-02
fliN	-1,14	4,99E-05
VC_RS05660	-1,12	9,93E-03
VC_RS00855	-1,12	2,41E-04
arcA	-1,12	9,12E-03
arcA	-1,12	9,12E-03

VC_RS18700	-1,11	4,29E-03
VC_RS00635	-1,11	3,88E-03
can	-1,11	1,35E-03
VC_RS09920	-1,11	7,19E-05
VC_RS11900	-1,10	1,07E-03
ycfP	-1,09	1,73E-03
galM	-1,08	9,41E-03
VC_RS17495	-1,08	4,37E-05
VC_RS09885	-1,07	7,65E-04
VC_RS12600	-1,07	2,42E-02
VC_RS10600	-1,07	3,60E-04
VC_RS09255	-1,06	2,13E-02
VC_RS11255	-1,06	2,99E-03
oadA	-1,06	1,00E-02
oadA	-1,06	1,00E-02
nudF	-1,05	2,57E-03
VC_RS06640	-1,05	6,18E-04
VC_RS15915	-1,05	6,89E-04
rhtB	-1,04	1,80E-02
rimI	-1,04	3,82E-02
minE	-1,04	1,57E-02
VC_RS17175	-1,04	4,67E-04
VC_RS00770	-1,03	7,83E-03
VC_RS12105	-1,03	1,93E-02
hupA	-1,03	2,50E-03
VC_RS06960	-1,02	3,49E-02
VC_RS10580	-1,02	6,78E-05
VC_RS10825	-1,02	4,93E-02
VC_RS11450	-1,01	1,11E-02
VC_RS03100	-1,01	8,64E-03
chiS	-1,00	7,43E-04

Table S3. RNA-seq V. cholerae WT/Δtgt, in MH and TOB. Only significant differences higher than 2-fold are shown.

MH					
locus_tag	old_locus_tag	gene	baseMean	log2FC WT/Δtgt	padj
VC_RS03715	VC0741,VC_0741	tgt	3412	6,91	3,3E-168
VC_RS13030	VC2706,VC_2706	yhhQ	5207	5,12	4,6E-148
VC_RS17680	VC_A0913,VCA0913	hutB	298	3,23	1,1E-06
VC_RS17670	VC_A0911,VCA0911	exbB	234	3,18	5,8E-07
VC_RS17690	VC_A0915,VCA0915	hutD	131	2,91	3,5E-05
VC_RS17675	VC_A0912,VCA0912	exbD	329	2,88	1,6E-09
VC_RS17685	VC_A0914,VCA0914	btuC/fecCD	362	2,80	2,7E-05
VC_RS03875	VC0773,VC_0773	entC	64	2,53	2,4E-04
VC_RS16165	VC_A0576,VCA0576	hutA	4750	2,51	5,1E-06
VC_RS17665	VC_A0910,VCA0910	tonB1	400	2,46	9,5E-07
VC_RS14430	VC_A0229,VCA0229	febD	356	2,44	1,4E-07
VC_RS17655	VC_A0908,VCA0908	hutX	1037	2,37	9,5E-07
VC_RS14435	VC_A0230,VCA0230	fhuC	617	2,34	1,7E-04
VC_RS17660	VC_A0909,VCA0909	hutW	1132	2,23	7,3E-07
VC_RS02435	VC0475,VC_0475	cirA	826	2,02	1,7E-03
VC_RS14425	VC_A0228,VCA0228	fepD	454	2,02	1,9E-07
VC_RS17650	VC_A0907,VCA0907	hutZ	3146	1,87	8,8E-06
VC_RS17955	VC_A0977,VCA0977	yejF	454	1,81	3,9E-08
VC_RS14420	VC_A0227,VCA0227	gcvH	2378	1,78	1,4E-05
VC_RS17950	VC_A0976,VCA0976		103	1,70	2,7E-02
VC_RS08170	VC1688,VC_1688	mglC	137	1,65	1,2E-02
VC_RS07460	VC1542,VC_1542	ligA	54	1,64	1,3E-04
VC_RS03070	VC0606,VC_0606	glnK	174	1,59	7,0E-03
VC_RS07475	VC1545,VC_1545	exbB	306	1,54	1,3E-04
VC_RS07470	VC1544,VC_1544	exbD	354	1,46	4,2E-04
VC_RS16600	VC_A0676,VCA0676	napF	1952	1,45	4,1E-02
VC_RS13690	VC_A0064,VCA0064	thiS	198	1,44	1,8E-03
VC_RS13695	VC_A0065,VCA0065	thiG	180	1,42	6,3E-04
VC_RS01835	VC0365,VC_0365	bfr	2422	1,39	1,1E-06
VC_RS07465	VC1543,VC_1543		1162	1,39	3,2E-04
VC_RS10685	VC2210,VC_2210	viuB	550	1,34	8,9E-04
VC_RS02430	VC0474,VC_0474	irgB	157	1,33	1,8E-02
VC_RS07595	VC1572,VC_1572		27	1,28	2,9E-02
VC_RS00985	VC0201,VC_0201	fhuC	92	1,27	3,2E-02
VC_RS00980	VC0200,VC_0200	fhuA	2454	1,25	3,7E-03
VC_RS07600	VC1573,VC_1573	fumC	197	1,25	9,7E-05
VC_RS10690	VC2211,VC_2211	viuA	527	1,24	4,5E-05
VC_RS07480	VC1546,VC_1546	exbB	303	1,23	2,0E-03
VC_RS03900	VC0778,VC_0778	fepG	53	1,19	4,6E-02
VC_RS03080	VC0608,VC_0608	fbpA	4516	1,18	1,3E-04

VC_RS13685	VC_A0063,VCA0063	ptrB	280	1,16	5,1E-03
VC_RS04975	VC1009,VC_1009		505	1,16	1,1E-05
VC_RS02570	VC0504,VC_0504	susC (tonB-like)	42	1,11	3,2E-02
VC_RS06170	VC1265,VC_1265	cytochrome C	511	1,10	1,3E-02
VC_RS07485	VC1547,VC_1547	exbB	692	1,09	6,0E-04
VC_RS05755	VC1174,VC_1174	trpE	263	1,07	9,7E-05
VC_RS03865	VC0771,VC_0771	vibB	412	1,06	1,1E-03
VC_RS16595	VC_A0675,VCA0675	narQ	770	1,03	4,9E-02
VC_RS16075	VC_A0558,VCA0558	yfjD	516	1,03	2,5E-02
VC_RS01830	VC0364,VC_0364	bfd	321	1,02	8,2E-03
VC_RS14440	VC_A0231,VCA0231	yqhC	272	1,00	2,7E-02
VC_RS02480	VC0486,VC_0486	srlR	748	1	3,2E-03
VC_RS12970	VC2694,VC_2694	sodA	503	0,80	5,1E-03

TOB

locus_tag	old_locus_tag	gene	baseMean	log2FoldChange WT/Δtgt	padj
VC_RS03715	VC0741,VC_0741	tgt	3412	5,991	5,0E-181
VC_RS13030	VC2706,VC_2706	yhhQ	5207	4,392	6,2E-114
VC_RS02575	VC0505,VC_0505		8	3,806	2,8E-02
VC_RS00075	VC0018,VC_0018	ibpA	4235	1,919	1,5E-03
VC_RS04265	VC0855,VC_0855	dnaK	17310	1,863	3,5E-03
VC_RS02570	VC0504,VC_0504	susC (tonB)	42	1,823	2,1E-04
VC_RS04385	VC0885,VC_0885		97	1,812	1,7E-03
VC_RS03575	VC0711,VC_0711	clpB	2525	1,688	1,2E-02
VC_RS04835	VC0977,VC_0977	cnoX	522	1,595	2,3E-03
VC_RS02995	VC0589,VC_0589	yadG	518	1,586	2,3E-02
VC_RS12835	VC2665,VC_2665	groES1	2421	1,555	4,6E-02
VC_RS18020	VC_A0989,VCA0989	dinF	136	1,511	2,5E-02
VC_RS04870	VC0985,VC_0985	htpG	9334	1,507	4,5E-02
VC_RS05980	VC1217,VC_1217	yjgM	88	1,406	7,7E-03
VC_RS04390	VC0886,VC_0886		208	1,381	5,8E-03
VC_RS16915	VC_A0744,VCA0744	glpK	1194	1,317	1,8E-09
VC_RS12880	VC2674,VC_2674	hslU	1673	1,268	1,6E-02
VC_RS12885	VC2675,VC_2675	hslV	365	1,261	5,9E-03
VC_RS00930	VC0188,VC_0188	prlC	2248	1,194	8,4E-03
VC_RS01320	VC0271,VC_0271	corC	728	1,155	1,2E-03
VC_RS02400	VC0468,VC_0468	gshB	1377	1,124	1,8E-04
VC_RS06455	VC1325,VC_1325	mglB	1478	1,089	8,0E-05
VC_RS09260	VC1920,VC_1920	lon	3601	1,066	2,3E-02
VC_RS02395	VC0467,VC_0467	ygqE	541	1,055	6,7E-04
VC_RS17520	VC_A0881,VCA0881		196	1,033	1,4E-02
VC_RS17525	VC_A0882,VCA0882		289	1,021	3,2E-03
VC_RS12360	VC2564,VC_2564	dbpA	618	-1,017	3,0E-02
VC_RS15790	VC_A0494,VCA0494	acetyltransferase	70	-1,028	3,7E-02

VC_RS03960	VC0792,VC_0792	yjfF oad	28	-1,029	2,6E-02
VC_RS14205	VC_A0179,VCA0179	psuT	156	-1,038	3,3E-02
VC_RS18615	VC_1646		27	-1,057	4,6E-02
VC_RS05270	VC1071,VC_1071	arsJ	117	-1,093	4,0E-03
VC_RS07060	VC1458,VC_1458	zot	640	-1,102	1,8E-02
VC_RS09405	VC1953,VC_1953	nupX	95	-1,131	2,3E-02
VC_RS18070	VC_A1000,VCA1000	leuE	62	-1,139	3,8E-02
VC_RS12345	VC2561,VC_2561	cobA	78	-1,143	3,3E-02
VC_RS15320			90	-1,171	1,4E-02
VC_RS06240	VC1279,VC_1279	betT	572	-1,246	9,9E-04
VC_RS15780	VC_A0492,VCA0492	RfbP-related protein	323	-1,262	8,5E-07
VC_RS07075	VC1461,VC_1461	cep ctx	2195	-1,282	1,9E-04
VC_RS12540	VC2600,VC_2600	yejM	397	-1,31	3,0E-03
VC_RS01360	VC0280,VC_0280	cadB	47	-1,346	5,1E-03
VC_RS16860	VC_A0732,VCA0732	ygiW	881	-1,417	1,5E-03
VC_RS18060	VC_A0998,VCA0998	nemA	385	-1,446	3,0E-02
VC_RS08700	VC1801,VC_1801		74	-1,462	2,6E-02
VC_RS01365	VC0281,VC_0281	cadA ldcI	60	-1,489	1,7E-03
VC_RS07640	VC1581,VC_1581	nuoL	56	-1,502	5,4E-03
VC_RS18100	VC_A1006,VCA1006	osmC	77	-1,521	2,0E-03
VC_RS07080	VC1462,VC_1462	rstB2	4846	-1,523	1,2E-04
VC_RS17365	VC_A0847,VCA0847	yjeH	141	-1,535	3,6E-04
VC_RS05275	VC1073,VC_1073		235	-1,617	1,0E-05
VC_RS08705	VC1802,VC_1802		35	-1,77	8,5E-03
VC_RS08695			66	-1,778	1,3E-03
VC_RS08680	VC1798,VC_1798	eha	131	-1,804	2,2E-05
VC_RS08690	VC1800,VC_1800		183	-1,851	8,0E-05
VC_RS07065	VC1459,VC_1459	ace	152	-1,939	4,0E-02
VC_RS08685	VC1799,VC_1799	phage transposase	302	-2,376	1,4E-08
VC_RS07040	VC1454,VC_1454	rstA1	29530	-2,705	1,9E-04
VC_RS07070	VC1460,VC_1460	orfU ctx	1156	-2,774	3,9E-08
VC_RS07085	VC1463,VC_1463	rstA2	29040	-2,893	5,1E-05

Table S4: Primers, plasmids and strains

gene expressions from pSEVA

plasmid in strain TOP10	name	primers used for gene amplification
M027	pSEVA238	MCSSEVA238-5 GCAAGAAGCGGATACAGGAG MCSSEVA238-3 GGTTTTCCCAGTCACGACGC
R591	pSEVA-tgt	5tgtEcoRI CGCGGAATTCGTGAAATTAAAATTTGAACTG and 3tgtXbaI CGCGTCTAGATCAGGCTTTGTCTTTTTGTAGTGG
Q298	pSEVA-rsxA	ZIP753 GCCCGAATTCCATTTGCCACTTATTGCG and ZIP754 GCCGCCGAATTCTTACAGTTTCACCAATCCGGTAAAGCC
Q294	pSEVA-soxR	ZIP757 GGGGCCCCCCCCCGAATTCGTAAAGCGTTTTTTTAATAAAACGGG and ZIP758 CCGAATTCTTAACGGCTCCACTCTTCTGGATGCGATAAGCG
Q291	pSEVA-katG	ZIP755 GCGCGCCCCGAATTCATTTCCCATTTAGTGAAAAGGG and ZIP756 GAATTCTTACATCGCGGCCAGTTTTGCCACC

tRNA overexpression fragments cloned in pTOPO-blunt-kanamycin R (Ptrc promoter and VCt002 terminator are underlined, anticodon in red)

plasmid in TOP10	name	sequence
L961	Ptrc-eco-tRNA-Tyr wtGUA	GAGCTGTTGACAATTAATCATCCGGCTCGTATAATGTGTGGGGTGGGGTTCCCGAGCG GCCAAAGGGAGCAGACTGTAAATCTGCCGTCACAGACTTCGAAGGTTCGAATCCTTCC CCCACCACCACTTATTCGAGCTTAAGCTCAAAAAACTACA
M660	Ptrc-eco-tRNA-Tyr mutAUA	GAGCTGTTGACAATTAATCATCCGGCTCGTATAATGTGTGGGGTGGGGTTCCCGAGCG GCCAAAGGGAGCAGACTATAAATCTGCCGTCACAGACTTCGAAGGTTCGAATCCTTCC CCCACCACCACTTATTCGAGCTTAAGCTCAAAAAACTACA
L957	Ptrc-eco-tRNA-Asp wt GUC	GAGCTGTTGACAATTAATCATCCGGCTCGTATAATGTGTGGGGAGCGGTAGTTCAGTC GGTTAGAATACCTGCCTGTCACGCAGGGGGTCGCGGGTTCGAGTCCCGTCCGTTCCGC CACTTATTCGAGCTTAAGCTCAAAAAACTACA
L960	Ptrc-vch-tRNA-Tyr wtGUA	GAGCTGTTGACAATTAATCATCCGGCTCGTATAATGTGTGGGGAGGGGTTCCCGAGTG GCCAAAGGGAGCAGACTGTAAATCTGCCGGCTCCGCCTTCGATGGTTCGAATCCGTCC CCCTCCACCACTTATTCGAGCTTAAGCTCAAAAAACTACA
L959	Ptrc-vch-tRNA-Tyr mutAUA	GAGCTGTTGACAATTAATCATCCGGCTCGTATAATGTGTGGGGAGGGGTTCCCGAGTG GCCAAAGGGAGCAGACTATAAATCTGCCGGCTCCGCCTTCGATGGTTCGAATCCGTCC CCCTCCACCACTTATTCGAGCTTAAGCTCAAAAAACTACA
L956	Ptrc-vch-tRNA-Asp wtGUC	GAGCTGTTGACAATTAATCATCCGGCTCGTATAATGTGTGGGGAGCGGTAGTTCAGTC GGTTAGAATACCGGCCTGTCACGCCGGGGGTCGCGGGTTCGAGTCCCGTCCGCTCCG CCACTTATTCGAGCTTAAGCTCAAAAAACTACA
L955	Ptrc-vch-tRNA-mutAspAUC	GAGCTGTTGACAATTAATCATCCGGCTCGTATAATGTGTGGGGAGCGGTAGTTCAGTC GGTTAGAATACCGGCCTATCACGCCGGGGGTCGCGGGTTCGAGTCCCGTCCGCTCCGC CACTTATTCGAGCTTAAGCTCAAAAAACTACA
M651	Ptrc-vch-tRNA-Asn wtGUU	GAGCTGTTGACAATTAATCATCCGGCTCGTATAATGTGTGGTCCTCCTTAGCTCAGTCG GTAGAGCGACGGACTGTTAATCCGCAGGTCGCTGGTTCAAGTCCAGCAGGAGGAGCC ACTTATTCGAGCTTAAGCTCAAAAAACTACA
L962	Ptrc-vch-tRNA-Asn mutAUU	GAGCTGTTGACAATTAATCATCCGGCTCGTATAATGTGTGGTCCTCCTTAGCTCAGTCG GTAGAGCGACGGACTATTAATCCGCAGGTCGCTGGTTCAAGTCCAGCAGGAGGAGCC ACTTATTCGAGCTTAAGCTCAAAAAACTACA
M646	Ptrc-vch-tRNA-HIS wtGUG	GAGCTGTTGACAATTAATCATCCGGCTCGTATAATGTGTGGGTGGCTATAGCTCAGTT GGTAGAGCCCCGGATTGTGATTCCGGTTGTCGTGGGTTCGAGCCCCATTAGCCACCCC ACTTATTCGAGCTTAAGCTCAAAAAACTACA
L997	Ptrc-vch-tRNA-HIS mutAUG	GAGCTGTTGACAATTAATCATCCGGCTCGTATAATGTGTGGGTGGCTATAGCTCAGTT GGTAGAGCCCCGGATTATGATTCCGGTTGTCGTGGGTTCGAGCCCCATTAGCCACCCC ACTTATTCGAGCTTAAGCTCAAAAAACTACA
M653	Ptrc-vch-tRNA-Phe wtGAA	GAGCTGTTGACAATTAATCATCCGGCTCGTATAATGTGTGGGCCCGGATAGCTCAGTC GGTAGAGCAGAGGATTGAAAATCCTCGTGTCGGTGGTTCGATTCCGCCTCCGGGCACC ACTTATTCGAGCTTAAGCTCAAAAAACTACA

translational fusions ordered in pUC_IDT (carbenicillin R)

plasmid in strain DH5α	name	sequence

R973	Ptrc-rsxATAC-gfp	TTGACAATTAATCATCCGGCTCGTATAATGTGTGGAATTGTGAGCGGATAACAATTTCACACAGGA AACAGCGCCGCATGACCGAATACCTTTTGTTGTTAATCGGCACCGTGCTGGTCAATAACTTTGTAC TGGTGAAGTTTTTGGGCTTATGTCCTTTTATGGGCGTATCAAAAAAACTAGAGACCGCCATTGGCA TGGGGTTGGCGACGACATTCGTCCTCACCTTAGCTTCGGTGTGCGCTTACCTGGTGGAAAGTTAC GTGTTACGTCCGCTCGGCATTGAGTACCTGCGCACCATGAGCTTTATTTTGGTGATCGCTGTCGTA GTACAGTTCACCGAAATGGTGGTGCACAAAACCAGTCCGACACTCTACCGCCTGCTGGGCATTTTC CTGCCACTCATCACCACCAACTGTGCGGTATTAGGGGTTGCGCTGCTCAACATCAACGAAAATCAC AACTTTATTCAATCGATCATTTACGGTTTTGGCGCTGCTGTTGGCTTCTCGCTGGTGCTCATCTTGT TCGCTTCAATGCGTGAGCGAATCCATGTAGCCGATGTCCCCGCTCCCTTTAAGGGCGCATCCATTG CGATGATCACCGCAGGTTTAATGTCTTTGGCCTTTATGGGCTTTACCGGATTGGTGAAACTGGCTA GCAAAGGAGAAGAACTTTTCACTGGAGTTGTCCCAATTCTTGTTGAATTAGATGGTGATGTTAATG GGCACAAATTTTCTGTCAGTGGAGAGGGTGAAGGTGATGCTACATACGGAAAGCTTACCCTTAAA TTTATTTGCACTACTGGAAAACTACCTGTTCCATGGCCAACACTTGTCACTACTTTGACCTATGGTG TTCAATGCTTTTCCCGTTATCCGGATCATATGAAACGGCATGACTTTTTCAAGAGTGCCATGCCCGA AGGTTATGTACAGGAACGCACTATATCTTTCAAAGATGACGGGAACTACAAGACGCGTGCTGAAG TCAAGTTTGAAGGTGATACCCTTGTTAATCGTATCGAGTTAAAAGGTATTGATTTTAAAGAAGATG GAAACATTCTCGGACACAAACTCGAGTACAACTATAACTCACACAATGTATACATCACGGCAGACA AACAAAAGAATGGAATCAAAGCTAACTTCAAAATTCGCCACAACATTGAAGATGGAGGCGTTCAA CTAGCAGACCATTATCAACAAAATACTCCAATTGGCGATGGCCCTGTCCTTTTACCAGACAACCATT ACCTGTCGACACAATCTGCCCTTTCGAAAGATCCCAACGAAAAGCGTGACCACATGGTCCTTCTTG AGTTTGTAACTGCTGCTGGGATTACACATGGCATGGATGAGCTCTACAAATAA
R972	Ptrc-rsxATATWT-gfp	TTGACAATTAATCATCCGGCTCGTATAATGTGTGGAATTGTGAGCGGATAACAATTTCACACAGGA AACAGCGCCGCATGACCGAATATCTTTTGTTGTTAATCGGCACCGTGCTGGTCAATAACTTTGTAC TGGTGAAGTTTTTGGGCTTATGTCCTTTTATGGGCGTATCAAAAAAACTAGAGACCGCCATTGGCA TGGGGTTGGCGACGACATTCGTCCTCACCTTAGCTTCGGTGTGCGCTTATCTGGTGGAAAGTTACG TGTTACGTCCGCTCGGCATTGAGTATCTGCGCACCATGAGCTTTATTTTGGTGATCGCTGTCGTAG TACAGTTCACCGAAATGGTGGTGCACAAAACCAGTCCGACACTCTATCGCCTGCTGGGCATTTTCC TGCCACTCATCACCACCAACTGTGCGGTATTAGGGGTTGCGCTGCTCAACATCAACGAAAATCACA ACTTTATTCAATCGATCATTTATGGTTTTGGCGCTGCTGTTGGCTTCTCGCTGGTGCTCATCTTGTTC GCTTCAATGCGTGAGCGAATCCATGTAGCCGATGTCCCCGCTCCCTTTAAGGGCGCATCCATTGCG ATGATCACCGCAGGTTTAATGTCTTTGGCCTTTATGGGCTTTACCGGATTGGTGAAACTGGCTAGC AAAGGAGAAGAACTTTTCACTGGAGTTGTCCCAATTCTTGTTGAATTAGATGGTGATGTTAATGG GCACAAATTTTCTGTCAGTGGAGAGGGTGAAGGTGATGCTACATACGGAAAGCTTACCCTTAAAT TTATTTGCACTACTGGAAAACTACCTGTTCCATGGCCAACACTTGTCACTACTTTGACCTATGGTGT TCAATGCTTTTCCCGTTATCCGGATCATATGAAACGGCATGACTTTTTCAAGAGTGCCATGCCCGA AGGTTATGTACAGGAACGCACTATATCTTTCAAAGATGACGGGAACTACAAGACGCGTGCTGAAG TCAAGTTTGAAGGTGATACCCTTGTTAATCGTATCGAGTTAAAAGGTATTGATTTTAAAGAAGATG GAAACATTCTCGGACACAAACTCGAGTACAACTATAACTCACACAATGTATACATCACGGCAGACA AACAAAAGAATGGAATCAAAGCTAACTTCAAAATTCGCCACAACATTGAAGATGGAGGCGTTCAA CTAGCAGACCATTATCAACAAAATACTCCAATTGGCGATGGCCCTGTCCTTTTACCAGACAACCATT ACCTGTCGACACAATCTGCCCTTTCGAAAGATCCCAACGAAAAGCGTGACCACATGGTCCTTCTTG AGTTTGTAACTGCTGCTGGGATTACACATGGCATGGATGAGCTCTACAAATAA
R975	Ptrc-gfpTAC	GAGCTGTTGACAATTAATCATCCGGCTCGTATAATGTGTGGAATTGTGAGCGGATAACAATTTCAC ACAGGAAACACATATGCGTAAAGGAGAAGAACTTTTCACTGGAGTTGTCCCAATTCTTGTTGAATT AGATGGTGATGTTAATGGGCACAAATTTTCTGTCAGTGGAGAGGGTGAAGGTGATGCAACATAC GGAAAACTTACCCTTAAATTTATTTGCACTACTGGAAAACTACCTGTTCCATGGCCAACACTTGTCA CTACTTTCGGTTACGGTGTTCAATGCTTTGCGAGATACCCAGATCATATGAAACAGCATGACTTTTT CAAGAGTGCCATGCCCGAAGGTTACGTACAGGAAAGAACTATATTTTTCAAAGATGACGGGAACT ACAAGACACGTGCTGAAGTCAAGTTTGAAGGTGATACCCTTGTTAATAGAATCGAGTTAAAAGGT ATTGATTTTAAAGAAGATGGAAACATTCTTGGACACAAATTGGAATACAACTACAACTCACACAAT GTATACATCATGGCAGACAAACAAAAGAATGGAATCAAAGTTAACTTCAAAATTAGACACAACAT TGAAGATGGAAGCGTTCAACTAGCAGACCATTACCAACAAAATACTCCAATTGGCGATGGCCCTG TCCTTTTACCAGACAACCATTACCTGTCCACACAATCTGCCCTTTCGAAAGATCCCAACGAAAAGA GAGACCACATGGTCCTTCTTGAGTTTGTAACAGCTGCTGGGATTACACATGGCATGGATGAACTAT ACAAATAA
R974	Ptrc-gfpTAT	GAGCTGTTGACAATTAATCATCCGGCTCGTATAATGTGTGGAATTGTGAGCGGATAACAATTTCAC ACAGGAAACACATATGCGTAAAGGAGAAGAACTTTTCACTGGAGTTGTCCCAATTCTTGTTGAATT AGATGGTGATGTTAATGGGCACAAATTTTCTGTCAGTGGAGAGGGTGAAGGTGATGCAACATAT GGAAAACTTACCCTTAAATTTATTTGCACTACTGGAAAACTACCTGTTCCATGGCCAACACTTGTCA CTACTTTCGGTTATGGTGTTCAATGCTTTGCGAGATATCCAGATCATATGAAACAGCATGACTTTTT CAAGAGTGCCATGCCCGAAGGTTATGTACAGGAAAGAACTATATTTTTCAAAGATGACGGGAACT ATAAGACACGTGCTGAAGTCAAGTTTGAAGGTGATACCCTTGTTAATAGAATCGAGTTAAAAGGT ATTGATTTTAAAGAAGATGGAAACATTCTTGGACACAAATTGGAATATAACTATAACTCACACAAT GTATATATCATGGCAGACAAACAAAAGAATGGAATCAAAGTTAACTTCAAAATTAGACACAACAT TGAAGATGGAAGCGTTCAACTAGCAGACCATTATCAACAAAATACTCCAATTGGCGATGGCCCTG TCCTTTTACCAGACAACCATTATCTGTCCACACAATCTGCCCTTTCGAAAGATCCCAACGAAAAGAG AGACCACATGGTCCTTCTTGAGTTTGTAACAGCTGCTGGGATTACACATGGCATGGATGAACTATA TAAATAA

plasmid in strain (WT/*Δtgt*)	codon replacement	introduction of point mutation in circular pTOPO-TA (kanamycin R) by PCR using primers :
N509/N511	bla wt	Tyr103TAC Asp129GAT
N512/N514	bla Tyr103TAC > Tyr TAT synonymous	ZIP555 GACTTGGTTGAGTATTCACCAGTCACAGAAAAGC ZIP556 TCTGTGACTGGTGAATACTCAACCAAGTCATTCTGAGAATAG
plasmid in strain TOP10	primers for transcriptional fusion PrsxA-gfp	
Q282	ZIP796 ZIP812 ZIP813 ZIP200	GGATACAAAAAAGTAAACCC CTCCTTTACGCATAGTTATATAAATGTTTGCTTCCGATCCCGGCATTATCCTG CAGGATAATGCCGGGATCGGAAGCAAACATTTATATAACTATGCGTAAAGGAG TATCAAGCTTATTTGTATAGTTCATCCATGCC
target for amplification	primers for q-RT-PCR tRNAs	
tRNATyr	ZIP719 ZIP720	GGAGGGGTTCCCGAGTGG GGTGGAGGGGGACGGATT
tRNAAsp	ZIP721 ZIP722	GGAGCGGTAGTTCAGTCG TGGCGGAGCGGACGGGAC
tRNAHis	ZIP723 ZIP724	GTGGCTATAGCTCAGTTG TGGGGTGGCTAATGG
tRNAAsn	ZIP725 ZIP726	TCCTCCTTAGCTCAGTCGG TGGCTCCTCCTGCTGG
gyrA	gyrA_F gyrA_R	AAT GTG CTG GGC AAC GAC TG GAG CCA AAG TTA CCT TGG CC
target for amplification	primers for digital-RT-PCR fluorescent probes	
tgt		fwd CAA CAC CAC TGG ATC CTC ATT rev GGT AGT AAC GCA GGT TAT GG 5' - [FAM] A CCT GCA TCA TCT GGA TCG CTG TAA - 3' [BHQ2]
rsxA		fwd TCA CGC ATT GAA GCG AAC rev CAC CAA CTG TGC GGT ATT AG 5' - [FAM] A GCG CCA AAA CCA TAA ATG ATC GAT - 3' [BHQ2]
gyrA		fwd AAT GTG CTG GGC AAC GAC TG rev GAG CCA AAG TTA CCT TGG CC 5' - [CY5] - CAC CCT CAT GGT GAC AGT GCG GTT T - 3' [BHQ2]
Strains		
V. cholerae	strain #	reference
N16961 hapR+	F606	laboratory collection
N16961 hapR+ ΔlacZ	K329	Babosan et al, 2022
Δtgt::spec	J420	Babosan et al, 2022
ΔtolA::kan	J983	Negro et al, 2019
Δcrp::kan	Q081	Deletion of *crp* in F606 as described in Lang et al, 2021
ΔrluF::kan	M567	Babosan et al, 2022
ΔrluF::kan Δtgt::spec	M569	Deletion of *rluF* in J420, as described for deletion of *rluF* in WT in Babosan et al, 2022
E. coli	strain #	construction
MG1655	C349	laboratory collection
Δtgt::kan	J233	P1 transduction of tgt::kan from Keio collection into MG1655
Δtgt	R181	Kanamycin resistance cassette was removed using the FLP/FRT system (Zhu et al, 1995)
ΔrsxA::kan	R207	P1 transduction of tgt::kan from Keio collection into MG1655
Δtgt ΔrsxA::kan	R223	P1 transduction of rsxA::kan from Keio collection into R181 *Δtgt*

Supplementary figure legends

Figure S1. No effect of *rluF* deletion on fitness in *V. cholerae* WT and *Δtgt* strains. In vitro competition experiments of *V. cholerae* WT and mutant strains in the absence or presence of sub-MIC aminoglycosides tobramycin TOB and gentamicin (GEN) (50% of the MIC, TOB 0.6 µg/ml, GEN 0.5 µg/ml). MH: no antibiotic treatment. The Y-axis represents $\log_{10}$ of competitive index calculated as described in the methods. A competitive index of 1 indicates equal growth of both strains. The X-axis indicates growth conditions. For multiple comparisons, we used one-way ANOVA on GraphPad Prism. **** means $p<0.0001$, * means $p<0.05$. Number of replicates for each experiment: $3<n<10$.

Figure S2. Impact of tRNA overexpression on fitness during growth in sub-MIC TOB. A. Absence of *tgt* does not visibly affect endogenous tRNA-GUN levels. qRTPCR. A: relative tRNA abundance in *Δtgt* compared to WT strain in the absence of treatment (NT) and in the presence of sub-MIC tobramycin (TOB). **B.** In vitro competition experiments between *V. cholerae* WT and *Δtgt* strains, carrying a plasmid overexpressing the indicated tRNA; in the absence (NT) or presence of sub-MIC tobramycin (50% of the MIC, TOB 0.6 µg/ml). NT: no antibiotic treatment. The Y-axis represents $\log_{10}$ of competitive index calculated as described in the methods. A competitive index of 1 indicates equal growth of both strains. The X-axis indicates which tRNA is overexpressed, from the high copy pTOPO plasmid. The anticodon sequence is indicated (e.g. $tRNA^{Tyr}_{AUA}$ decodes the TAT codon). The following tRNAs-GUN are the canonical tRNAs which are present in the genome, and modified by Tgt: Tyr_{GUA}, His_{GUG}, Asn_{GUU}, Asp_{GUC}. The following tRNAs-AUN are synthetic tRNAs which are not present in the genome: Tyr_{AUA}, His_{AUG}, Asn_{AUU}, Asp_{AUC}. $tRNA^{Phe}_{GAA}$ is used as non Tgt-modified control. p0 is the empty plasmid. For multiple comparisons, we used one-way ANOVA on GraphPad Prism. **** means $p<0.0001$, * means $p<0.05$. Number of replicates for each experiment: $3<n<8$. In A, only significant differences are indicated. ns means non-significant.

Figure S3. Post-transcriptional upregulation of RsxA in *Δtgt* due to a Tyr codon bias towards TAT and toxicity in sub-MIC TOB. ABC. Translational fusion of TAC and TAT versions of *rsxA* to *gfp* (A. 4 hours exponential phase cultures, B. overnight stationary phase cultures). **DEF**. TAC and TAT versions of *gfp* alone (C. 4 hours exponential phase cultures without antibiotics, D. in the presence of sub-MIC TOB), measured by flow cytometry. Y-axis represents mean fluorescence. **C and F** show representative examples of fluorescence observed with indicated reporters.

Figure S4. *rsxA* levels impact growth in the presence of sub-MIC TOB. ABCD. Growth curves in microtiter plate reader, in *V. cholerae* in indicated conditions**.** P-tgt+: pSEVA expressing *tgt*. P-rsx+: pSEVA expressing *rsxA*. P-control: empty pSEVA. **E**. Growth curves in microtiter plate reader, in *E. coli* WT and *Δtgt* in MH or in the presence of tobramycin at the indicated concentrations (in µg/mL). **F.** Left: Competition experiments in *E. coli*, with indicated strains. Right: Relative OD 620 nm of indicated strain comparing growth in TOB (0.4 µg/ml) divided by growth in the absence of treatment.

Figure S5. Codon usage. A and B: Tyrosine codon usage in A: *V. cholerae* and B: *E. coli* in the whole genome and selected groups of genes. Red indicates positive codon usage bias, i.e. TAT bias. Blue indicates negative codon usage bias for TAT, i.e. TAC bias. **CDE.** Gene ontology enrichment analysis in *V. cholerae* of **C:** overrepresented gene categories with TAT usage bias**. D:** underrepresented gene categories with TAT usage bias**. E:** overrepresented gene categories with TAC usage bias.